

Magnetic Nanostructures

K. Bennemann

Institute of Theoretical Physics FU-Berlin

Arnimallee 14, 14195 Berlin

keywords: Magnetism, Nanostructures

Contents

1	<i>Introduction</i>	2
1.1	<i>Magnetic Clusters</i>	3
1.2	<i>Magnetic Films</i>	5
1.3	<i>Tunnel Junctions</i>	8
2	<i>Theory</i>	10
2.1	<i>Magnetism : Electronic theory</i>	12
2.2	<i>Magnetism : Heisenberg type theory</i>	14
2.3	<i>Electronic Structure of Mesoscopic Systems : Balian–Bloch type theory</i>	15
2.4	<i>Magnetooptics</i>	20
2.5	<i>Magnetization Dynamics</i>	27
2.6	<i>Theory for Magnetic Films during Growth : Nonequilibrium Magnetic Domain Structure</i>	27
2.7	<i>Tunnel Junctions: Spin Currents</i>	29
2.8	<i>Quantum dot Systems</i>	34
3	<i>Results</i>	35
3.1	<i>Small Magnetic Particles</i>	35
3.1.1	<i>Single Magnetic Clusters</i>	35
3.1.2	<i>Ensemble of Clusters</i>	41
3.2	<i>Thin Magnetic Films</i>	42
3.2.1	<i>Magnetic Structure</i>	45
3.2.2	<i>Reorientation Transition of the Magnetization</i>	45
3.2.3	<i>Magnetooptics</i>	48
3.2.4	<i>Nanostructured Thin Films with Magnetic Domains</i>	51
3.3	<i>Tunnel Junctions: Magnetic Effects</i>	58
4	<i>Summary</i>	64

Abstract

Characteristic results of magnetism in small particles and thin films are presented. As a consequence of the reduced atomic coordination in small clusters and thin films the electronic states and density of states modify. Thus magnetic moments and magnetization are affected. In tunnel junctions interplay of magnetism, spin currents and superconductivity are of particular interest. Results are given for single transition metal clusters, cluster ensembles, thin films and tunnel systems.

1 Introduction

Due to advances in preparing small particles, thin films, film multilayers and tunnel junctions the area of nanostructures in physics has received increased interest. Clearly engineering on an atomic scale condensed matter offers many possibilities regarding new physics and technical applications.

Of particular interest is the occurrence of magnetism in nanostructures like single transition metal clusters (Ni, Co, Fe etc.), ensembles of such clusters, for example in lattice like arrangements[1], ferromagnetic thin films, multilayers of such films [2] and tunnel junctions[3]. The latter are of interest, for example, regarding switching of electric, charge and spin currents. Size and orientation of magnetic moments and magnetization depend in general sensitively on atomic environment, atomic coordination (surfaces, interfaces etc.).

Of course, one expects that magnetic fluctuations are significant due to the reduced dimension of nanostructures. Regarding magnetic anisotropy, this will play an important role in general and also with respect to the role played effectively by the magnetic fluctuations. Due to magnetic anisotropy phase transitions occur in reduced dimensions and ultrathin films.

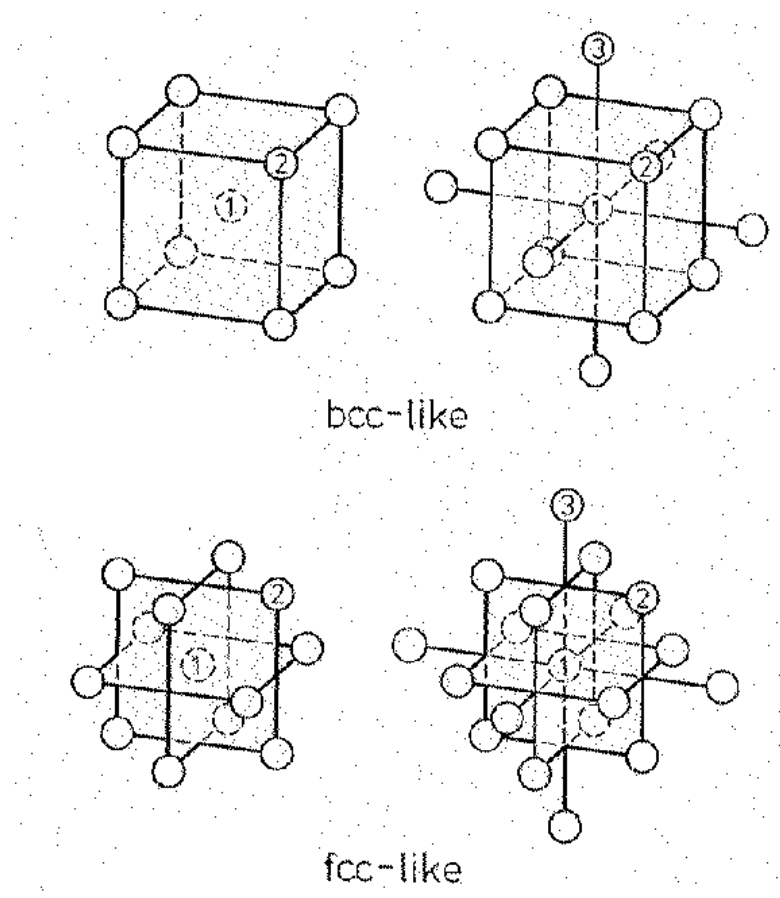


Figure 1: Illustration of b.c.c.– and f.c.c. like clusters. Different atomic shells surrounding the center 1 are labelled by 2, 3 etc.

In general the topology of the nanostructure affects strongly the electronic structure and the orientation of the magnetization, its domain structure, and magnetic relaxation. The electron energy spectrum gets discrete and quantum well states (QWS) occur in thin films.

Note, in nanostructured thin films magnetic domain structure is frequently present. The size of the domains and their relaxation depends on atomic structure of the film, anisotropy and temperature. The reversal of a domain magnetization may be relatively slow, but may speed up at nonequilibrium for example due to hot electrons.

In growing thin films interesting nonequilibrium behavior may result from the interdependence of atomic morphology of the nanostructure and its magnetic domain formation. This may be seen observing time resolved properties of growing nanostructures. Thus, it is of interest to study, time resolved, the occurrence of uniform ferromagnetism in thin films as a function of film thickness and domain density and size, in general on growth conditions for producing nanostructures.

For tunneling interplay of magnetism and superconductivity is of particular interest. Between two magnets one expects as a result of the spin continuity equation and Landau–Lifshitz equation Josephson like spin currents.

In the following magnetic nanostructures having different geometry and tunneling are discussed:

1.1 Magnetic Clusters

While small clusters may have a complicated atomic structure, this will tend to become bulk like for larger ones. Hence, approximately one may assume first liquid like structures as the number of atoms N in the cluster increases and then bulk like structures for larger clusters. The cluster volume V is given by $V \sim N^3$ and the surface area by $S \sim N^{2/3}$ [1].

In Fig.1 f.c.c.- and b.c.c. like cluster structures are shown. These may approximate magnetic transition metal clusters. In such clusters DOS and magnetic moments are site dependent.

In Fig.2 the discretization of the electron energy spectrum of such clusters is illustrated. Levels are occupied up to the Fermi–level ε_F and interesting odd, even effects occur as a function of cluster size (number N of atoms).

The magnetism of the cluster is characterized by its atomic shell (i) dependent magnetic moments $\mu_i(N)$, by the magnetization $M(T, N)$ and Curie–temperature $T_c(N)$. These magnetic properties may be calculated using an electronic theory and for example a tight–binding Hubbard like hamiltonian, or on a more phenomenological level a Heisenberg hamiltonian including magnetic anisotropy. Thus, one may estimate the Curie–temperature from

$$T_c \sim aJq_{eff}(N) \quad , \quad (1)$$

where a is a fitting parameter, J the interatomic exchange coupling integral and q_{eff} the effective coordination number [2].

In Fig.2 size effects for the electronic structure are sketched. Note, screening of Coulombic interactions and width of d–electron states varies with cluster size and affects thus magnetic activity. Also spacing of the n electronic states is

$$\delta \approx \varepsilon_F/n \approx (\hbar v_F/R)(k_F R)^{-2}(N(0)V)^{-1} \quad . \quad (2)$$

Here, ε_F is the Fermi energy and v_F and k_F the corresponding Fermi velocity and wave–vector. V refers to the volume and $N(0)$ to the density of states (D.O.S.) at ε_F . One expects for $T > \delta$ that the discretization plays no great role. However, discretization might affect

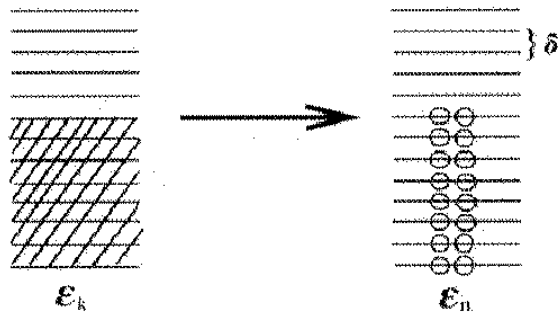


Figure 2: Sketch of size effects in small clusters having a diameter R and n electrons with energy ε_n . The spacing of the electronic energy levels is δ . ($\varepsilon_k \rightarrow$ discrete spectrum as particle size decreases). The electronic spectrum exhibits shell structure which reflects characteristically the atomic structure. Many properties should reflect this, in particular magnetism and superconductivity.

many properties in grains and quantum dots, in particular magnetism and superconductivity (formation of magnetic moments, magnetization, size of Cooper pairs, superfluid density etc.).

The local electron density of states of atom i is given by $N_i(\varepsilon, N)$ and generally spin dependent ($N_{i\sigma}(\varepsilon, N)$). This determines occurrence and size of local magnetic moments. Their direction is determined by magnetic anisotropy. Note, besides spin magnetism also orbital one occurs and is typically enhanced compared with bulk one. Also generally the orbital magnetism is dependent on atomic site.

Mie-scattering by spherical small particles is an interesting phenomena. One expects that magnetism leaves a characteristic fingerprint on the Mie-scattering profile. The magnetic field of the incident light couples to the cluster magnetization. This affects the Mie scattering in particular the backscattering intensity [4].

This effect of magnetism on Mie scattering needs be studied more. It offers an interesting alternative to deflection experiments by a magnetic field regarding study of small particle magnetism.

In Fig.3 an ensemble of clusters (or quantum dots) arranged on a lattice is shown. In general the lattice sites may be occupied by ferromagnetic (or paramagnetic) clusters or may be empty. Dependent on the cluster pattern one gets rich physical behavior. For example, while the single clusters are ferromagnetic, for larger spacing between the clusters one might get (for higher temperature) no global magnetization of the whole cluster ensemble. For dense spacings of the grains, dots and sufficient strong interaction amongst them, local and also global magnetization may occur as a function of temperature T . Note, typically $T_{ci}(N) > T_c$, where i refers to the cluster i and T_c to the Curie-temperature of the ensemble, cluster lattice. Of course, also antiferromagnetism may occur.

In general interesting phase diagrams are expected for an ensemble of magnetic grains (quantum dots). One gets for interactions $J > 0$ and $J < 0$ ferromagnetism or antiferromagnetism for the grain ensemble. For a mixture of grains, for example a mixture of superconducting and ferromagnetic ones, one may observe like for alloys interesting behavior and one may get Josephson currents between the dots and due to electronic charge transfers odd-even occupation effects, etc.

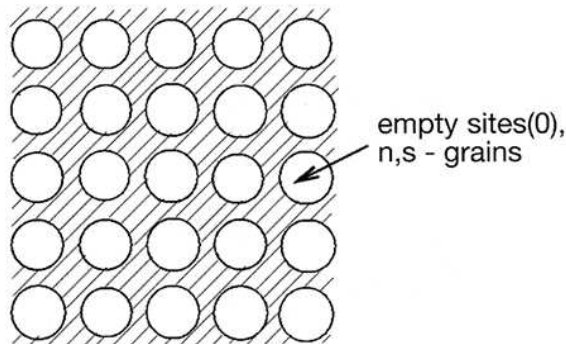


Figure 3: Illustration of an ensemble of small particles (grains) arranged in a lattice. The lattice sites may be empty or occupied by ferromagnetic, paramagnetic, or superconducting clusters, for example. Removing irregularly clusters from the lattice sites creates all sorts of nanostructures. Electrons move via hopping and tunneling between the lattice sites.

An interesting example of an important nanostructure is an ensemble of quantum dots, an anti-dot lattice for example. In Fig.4 an anti-dot lattice immersed in a medium is sketched. Here, the anti-dots repel electrons moving for example between the quantum dots. An external magnetic field B will change, deform the electron orbits spin-dependently and this may yield interesting behavior of the electronic properties of the system. Sensitive quantum mechanical interferences appear in such nanostructures. As indicated in Fig.4 a few electronic orbits may determine mostly the electronic structure, see theory by Stampfli *et al.* [5]. Quantum mechanical interference cause characteristic oscillations in the electronic density of states (DOS). These may be spin dependent.

In summary, these are some cluster like nanostructures. Regarding magnetism transition-metal and rare-earth atoms, metal-oxydes etc. are particularly interesting. The dependence of magnetic spin and orbital moments and spin correlations on particle size and temperature are of interest. Magnetic moments, Curie temperature and magnetization control the magnetic behavior [1, 2, 6, 7, 8, 9, 10].

1.2 Magnetic Films

For ultrathin films one may get magnetic behavior which could differ drastically from the one for thick ferromagnetic films. The latter are approaching as a function of film thickness d the bulk behavior (b), for the Curie-temperature one finds $T_c(d) \rightarrow T_{c,b}$ as film thickness d increases. The increase of $T_c(N)$ for increasing thickness of the ferromagnetic film is often described by the scaling law $\Delta T_c/T_{cb} \propto N^{-\lambda}$, or more empirically by $\Delta T_c/T_c(N) \propto N^{-\lambda'}$ with non-universal exponent λ' which fits better experiments, for details see Jensen *et al.* [2].

Note, in ultrathin films, one or two atomic layers thick, ferromagnetism results from magnetic anisotropy (spin-orbit coupling etc.) suppressing two-dimensional magnetic fluctuations.

Various film structures are shown in Fig.5. Neighboring magnetic films may order parallel or antiparallel. Approximately, first for ultrathin films $T_c(d) \sim d$ typically. As the thickness of the film increases the Curie-temperature approaches the bulk one. Generally one gets for multilayer structures a rich variety of magnetic phase diagrams. For example, the change of the magnetization upon increasing the Cu-spacer thickness of a $(\text{Co}/x\text{Cu}/\text{Ni})$ film system

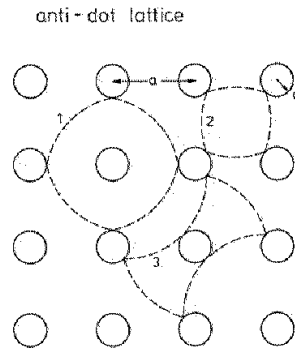


Figure 4: Magnetic field effects on polygonal electron paths in an anti-dot lattice. Here, a denotes the spacing of the anti-dots with radius d . The electrons move between the dots and are repelled by the anti-dot potential and thus selectively the polygonal paths 1, 2, 3 etc. yield the most important contribution to the spin dependent D.O.S., magnetoresistance, etc. Details of the theory determining the electronic structure of such mesoscopic systems are given by Stampfli *et al.*

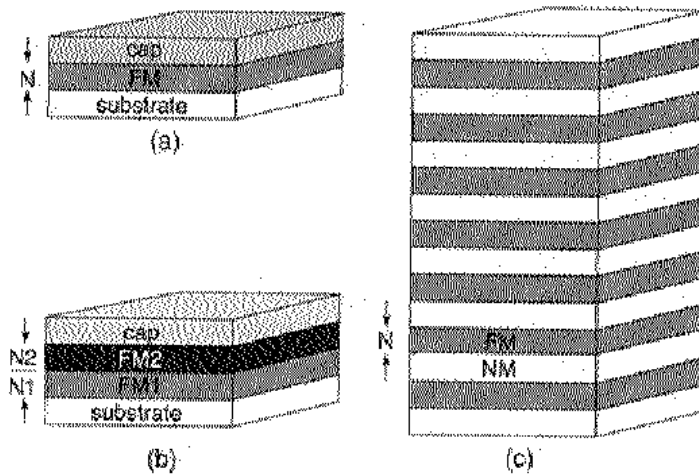


Figure 5: Thin magnetic film structures are shown. Typical configurations are given. (a) Thin ferromagnetic film of thickness N on a substrate, (b) two ferromagnetic films (FM1, FM2) on a substrate and (c) multilayer film structure. The ferromagnetic films are separated by a nonmagnetic one (NM). At the surface the magnetic film may be covered by nonmagnetic material (cap). Of particular importance is the interplay of magnetism of magnetic thin films of a film multilayer system.

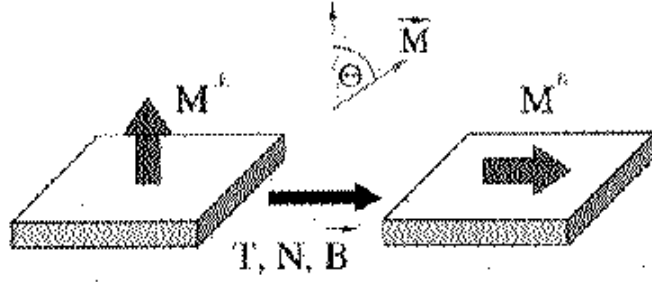


Figure 6: The reorientation transition $M_{\perp} \rightarrow M_{\parallel}$ of the magnetization at the surface or interface of films is shown. This transition may be induced by temperature T , increasing film thickness N and film morphology and external magnetic field B .

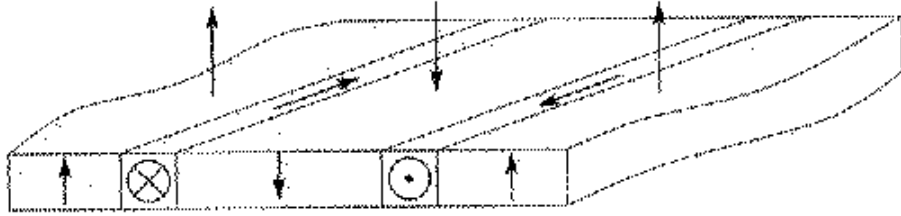


Figure 7: Illustration of a magnetic stripe domain phase of a thin film. Neighboring domains are antiferromagnetically oriented and separated by Bloch type domain walls. The magnetic structure is generally controlled by the film morphology and magnetic anisotropy. Of course, dependent on this other domain structures may result, see Jensen *et al.*.

reflects characteristically the coupling between the two ferromagnets Ni and Co. For a detailed discussion of theoretical and experimental results see Jensen *et al.* [2, 6, 7, 9, 10, 11].

Magnetic anisotropy controls the orientation of the magnetization, $\vec{M}(T, d, \dots)$, at the surface of the film. Dependent on temperature T , film thickness and structure and effective magnetic field \vec{B} the orientation of the surface magnetization \vec{M} may change from perpendicular M_{\perp} to parallel one M_{\parallel} , $M_{\perp} \rightarrow M_{\parallel}$. This reorientation transition, important for example for magnetic recording, is illustrated in Fig.6 [7].

Obviously, the orientation of the magnetization at surfaces is related to the magnetic domain structure occurring in thin films. This is also clear from the illustration of domain structure in Fig.7.

As expected on general physical grounds, dependent on film growth conditions one gets for thin film growth on a substrate a variety of nanostructures. This is illustrated in Fig.8. For a growing film the accompanied magnetism may not be at equilibrium, but changing as the film topology changes. One has a nonequilibrium situation and magnetic structure changes due to magnetic relaxation, of domains *etc.*. The latter may be relatively slow. Various pattern of magnetic domains occur in general. Then reversal of local domain magnetization occur on a ps (picosecond) to ns (nanosecond) time scale and change the global film magnetization as

function of time, see for example studies by Brinzanik, Jensen, Bennemann.

Similarly as in the case of cluster ensembles on a lattice the magnetic domains resulting in nanostructured films may be dense or separated by larger distances. Correspondingly the domains are dominantly coupled via exchange or dipolar interactions, for example. This then will be reflected in the global magnetization, size of magnetic domains and in particular magnetic relaxation during film growth.

In Fig.9 the growth of a thin film resulting from atom by atom deposition at the surface is shown. For simplicity fast diffusion of chemisorbed atoms is assumed. Growing of a film occurs, since deposited atoms prefer to sit next to already deposited atoms thus gaining optimally cohesion. As time progresses islands of deposited atoms coalesce and nanostructured film is formed. Of course, via diffusion of the deposited atoms the film structure depends somewhat on the film structure of the substrate. Thus, one may get island formation, striped structures and quasi uniform growth, see calculations by Jensen *et al.* It is remarkable that already simple growth models yield most of the observed structures during film growth.

Regarding magnetization this reflects the nanostructure and typically magnetic domains occur before global uniform film magnetization is present.

In thin films one expects quantum-well states (Q.W.S.) which will change characteristically with film thickness. Such states were calculated for example by Hübner, Luce *et al.* For details see Bennemann in Nonlinear Optics in Metals (Oxford University Press) [12]. The confinement in thin films causes the Q.W.S. In FM films these states are spin split reflecting characteristically magnetism. In Fig.10 QWS are sketched and their parity is indicated by (+) and (-).

Magneto-optics (S.H.G.: Second harmonic light generation) will reflect magnetism sensitively. Thus in particular for magnetic nano film structures with spin split Q.W.S. one will get interesting optical properties reflecting characteristically magnetism. This is illustrated in Fig.11. Optical interferences involving QWS cause oscillations in the MSHG as a function of film thickness.

This summarizes then interesting nanostructures consisting of films. Film multilayers offer particularly interesting magnetic pattern. Neighboring films interact largely via exchange coupling and this controls the magnetic behavior of each film and the global one. For example transport properties like the magnetoresistance depend on the relative orientation of the magnetization of neighboring films. During film growth magnetic relaxation controlled by anisotropy plays an important role. This is reflected in the nonequilibrium magnetization of the film and its relaxation towards the equilibrium one.

1.3 Tunnel Junctions

Tunnel junctions involving magnetism are interesting microstructures, in particular regarding quantum mechanical behavior, switching devices and charge- and spin currents and their interdependence. Coupling of the magnetic order parameter phases, for both ferromagnets and antiferromagnets, on both sides of the tunnel medium yields Josephson like (spin) currents, driven by the phase difference, for details see study by Nogueira *et al.* and others. Obviously, this will depend on the magnetic state of the medium through which tunnelling occurs, on spin relaxation. The effective spin coupling between N_1 and N_3 depends on the spin susceptibility of N_2 and $J_{eff} = J_{eff}(\chi)$. Note, from the continuity equation follows

$$\vec{j}_T \propto J_{eff} \vec{S}_1 \times \vec{S}_3 + \dots \quad (3)$$

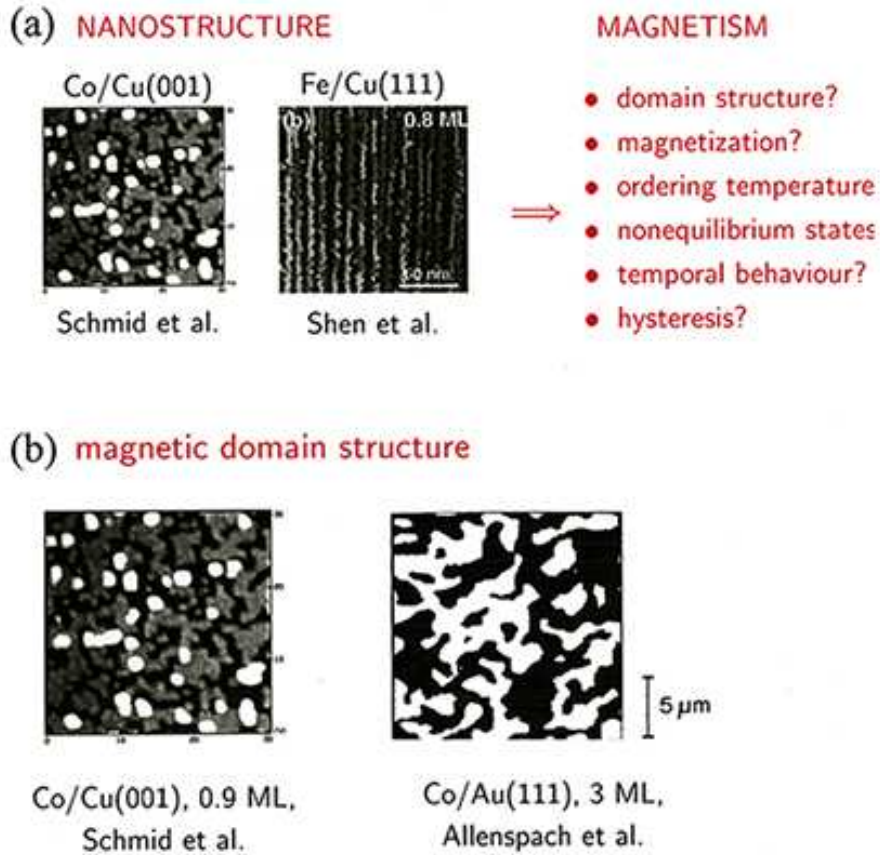


Figure 8: Nanostructures of ultrathin films and accompanying magnetic domain structures. The upper Fig.(a) shows various observed atomic nanostructures. Questions are listed regarding dependence of the resulting magnetic structures on film topology. Co/Cu(001) refers to 0.9ML of Co (black:substrate, grey:first layer, white:2.adatom layer), Fe/Cu(111)to 0.8ML of Fe (grey: chains of Fe atoms which will coalesce for increasing Fe coverage). Fig.(b) The obtained magnetic domain structures are given. Only domain structure at surface is shown. Magnetic domains for Co/Cu (white: 2. layer, grey: 1. layer). The irregularly shaped domains (white) for Co/Au have a perpendicular magnetization and lateral size of about 1 μ m. Note, such structures are observed in various experiments. Typically magnetic domain size increases with increasing film thickness. Increasing for Co/Au the Co film thickness to 6ML turns their magnetization to in-plane (reorientation transition).

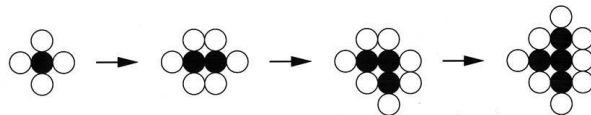


Figure 9: Illustration of simple (Eden type) growth of a thin film (for a square lattice). One assumes fast surface diffusion and uses a Monte Carlo simulation of molecular beam epitaxial (MBE) film growth. Surface atomic sites are indicated. Successively deposited atoms are given in black and due to cohesive energy prefer to cluster.

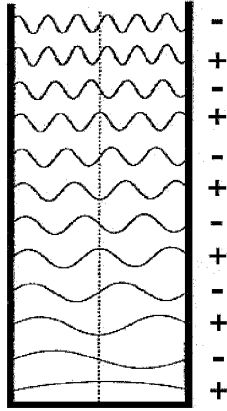


Figure 10: Sketch of electronic Q.W.S. in a thin film and resulting from the confinement of the electrons. Such QWS occur for example in a Co/xML Cu/Co film system. Describing the film confinement by a square well potential one gets already quite properly such QWS and which parity is indicated by (+) and (-). Note, parity changes for increasing quantum number.

The tunneling is sketched in Fig. 12.

Clearly tunnelling allows to study magnetic effects, ferromagnetic versus antiferromagnetic configurations of the tunnel system ($\uparrow| T |\uparrow$), or ($\uparrow| T |\downarrow$) and interplay of magnetism and superconductivity ($T \equiv S.C.$), as for example for junctions (FM/SC/FM) or (SC/FM/SC). Such junctions may serve as detectors for triplet superconductivity (TSC) or ferromagnetism (FM), antiferromagnetism (AF). Of course tunnelling is different for parallel or antiparallel magnetization of M_1 and M_3 . Also importantly, tunnel junctions may serve to study Onsager theory on a molecular-atomistic scale.

Electron and Cooper pair transfer between two quantum dots exhibits interesting behavior, for example v.Stückelberg oscillations due to bouncing back and forth of electrons if an energy barrier is present. Then assistance of photons is needed to overcome the energy barrier. The current (spin-, charge current) may depend on the pulse shape and duration, see Garcia, Grigorenko *et al.*

Summary: For illustrating reasons various interesting nanostructures like clusters, films and tunnel junctions with important magnetic effects are discussed. In the next chapter some theoretical methods useful for calculations are presented. Then results obtained this way are given.

It is important to note that for illustrational purposes the physics has been simplified. Mostly, the analysis can be improved straightforwardly. However, likely this will not change the physical insights obtained from the simplified analysis. For more details see for clusters studies by Pastor *et al.* [1, 6] and by Stampfli *et al.* [5], and for films research by Jensen *et al.* [2, 7, 8], and for tunnel junctions studies by Nogueira, Morr *et al.* [3].

2 Theory

In general theory for nanostructures must allow for a local, atomic like analysis of the electronic structure. Using Hubbard hamiltonian and tight-binding type theory one may determine (a) $N_{i\sigma}(\epsilon, \dots)$, the electron density of states at an atomic site i and for spin σ , dependent on

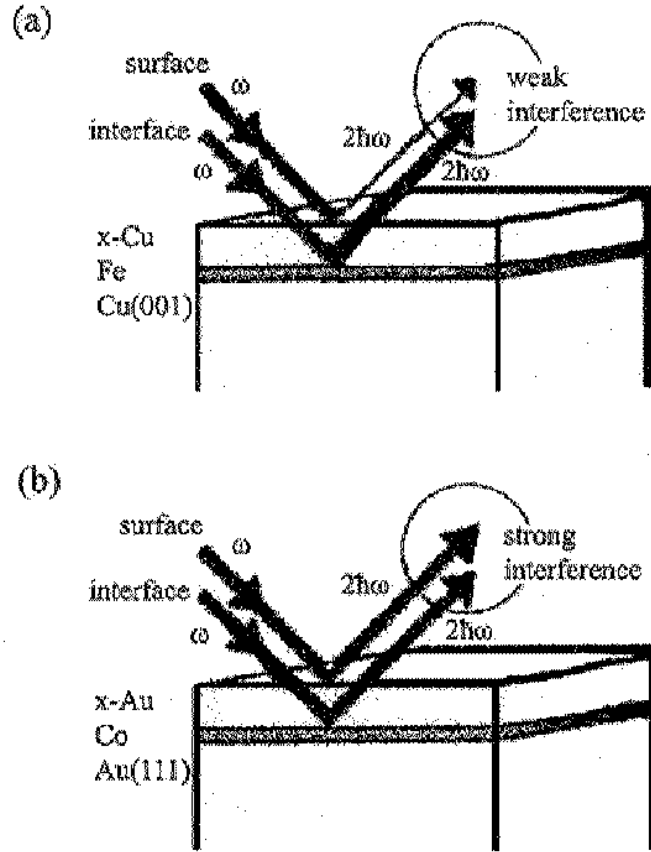


Figure 11: Illustration of magnetic S.H.G.(MSHG) resulting for thin films with Q.W.S.. Note, in magnetic films the Q.W.S. are spin polarized and their energies depend on film thickness. Thus, SHG involving QWS exhibits film thickness dependent effects. Oscillations in the magneto-optical signals occur. The interference of S.H.G. from the surface and the interface (film/substrate) yields a sensitive detection of magnetism. Characteristic differences occur for (a) weak interference and (b) strong interference. This is observed for example for $x\text{Cu}/\text{Fe}/\text{Cu}$ (weak interference) and $x\text{Au}/\text{Co}/\text{Au}$ structures (strong interference), respectively. Here, x refers to the number of layers of the top film.

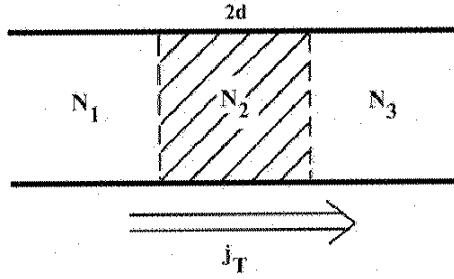


Figure 12: A tunnel junction ($N_1 | N_2 | N_3$), where N_i refers to the state, magnetic, superconducting, normal. The current j_T may refer to spin- or charge transport and may be driven by the phase difference $\Delta\varphi = \varphi_3 - \varphi_1$, for example. Both spin and charge current may couple in general. The continuity equation for the magnetization, $(\partial_t M_i + \partial_\mu j_{i\mu,s} = 0)$, indicates that magnetic dynamics $M(t)$ may induce spin currents j_s . As a consequence interesting nonequilibrium behavior is expected. Note, applying a voltage V to the sketched tunnel system may yield a two-level system (resembling a qubit, etc.)

the local atomic configuration surrounding atom i ,

(b) μ , the atomic like magnetic moment, as a function of particle size (cluster size or film thickness),

(c) M , the magnetization and the Curie-temperature (T_c).

Note, all properties result from the electronic Green's function $G_{i\sigma}(\epsilon, \dots)$. Including spin-orbit coupling (V_{so}) yields magnetic anisotropy. Thus, also

(d) orbital magnetism

is obtained. Note, anisotropy and orbital magnetism get typically for nanostructures more important.

Alternatively to an electronic theory one may use on a more phenomenological level the Heisenberg hamiltonian including magnetic anisotropy to analyze magnetism in nanostructures.

2.1 Magnetism : Electronic theory

To determine the size and structural dependence of the magnetic properties of small transition metal clusters the Hubbard hamiltonian for d -electrons which are expected to contribute dominantly is used (see Pastor *et al.* [1, 6] and Moran-Lopez *et al.* [10])

$$H = \sum_{i=j} t_{ij} c_{i\sigma}^+ c_{i\sigma} + H' \quad , \quad (4)$$

$$H' = \sum_i \epsilon_{i\sigma} n_{i\sigma} - E_{dc} \quad , \quad (5)$$

and effective on-site electron energies

$$\epsilon_{i\sigma} = \epsilon^0 + U\Delta n_i - \sigma \frac{J}{2} \mu_i \quad . \quad (6)$$

Here, $c_{i\sigma}^+$ and $c_{i\sigma}$ are the usual creation and annihilation operator for electrons on site i and with spin σ and t_{ij} denotes the distance dependent hopping integral. Note, i, j refer to atomic sites and includes orbital character ($d_i : e_g, t_{2g}$ orbitals, s, p -orbitals). H' describes interactions (in

the unrestricted Hartree–Fock approximation). The effective intraatomic Coulomb interaction are denoted by U and the exchange interaction by J ($J = U_{\uparrow\downarrow} - U_{\uparrow\uparrow}$, $U = (U_{\uparrow\downarrow} + U_{\uparrow\uparrow})/2$). Here, $U_{\sigma\sigma'}$, refers to electron spins σ, σ' . $E_{dc} = (1/2) \sum_{i,\sigma} (\epsilon_{i\sigma} - \epsilon^0) \langle n_{i\sigma} \rangle$ corrects for double counting as usual. The charge transfer Δn_i is given by $\Delta n_i = n_i - n^0$, $n^0 = (1/n) \sum_i n_i$.

The quasi local magnetic moment at site i is given by

$$\mu_i \propto \langle n_{i\uparrow} - n_{i\downarrow} \rangle \quad , \quad (7)$$

with $\langle n_{i\sigma} \rangle = \int_{-\infty}^{\epsilon_F} d\epsilon N_{i\sigma}(\epsilon - \epsilon_{i\sigma})_t$. Here, $N_{i\sigma}(\epsilon)$ is the density of states (DOS) at site i for electrons with spin σ (and at time t).

This theory applies also to thin films. Then, i may refer to film layer and one should keep μ_i and $p_i^{+,-}$.

To calculate the magnetization $M(T)$ one must take into account the orientation of the magnetic moments. Assuming a preferred magnetization axis one gets (Ising model, see Moran-Lopez *et al.*, Liu) [10]

$$M(T) \simeq \sum_i \{p_i^+ \mu_i^+(T) + p_i^- \mu_i^-(T)\} / \mu^+(0) \quad . \quad (8)$$

The probabilities $p_i^{+,-}$ refer to finding moments $\mu_i^{+,-}$ pointing parallel or antiparallel to the preferred magnetization axis. For simplicity one may use the approximation $p_i^{+,-} = p^{+,-}$. Assuming spherical like clusters, then i refers to the atomic shell of the cluster and $\mu_i^{+,-}$ to the magnetic moment within shell i pointing in the direction of the magnetization (+) and in opposite direction (−), respectively.

Then one determines the order parameter ($\propto M$)

$$\mu_i = p_i^+ - p_i^- \simeq p^+ - p^- \quad (9)$$

($\mu_i \approx \mu$) from minimizing the free–energy

$$F = \Delta E - TS \quad . \quad (10)$$

Here, the entropy S is given by

$$S \simeq -kN \{p^+ \ln p^+ + p^- \ln p^-\} \quad , \quad (11)$$

and $\Delta E = E(\mu) - E(0)$. The electronic energy is calculated using a hamiltonian H , for example Eq.(4). For calculating the Green's functions the electronic energies are determined from

$$\epsilon_{i\sigma}^{+,-} \simeq \epsilon_{i\sigma}^0 - \sigma J \sum_j \mu_i^{+,-} \mu_j^{+,-} \quad . \quad (12)$$

Note, $\epsilon_{i\sigma}^+ \simeq \epsilon_{i\sigma}^0 - \sigma \mu_i^+ J \sum_j \{p^+ \mu_j^+ + p^- \mu_j^-\}$. The Curie–temperature is given by $M(T_c) = 0$.

A similar analysis can be performed using functional–integral theory as developed by Hubbard *et al.*, see Pastor *et al.* [6].

Note, as already mentioned this theory can also be used for films. Then i may refer to the film layer, etc..

The magnetization can also be determined using the Bragg–Williams approximation. Assuming for simplicity Ising type spins one finds for the magnetization (see Jensen, Dreyssé *et al.*)

$$M_i(T) = \tanh\{\beta J \mu_i (z_0 M_i \mu_i + z_1 M_{i+1} \mu_{i+1} + z_{-1} M_{i-1} \mu_{i-1}) - \Delta h_i\} \quad . \quad (13)$$

Here, $\beta = 1/kT$, z_0, z_1, z_{-1} are nearest neighbor coordination numbers and Δh_i denotes the Onsager reaction field. Referring to cluster shells (film layer) z_0 gives the neighboring atoms of i within shell (layer) i and z_{-1} and z_1 the nearest neighbor atoms in the shell (layer) below and above, respectively. It is

$$\Delta h_i = (\beta J \mu_i)^2 M_i \{ z_0 \mu_i^2 (1 - M_i^2) + z_1 \mu_{i+1}^2 (1 - M_{i+1}^2) + z_{-1} \mu_{i-1}^2 (1 - M_{i-1}^2) \} \quad (14)$$

Applying these expressions to films one has $z_1 = 0$ (and $\mu_1 = 0$) if i refers to the surface plane and $z_{-1} = 0, \mu_{-1} = 0$ if i refers to the film layer on a nonmagnetic substrate.

Note, for $T \leq T_c$ the Eq.(13) can be linearized yielding a (tridiagonal) matrix equation which largest eigenvalue gives $T_c(d)$. For the hamiltonian H one may use the Heisenberg one, for example.

Orbital magnetism, anisotropy: Adding spin-orbit interaction V_{so} to Eq.(4), $H \rightarrow H + V_{so}$, and using

$$V_{so} = -v \sum_{\alpha, \beta} (\vec{L}_i \cdot \vec{S}_i)_{\alpha, \beta} c_{\alpha}^{\dagger} c_{\beta} \quad , \quad (15)$$

one may also determine magnetic anisotropy and also orbital magnetic moments ($\langle L_i \rangle$). $(\vec{L}_i \cdot \vec{S}_i)_{\alpha, \beta}$ refers to intra-atomic matrix elements between orbitals α, β . Of course, the orbital moment \vec{L}_i depends on cluster atom i and on orientation δ of \vec{S} with respect to structural axis: $\vec{L}_i \rightarrow L_{i, \delta}$ (see Pastor *et al.* [6]). In case of films i refers to the film layer.

Note, in clusters and thin films and at surfaces the spin-orbit coupling and orbital magnetism is typically enhanced. Orbital magnetism may play an interesting role for nanostructures.

2.2 Magnetism : Heisenberg type theory

One may also calculate the magnetism in nanostructures by using the Heisenberg type hamiltonian, including magnetic anisotropy (see Jensen *et al.* [2, 7, 8, 9, 11]). As known magnetic anisotropy controls the magnetic structure like direction of the magnetization, domains, their size, shape, in thin films and at interfaces in particular. Then one determines the magnetic structure resulting from the quasi local magnetic moments (\vec{S}_i) using the hamiltonian

$$H = -\frac{1}{2} J \sum_{i,j} \vec{S}_i \cdot \vec{S}_j + \frac{1}{2} A \sum_{i,j} \left(\frac{\vec{S}_i \cdot \vec{S}_j}{r_{ij}^3} - 3 \frac{(\vec{S}_i \cdot \vec{r}_{ij})(\vec{S}_j \cdot \vec{r}_{ij})}{r_{ij}^5} \right) + H_{anis.} \quad , \quad (16)$$

with exchange anisotropy hamiltonian

$$H_{anis.} = -\frac{1}{4} K \sum_{i,j} S_i^z S_j^z - \frac{1}{4} D \sum_{i,j} (S_i^x S_j^x + S_i^y S_j^y) \quad . \quad (17)$$

Here, K and D are uniaxial and quartic in-plane (exchange) anisotropy constants, respectively. Note, in H the first term is the Heisenberg exchange interaction and the second term refers to the magnetic dipole interaction, and $A = \mu_0 (g \mu_B)^2 / a_0^3$. \vec{S}_i denotes Heisenberg spins (for Ising model spin $\frac{1}{2}$) at site i . The second term in Eq.(16), which results as interaction amongst magnetic moments in classical electrodynamics, reduces in particular at surfaces the magnetization normal to the surface. it gives the demagnetization field and is called the shape

anisotropy. Although this long-range magnetic dipole coupling is usually much smaller than the exchange one, it is on a mesoscopic length scale typically very important and determines the magnetic domain structure.

Of course, the parameters, in particular K and D may depend on i, j (shell, film layer). Typically anisotropy is larger at surfaces, interfaces. The interplay of K and D , which may depend on film thickness and temperature ($K \rightarrow K_i$, where i refers to film layer), determines the normal and in-plane magnetization at surfaces and the reorientation transition (see Jensen *et al.*). Note, one has also higher order anisotropy constants like K_4 due to noncollinearity of the spins (approximately $K_4 \propto J^{-1}$), see Jensen *et al.*, which may play a role. It is also important to note that exchange and dipolar coupling have a different distance dependence. The parameters in particular the anisotropy ones depend in general on temperature. Of course, temperature induces changes of the atomic structure and this plays a role for thin films and for films during growth on a substrate.

Applying standard methods of statistical mechanism one gets the free-energy F , the magnetization and phase-diagrams in terms of J and the anisotropy forces for clusters and thin films and also for nanostructured films with magnetic domain structure. For a more detailed analysis see in particular P. Jensen *et al.*. The magnetic phase diagram (P.D.) follows from minimizing the free-energy.

From Eq.(16) follows the magnetic reorientation transition, for example as driven by temperature:

$$M_{\perp} \rightarrow_{T_R} M_{\parallel} \quad (18)$$

occurring at temperature T_R . Note, the temperature dependence of the effective anisotropy parameters and of the dipole coupling is mainly determined by the magnetization. Minimizing the free-energy (anisotropy contribution to free-energy) gives the transition $M_{\perp} \rightarrow M_{\parallel}$ at temperature T_R , see Jensen *et al.* [7].

Note, the control parameters in Eq.(16) depend on atomic structure, morphology of the nananostructures, film thickness for example. Thus, T_R is affected.

The above Hubbard-tight-binding type electronic theory and the Heisenberg type phenomenological theory including magnetic anisotropy permit a calculation of the magnetic properties of nanostructures. A basic understanding of the dependence of magnetism in nanostructures on atomic configuration and on more global morphology is obtained.

Note, for alloys one may extend above theories using appropriate versions of C.P.A. like analysis (C.P.A: coherent potential approximation).

2.3 Electronic Structure of Mesoscopic Systems : Balian-Bloch type theory

The important electronic structure (shell structure) of mesoscopic systems like spherical clusters, discs, rings, (quantum) dots can be determined using a relatively simple theory developed by Stampfli *et al.* extending original work by Balian-Bloch (Gutzwiller) [5]. One assumes a square well like generally spin dependent potential (U_{σ}). The dominant contribution to the electronic structure (near the Fermi-energy and for electronic wavevector k_F^{-1} larger than atomic distance) results from (interfering) closed electronic orbital paths. Then the key quantity of the electronic structure of a quantum dot system, the density of states (DOS), can be calculated from (n =number of atoms in nanostructure) from the Green's function G . The Green's function $G(\vec{r}, \vec{r}')$ is derived by using multiple scattering theory, see Stampfli *et al.*. Interference

of different electron paths yields oscillations in the DOS *et al.*. This leaves a fingerprint on many properties.

Thus, for example, oscillations in the electronic structure of mesoscopic systems, in the magnetoresistance and other properties of quantum-dot systems can be calculated.

From the electronic Green's function G one determines the (generally spin dependent) density of states (DOS)

$$N_\sigma(E, n) = \frac{1}{2\pi i} \int_V d^d r \{G_\sigma(\vec{r}, \vec{r}, E + i\epsilon) - G_\sigma(\vec{r}, \vec{r}, E - i\epsilon)\}_{\vec{r}=\vec{r}} \quad . \quad (19)$$

One gets (\bar{N} = average DOS)

$$N_\sigma(E, n) = \bar{N}_\sigma(E, n) + \Delta N_\sigma(E, n) \quad , \quad (20)$$

where ΔN_σ refers to the oscillating part of the DOS due to interference of dominating closed electron paths in clusters, thin films, and ensemble of repelling anti-dots, see the theory by Stampfli *et al.*. Clearly the scattering can be spin-dependent (due to a potential U_σ) and can be manipulated by external magnetic fields B (s. cyclotron paths, Lorentz-force etc.) [5].

Under certain conditions regarding the potential felt by the electrons in the nanostructures (square-well like potentials etc., and states with $k^{-1} > a$, interatomic distance) one gets the result (see Stampfli *et al.* using extensions of the Balian-Bloch type theory)

$$\Delta N_\sigma(E, n) \simeq \sum_l A_{l\sigma}(E, n) \cos(kL_l + \phi_{l\sigma}) \quad . \quad (21)$$

Here, l refers to closed orbits (polygons) of length L , $k = \sqrt{|E| + i\delta}$, and $\phi_{l\sigma}$ denotes the phase shift characterizing the scattering potential and the geometry of the system. An external magnetic field affects $\Delta N_\sigma(E, n)$ via path deformation and phase shifts resulting from magnetic flux (see Aharonov-Bohm effect).

Clearly, the DOS in particular $\Delta N_\sigma(E, n)$ will be affected characteristically by the magnetism in various nanostructures, in quantum dot systems. For details of the Balian-Bloch like analysis see the theory by Stampfli *et al.* [5].

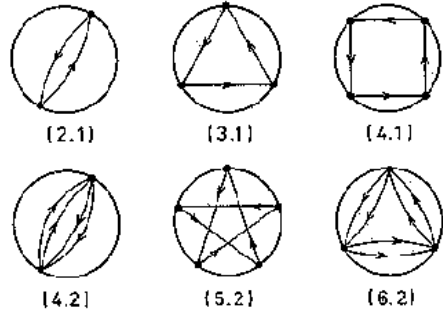
Note, the electronic structure due to the interferences of the dominant electronic states near the Fermi-energy described approximately by Eq.(21) results in addition to the one due to the atomic symmetry of the nanostructure (spherical one for clusters, 2d-symmetry for thin films, etc.). Thus, for example, one may find for magnetic clusters a phase diagram temperature vs. cluster size which dependent on magnetization exhibits phases where atomic (shell) structure and then spin dependent electronic structure dominates. Of course, for sufficiently large clusters these structures disappear.

The interference of closed electron orbits in magnetic mesoscopic systems like spherical clusters, discs, rings, thin films and quantum dot lattices causes spin dependently characteristic structure, oscillations in the DOS $N(E, n)$ (yielding corresponding ones for example in the cohesive energy, occupation of d, s electron states, Slater-Pauling curve for magnetism, magnetoresistance, etc.).

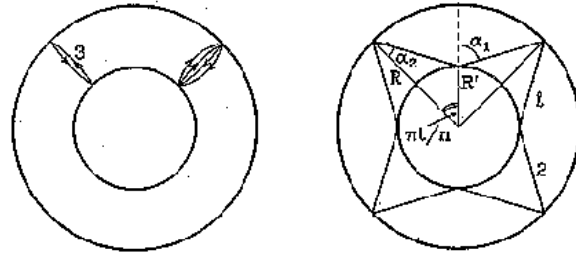
(a) Spherical Clusters: The properties of small spherical clusters follow from the DOS given approximately by

$$\Delta N_\sigma = \Delta N_o + \sum_{t=1}^{\infty} \sum_{p=2t+1}^{\infty} A_{t,p,\sigma} \sin \phi_{t,p,\sigma}, \quad (22)$$

(a) spheres, discs



(b) rings



(c) discs: $B \neq 0$

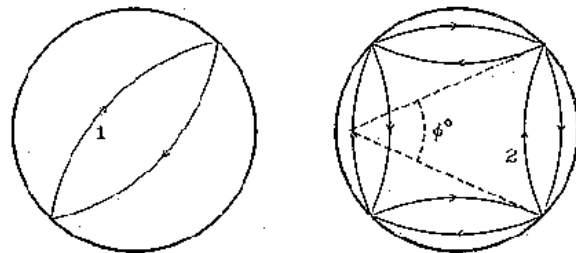


Figure 13: Examples of dominating electron paths characterized by (p,t) in (a) spheres, discs and (b) rings. Note, p and t refer to the number of corners and t to the one of circulations around the center, respectively, of the polygonal paths. In (c) the effect of an external magnetic field B is shown. Note, in particular for rings magnetic flux quantization may occur. Also the phase shift due to the Aharonov–Bohm effect may induce currents. For ferromagnets these are spin polarized.

where the orbits are characterized by the number of corners p and t describes how many times the center of the sphere is circled. Here, ΔN_o results for $p = 2t$ and turns out to be unimportant. For a detailed derivation of the amplitudes $A_{t,p,\sigma}$ and phases $\phi_{t,p,\sigma}$ see analysis by Stampfli *et al.* [5]. One gets

$$A_{t,p\sigma} = 2R^2 a_{t,p\sigma} \sqrt{\sin^3(\pi t/p)/p} \exp -(2pk_2 R \sin(\pi t/p)), \quad (23)$$

with $a_{t,p} = \sqrt{k_1 R/\pi} (-1)^t \cos(\pi t/p)$. Note, the amplitudes decrease rapidly for increasing number p of corners. The most important contributions to the DOS result from triangular, square and lower polygon orbits. The structure in the DOS affects many properties (conductivity, magnetoresistance, spin susceptibility χ , spin dependent ionization potential, etc.).

(b) Circular Rings: Circular rings with outer radius R_a and inner radius R_i are particularly interesting, since R_i/R_a controls which orbits are most important. For example, one may eliminate DOS contributions due to triangular orbits. One gets, see Fig.13 for illustration,

$$\Delta N = \Delta N_1 + \Delta N_2 + \Delta N_3, \quad (24)$$

where ΔN_1 results for orbits inside the ring (with $\pi t/p < \arccos(R_i/R_a)$) and which are also present for discs, ΔN_2 due to orbits scattered by the outer and inner surface of the ring and which circle around the center, and ΔN_3 results from ping-pong like orbits between R_a and R_i . In all cases one gets rapid oscillations (due to exponentials) and slower ones due to cos and sin functions.

Note, results for thin films follow for $R_a, R_i \rightarrow \infty$.

(c) Quantum Dots: The DOS of quantum dots is calculated similarly. Thus, one gets for example oscillations in the magnetoresistance r_σ , since $r_\sigma \propto N_\sigma^2(E, n)$.

Molecular fields and external magnetic field B will affect the electronic orbits, see Fig.13 for illustration. For discs, rings and quantum dots one gets phase shifts $\Delta\phi$ due to path deformation and the flux through the polygons. Note, the Lorentz force deforms the orbits. Also the magnetic flux due to a vector potential \vec{A} perpendicular to the discs plane for example gives a phase shift

$$\Delta\phi' = \oint \vec{A} \cdot d\vec{r} = \vec{B} \cdot \vec{S}, \quad (25)$$

where S is the area enclosed by the orbit. Note, structure in DOS due to Landau-levels may be included already in $N(E, n)$.

(d) Circular disc and quantum dots: For circular discs and quantum dots one gets (for square well like potentials) in Eq.(22) that $\Delta N_0 \approx 0$ and for the second term that mainly orbits with $p=2,3$ are important, since $A_{t,p,\sigma} \sim 1/p^{1/2}$. Note, now $a_{t,p\sigma} = (\alpha_{t,p\sigma}/2) \sqrt{1/(\pi k_1 R p)}$ and

$$A_{t,p} = \alpha_{t,p} R^2 [(1/\pi k_1 R p) \sin^3(\pi t/p)]^{1/2} \exp -[2pk_2 R \sin(\pi t/p)], \quad (26)$$

with $\alpha_{t,p} = 2$ for $p \neq 2t$ and $\alpha_{t,p} = 1$ for $p=2t$ and phases $\Phi_{t,p} = p[2k_1 R \sin(\pi t/p) - \pi/2 + \delta_{t,p}] + 3\pi/4$ as for spheres. Phases $\delta_{t,p}$ result from (possibly spin dependent) potential scattering at the surface of the system, see books on quantum mechanics [5], note $\delta_{t,p\sigma} = -\pi$ for $U \rightarrow \infty$. The phase shift δ affects level spacing (and vice versa) and appearance of electronic shell structure.

Magnetic field B : The magnetic field is taken to be perpendicular to the disc plane. Then one gets a change of the phase by

$$\Delta\Phi = \Delta\Phi_1 + \Delta\Phi_2, \quad (27)$$

where $\Delta\Phi_1 = pkR_c\Phi_c^0$, $\Phi_c^0 = 2\arcsin(R\sin(\Phi^0)/R_c)$, cyclotron orbit $R_c = k/B$ ($R_c \gg R$), is due to path deformation and $\Delta\Phi_2 = \Delta\Phi'$, see previous Eq., due to the enclosed flux (Aharonov–Bohm). The angle Φ_c^0 refers to the center of the cyclotron orbit, see Fig.13. Straightforward analysis gives

$$\Delta\Phi' = \pm BS_{\pm} \quad , \quad (28)$$

with

$$S_{+,-} = S_0 \pm \Delta \quad , \quad \Delta = (p/2)R_c^2(\phi_c^0 - \sin\phi_c^0) \quad . \quad (29)$$

Here, $2\phi^0 = (2\pi/p)t$, ϕ_c^0 is the angle seen from the center of the disc, see Fig., and for the cyclotron orbit one assumes $R \gg R_c$. \pm refers to clockwise and counterclockwise motion around the center of the orbit. Δ denotes the area resulting from path deformation due to field B. It is then

$$\Delta N_{\sigma}(E, B) \propto \sum_{t,p} A_{t,p\sigma} \cos(SB)(\dots) = \sum_{t,p} A_{t,p\sigma} \cos(S_0B) \sin\Phi_{t,p} \exp(-(pk_2(k_1/B)\Phi_c^0), \quad (30)$$

where $\Phi_{t,p}$ denote phase changes due to path deformation, see previous expression. Factor $\cos(S_0B)$ describes Aharonov–Bohm effect plus interference effects and gives oscillations periodic in B. Note, $\cos BS$ causes oscillations which are periodic in B, and oscillations change with (a-d). For large field B, $2R_c \leq (a-d)$, see Fig.4, path 1 and 3 disappears and only 2 remains (see Landau level oscillations with periodicity $(1/B)$, since $S \propto (1/B^2)$). $\Delta N \propto \cos(SB)$, $\phi_2 \propto SB$. The DOS oscillations are $\Delta N \propto \cos(SB)$, ($\Phi_2 \propto (SB)$).

The ratio (d/a) characterizes strength of antidot potential scattering. Of course, the oscillations in the DOS cause similar ones in the magnetoresistance, for example.

Antidot lattice: One assumes a 2d-lattice of antidots scattering via a repulsive potential the electrons. The lattice of antidots is illustrated in Fig.4 and Fig.14. Note, orbits 1, 2, 3 are most important. The scattering by the antidot lattice causes phase shifts $\Phi_{t,p\sigma}$. Note, the area S enclosed by the orbits 1, 2 and 3 is nearly independent of magnetic field B, such orbits occur for $2R_c > (a-d)$ and $R_c \propto 1/B$. One assumes that orbits are dephasing for distances much larger than lattice distance a. The oscillations in the DOS are given by (performing calculations similarly as for disc, see similar paths in Fig.13 and Fig.14)

$$\begin{aligned} \Delta N_{\sigma}(E, B) &= (\sqrt{2}(a-d)/k_1\pi) \sum_{t=1}^{\infty} (\sinh\varphi/\sinh(4t+1))\varphi^{1/2} \cos(BS) \sin\phi_{t,p} \\ &\times \exp(-4tk_2(k_1/B))\varphi_1 + \Delta N_r(E, B), \end{aligned} \quad (31)$$

with phases $\phi_{t,p} = 4t[k_1(k_1/B)\varphi_1 + B/2(k_1/B)^2(\varphi_1 - \sin\varphi_1) + \delta_{t,4t}] + \pi/2$, $\cosh\varphi = 2a/d - 1$, $\varphi_1 = 2\arcsin[(a-d)/(k_1/B)/\sqrt{2}]$, $S = 2t(a-d)^2$, etc., see Stampfli *et al.* [5]. The first term is due to path 1 and $\Delta N_r(E, B)$ due to path 2, 3 etc..

Note, Eq.32 takes into account that path reflections result from small antidots (rather than from spherical surfaces of discs with varying curvature). The oscillations of ΔN_{σ} periodic in B result for orbits 1, 2, 3, 4 and change with (a-d). For very small field B, note $R_c \propto (1/B)$, orbits become unstable and the large orbits get irregular due to dephasing. For increasing magnetic field B such that $2R_c \leq (a-d)$ first orbit 3 and then 1 disappears and only 2 survives. This orbit causes then for increasing field B Landau level oscillations with period $(1/B)$, since $S \propto R_c^2 \propto (1/B)^2$, flux $\sim SB$ and $\Delta N \propto \cos(SB)$. The oscillation periods are expected to decrease for decreasing lattice constant a and increasing magnetic field B. [5]

The oscillations in DOS $\Delta N_{\sigma}(E, B)$ affect many properties, in particular the magnetoresistance. A crossover from periodicity proportional in B to one in $(1/B)$ should occur for example for discs.

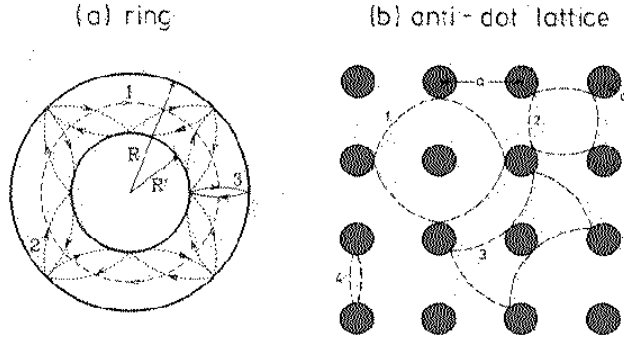


Figure 14: Effect of a magnetic field on various closed electron orbits, paths: (a) for a ring, (b) for a lattice of anti-dots, which scatter the electrons by a repulsive potential. Note, in particular for a narrow ring path 1 may dominate and magnetic flux quantization occurs. If the mean free path of the electrons is relatively large, as compared to the circumference of the ring, a magnetic field may induce a current driven by the phase shift due to the Aharonov–Bohm effect. On general grounds this current is expected to be spin polarized for ferromagnets and to decrease proportional to R^{-2} and for increasing temperature.

The theory by Stampfli *et al.* can be used also for a system of quantum dots on a lattice, including then hopping between the dots. Furthermore, an ensemble of magnetic and superconducting quantum dots may exhibit interesting behavior regarding (quantisation effects) magnetic flux etc..

Note, in general for lower dimensions ($3 \rightarrow 2$) degrees of freedom are reduced and one expects stronger oscillations of the DOS, for example in a magnetic field. The interference of the orbits yields generally rapid and slow oscillations. The spin dependence is calculated from the spin dependent scattering potential U_σ at the surfaces of the system.

Note, a ring may be viewed as an antidot enclosed by the metallic ring. The electrons are repelled by a strong repulsive potential from the inner core of the ring. If a magnetic field B is present, due to the flux quantization the electronic DOS reflects this and has fine structure as a result of the flux quantum $\phi_0 = 2\pi\hbar c/e$. Also a beating pattern of the oscillations may reflect interference of several paths dominating the electronic structure, see Figs.. These oscillations are also present in the electronic energy $E = \int d\varepsilon \varepsilon N(\varepsilon) + \dots$. As also discussed later the Aharonov–Bohm effect may induce a current in rings and discs etc. with interesting structure.

For further details of the analysis for rings and films see Stampfli *et al.* [5]. In particular these may exhibit interesting behavior at nonequilibrium (due to hot electrons, for example).

It is important to compare the results by Stampfli *et al.* using the Balian– Bloch type theory [5] with quantum mechanical calculations of the DOS. Then

$$N(E)_\sigma = \sum_m \delta(E - E_{m\sigma}), \quad (32)$$

where the eigenvalues $E_{m\sigma}$ of the state $|m\sigma\rangle$ are determined by the Schrödinger equation.

2.4 Magneto-optics

Interesting magneto-optical behavior is exhibited by magnetic films. Nonlinear optics, SHG is very surface sensitive and reflects the magnetic properties of the film. SHG is generated at the surface and at the interface surface/substrate or at the interface of two films.

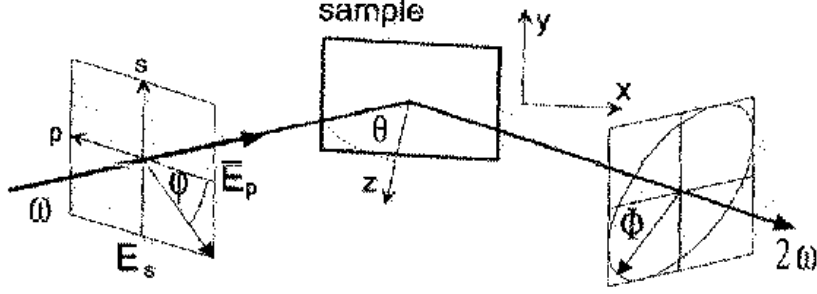


Figure 15: Optical configuration for incoming ω light and reflected 2ω light. Sketch of polarization of incoming and outgoing light characterized by the angle φ and Φ . z is normal to the surface and the crystal axes x, y are in the surface plane. θ denotes the angle of incidence.

In Fig.15 SHG at surfaces is shown (light $\omega \rightarrow 2\omega$). The 2ω -light is characterized by the response function $\chi_{ijl}(\vec{M}, \omega)$. The Fig. illustrates the optical configuration. Clearly, since the response depends on \vec{M} , note M_{\perp} and M_{\parallel} yield different $\chi_{ijl}(\vec{M})$, the reorientation transition of the magnetization can be studied optically.

For thin films the nonlinear susceptibility, response function χ^2 may be split into the contribution χ^s from the surface and χ^i from the interface. Then owing to the contribution $\chi^s \chi^i$ to the SHG intensity $I \propto |\chi|^2$ the relative phase of χ^s and χ^i is important. Furthermore, the magnetic contrast

$$\Delta I(2\omega, M) \propto I(2\omega, M) - I(2\omega, -M) \quad (33)$$

will reflect the film magnetism, since the susceptibility has contributions which are even and odd in M , see Bennemann *et al.* in Nonlinear Optics, Oxford University Press.[12]

Note, high resolution interference studies are needed to detect also for example lateral magnetic domain structures of films. Also polarized light reflects magnetism and in particular the magnetic reorientation transition, see Fig.16 and following results.

In magneto-optics (MSHG) using different combinations of polarization of the incoming and outgoing light, see Fig.15, one may analyze

$$\chi_{ijl}(\vec{M}). \quad (34)$$

Regarding the dependence on magnetization, for the susceptibility odd in magnetization one writes

$$\chi_{ijl}^o = \chi_{ijlm} M_m + \dots \quad (35)$$

(Note, $\chi = \chi^e + \chi^o$). Thus, in particular $\chi_{ijl}(M_c)$ changes characteristically for $c = x, y$, or z . For example, for incoming s-polarized light and outgoing p-polarized 2ω light, see Fig. 15 for illustration, the nonlinear susceptibility $\chi_{ijl}(M_y)$ dominates. Similarly $\chi_{ijl}(M_z)$ dominates in case of outgoing s-SHG polarization. For general analysis see Hübner *et al.*, Nonlinear Optics in Metals, Oxford Univ- Press.[12]

Regarding susceptibility χ^e and χ^o note further interesting behavior could result from terms which are higher order in the magnetization M ($\chi^e = \chi_0^e + aM^2 + \dots$, etc.) and χ_{ijl} reflects also the strength of the spin-orbit interaction. As discussed by Hübner *et al.* in case of

(a) $\vec{M} \parallel \vec{x}$ (longitudinal configuration), the tensor χ_{ijl} involves $\chi_{yxx}, \chi_{yyy}, \chi_{yzz}, \chi_{zxx}, \chi_{zyy}, \chi_{zzz}, \dots$ and in case of

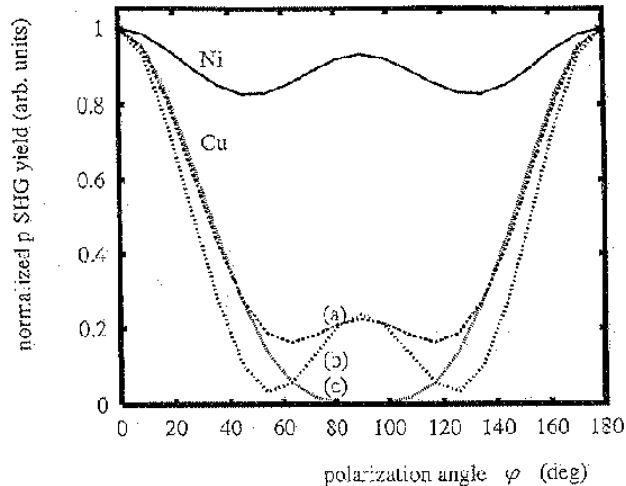


Figure 16: Polarization dependence of SHG. Note, the difference between magnetic Ni and nonmagnetic Cu. The angle φ refers to the incoming light polarization. Curves (a), (b), (c) for Cu result from using different input parameter for the diffraction index $n(\omega)$ and for $k(\omega)$, see calculations by Hübner *et al.*.

(b) $\vec{M} \parallel \vec{z}$ (polar configuration, optical plane x, z) elements χ_{zxx} , χ_{zzz} , χ_{xyz} and χ_{xxz} of susceptibility χ_{ijl} occur.

For longitudinal configuration and polarization combination $s \rightarrow p$ χ_{zyy} and for $p \rightarrow s$ χ_{yxx} , χ_{yzz} are involved. Furthermore, in case of polar configuration and polarization combinations $s \rightarrow p$ element χ_{zxx} and for $p \rightarrow s$ the element χ_{xyz} occur. This demonstrates clearly that Nolimoke as well as Moke can observe the magnetic reorientation transition and other interesting magnetic properties of nanostructures.

In Fig.16 results by Hübner *et al.* for the polarization dependence of SHG-light are shown. Note, agreement with experiments is very good. Obviously magnetism is clearly reflected. Similar behavior regarding polarization dependence is expected for the magnetic transition metals Cr, Fe, and Co. Due to $\langle d | z | d \rangle \approx \langle d | x | d \rangle$ for the dipole transition matrix elements one gets typically same results for s- and p-polarized light. To understand the behavior of Cu, note $\langle s | z | s \rangle \approx \langle s | x | s \rangle \approx 0$. Curves (a) and (b) refer to wavelengths exciting and not exciting the Cu d -electrons, respectively. Generally as physically expected $I_s(p-SH)_{NM} \rightarrow_{\omega} I_s(p-SH)_{TM}$. Again for a detailed discussion of the interesting polarization dependence see magnetooptics and discussion by Hübner *et al.*

In particular, interesting magneto-optical behavior of SHG and Moke results also from the spin-dependent quantum-well states (Q.W.S.) occurring in thin films. These states result from the square-well potential representing the confinement of the electrons in a thin film. In magnetic films the resulting electron states are of course spin-split. Characteristic magnetic properties follow. In contrast to band like-states for the electrons in the film only Q.W.S. show a strong dependence on film thickness. Thus, to study film thickness dependent (optical) behavior SHG involving Q.W.S. needs be studied.

One expects characteristic behavior of the optical response, its magnitude and dependence on light frequency ω and \vec{M} . Characteristic oscillations in the MSHG signal occur, since QWS involved in resonantly enhanced SHG occur periodically upon increasing film thickness, see Fig. for illustration (note, SHG involving transitions $i \rightarrow j \rightarrow l$ and with one of these states being

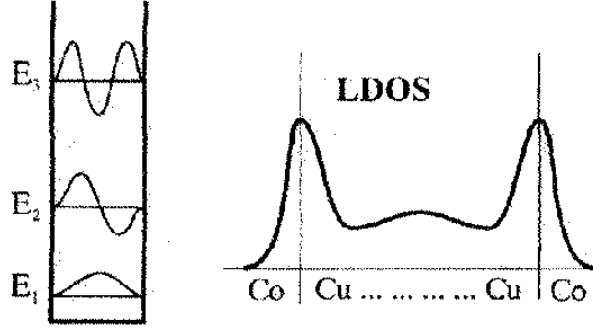


Figure 17: Illustration of quantum well states (QWS) due to confinement in a thin film of thickness d . Such states occur for example in a Co/10MLCu/Co film system. Note, the DOS of the QWS is strongly located at the interface. In magnetic films one gets generally spin split QWS. The parity of the QWS changes for increasing energy.

a QWS).

Clearly, the Q.W.S. energies shift with varying film thickness. Then SHG light intensity ($I_{2\omega}$) involving these states may oscillate as a function of film thickness and this in particular may reflect the magnetism of the film. Clearly, owing to the periodic appearance of Q.W.S. at certain energies for increasing film thickness, SHG involving these states may be resonantly enhanced and then oscillations occur as a function of film thickness.

A detailed analysis, see calculation of QWS by Luce, Bennemann, shows that the SHG periods depend on the parity of the Q.W.S., the position of the Q.W.S. within the Fermi-see or above, and on the interference of second harmonic light from the surface and interface film/substrate, etc. If this interference is important, then SHG response is sensitive to the parity of Q.W.S., light phase shift at the interface and inversion symmetry of the film. If this interference is not important, then SHG response and oscillations are different, see Fig.11 for illustration of the interference.

Thus, for an analysis of SHG involving QWS one may study:

(a) $\chi^i \simeq \chi^s$, when interference is important. Different behavior of SHG may result then if 1. QWS is involved as final state, 2. as intermediate state, or 3. both QWS as intermediate and final state matter. Note, for $\chi^s \chi^i \rightarrow (-1)$, for example due to inversion symmetric films or a phase shift π at the interface, the destructive interference yields no SHG-signal. Also if a final QWS near the Fermi-energy (and which may set the period of SHG-oscillation) has even parity, then in contrast to a QWS with odd parity no SHG signal occurs, since for the latter the product of the three dipole matrix elements is small.

(b) $\chi^i \neq \chi^s$, and interference is unimportant. Then different oscillation periods may occur. For example if a QWS above the Fermi-energy becomes available at film thickness d_1 for SHG then a first peak in SHG appears and then at film thickness $2d_1$ again at which previous situation is repeated, and so on. Of course, strength of signal depends on wavevector k in the BZ, DOS and frequency ω must fit optical transition. In case of a FM film then the resonantly enhanced SHG transitions are spin dependent and an enhanced magnetic contrast ΔI may occur.

If occupied QWS below the Fermi-energy are involved, then also oscillations occur, in particular due to DOS, see transition metals. If QWS below and above the Fermi-energy cause oscillations then the period of SHG may result from a superposition, as an example see the

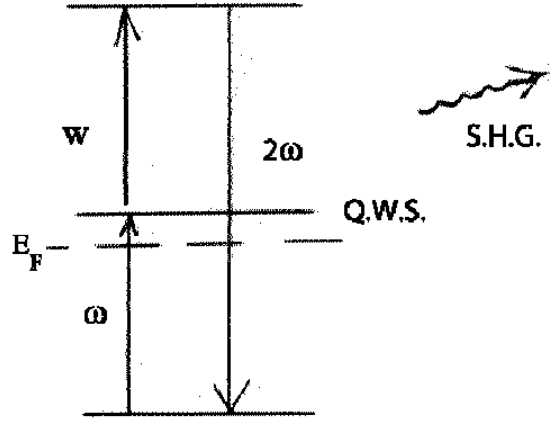


Figure 18: Illustration of electronic SHG transitions involving a QWS determining the oscillation period. If the QWS has even parity then resulting SHG is small. Only QWS with odd parity cause due to larger dipole matrix elements larger SHG and oscillations. In FM-films the QWS is spin split. Note, parity of QWS changes for increasing quantum number.

behavior of $x\text{Cu}/\text{Co}/\text{Cu}(001)$ films.

Characteristic properties of film SHG are listed in table 1. Various properties are listed for the case of no interference ($\chi^i \gg \chi^s$) and strong interference ($\chi^i \approx \chi^s$) of light from surface and interface. The first case is expected for a film system $x\text{Cu}/\text{Fe}/\text{Cu}(001)$, for example, since the interface Cu/Fe dominates due to the QWS of the Cu film and the large DOS of Fe near Fermi energy ε_F (see SHG transitions: $\text{Cu} \rightarrow_{\omega} \text{Fe} \rightarrow_{\omega} \text{QWS} \rightarrow_{2\omega} \text{Cu}$). Thus, $\chi^i \gg \chi^s$ and due to the QWS above ε_F one gets two and more SHG oscillation periods.

The case $\chi^i \approx \chi^s$ is expected for a film $x\text{Au}/\text{Co}(0001)/\text{Au}(111)$, for example, since no $\text{Co } d$ -states (see band structure of Co) are available as intermediate states for SHG transitions and the QWS in Au just below the Fermi-energy controls the SHG contribution, see Fig.18 for illustration. The parity of the QWS causes then oscillations $\Lambda = 2\Lambda_M$ (M refers to Moke), since clearly the 3 dipole (p) matrix elements $\langle d | p | \text{QWS} \rangle \langle \text{QWS} | p | d \rangle \langle d | p | d \rangle$ are much smaller if QWS has even symmetry (note, p is odd and d is odd).

The wave vector k dependence is controlled by the Brillouin zone structure (BZ). For a detailed discussion see Nonlinear Optics in Metals, Oxford University Press. [12]

The interesting S.H.G. (second harmonic light) interference resulting from surface s and interfaces i and reflecting sensitively magnetic properties of the film may be analyzed as follows. The SHG light intensity $I(2\omega)$ is approximately given by

$$I(2\omega) \sim |\chi_{ijl}|^2, \quad (36)$$

where χ denotes the nonlinear susceptibility. Note, χ may be split as (s :surface, i :interface)

$$\chi_{ijl}(2\omega) = \chi_{ijl}^s + \chi_{ijl}^i. \quad (37)$$

One gets

$$I(2\omega) \sim 2 |\chi_{ijl}^s|^2 + 2\chi_{ijl}^s \chi_{ijl}^i + \dots \quad (38)$$

Obviously the intensity $I(2\omega)$ depends on the resultant phase of the susceptibilities χ^s and χ^i .

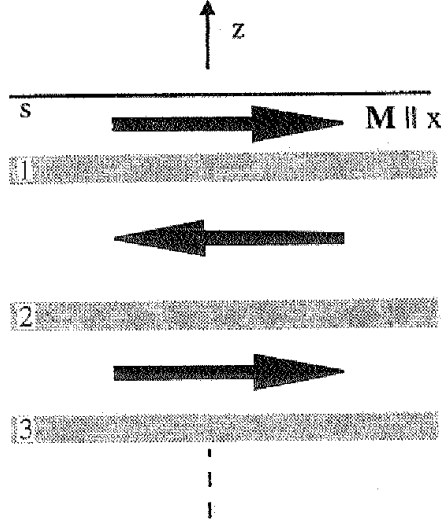


Figure 19: Multifilm system with antiferromagnetically ordered neighboring films. The shaded areas indicate interface regions important for SHG. Note, SHG results also at the surface. Typically approximately two atomic layers will contribute. The magnetization is assumed to be parallel to the surface which normal is in z -direction.

Then assuming, for example, that χ^s and χ^i are of nearly equal weight ($|\chi^s| \sim |\chi^i|$), it may happen that the 2.term in Eq.(38) cancels the first one, see for example inversion symmetry in films ($\chi_{ijl}^s \rightarrow -\chi_{ijl}^i$) or phase shift of the light by π at the interface.

If the interference of light from the surface and interface is negligible then different oscillations of the outcoming SHG light as a function of film thickness occur.

The weight of the optical transitions $i \rightarrow j \rightarrow l$ changes as the film thickness increases, see later discussion. Thus, Moke and Nolimoke oscillations occur.

Regarding optical properties, the morphology of the thin film and its magnetic domain structure should play a role in general.

Film multilayers: For magnetic film multilayers one expects interesting interferences and magnetic optical behavior. Assuming for example the structure shown in Fig.19, neglecting for simplicity QWS, one gets for SHG

$$I(2\omega) \sim |\chi_s(\vec{M}) + \chi_{int.1} + \chi_{int.2} + \dots|^2. \quad (39)$$

. Writing $\chi = \chi^e + \chi^o$, $\chi^o \sim M$, one has

$$I(2\omega) \sim |\chi_s^e + \chi_s^o(M) + \Sigma_i \chi_{int.i}^e + \dots|^2 \quad (40)$$

for the af structure. In the case of ferromagnetically aligned films it is

$$I(2\omega) \sim |\chi_s + \Sigma_i \chi_{int.i}(\vec{M})|^2. \quad (41)$$

Note, to detect magnetic domain structure experiments must achieve high lateral resolution, via interferences for example, etc. Of course surfaces with a mixture of domains with magnetization $M \perp$ and $M \parallel$ might yield a behavior as observed for the magnetic reorientation transition.

Table 1: Characteristics of SHG response from thin films. Its dependence on the film thickness involves QWS. The SHG oscillations reflect magnetic properties of the film.

	$ \chi^i \gg \chi^\delta $	$ \chi^i = \chi^\delta $
<i>k</i> selectivity	(<i>x</i> Cu/Fe/Cu(001) for example)	
	Strong magnetic signal due to strong (magnetic) interface contributions	Weak SHG signal, from only few <i>k</i> points and without strong interface contributions
	Sharp SHG peaks due to few contributing <i>k</i> points resulting in strong resonances	Doubled period and additional periods are frequency dependent
	Strong frequency dependence of the SHG oscillation of the QWS in the k_\perp direction	MOKE period absent; doubled and additional SHG period visible
	MOKE period and larger periods visible; no exact doubling of the MOKE period	
No <i>k</i> selectivity		(<i>x</i> Au/Co(0001)/Au(111) for example)
	Strong magnetic signal, since strong interface contribution Broad SHG peaks, since contributions come from many <i>k</i> points	Smaller magnetic contribution, since interface and (nonmagnetic) surface contributions are of the same magnitude
	Weak frequency dependence of the oscillation period	Broad, smooth peaks, since interference effects do not change magnitude
	MOKE period and larger periods present	SHG oscillation periods rather independent of the frequency, since the SHG signal is caused by the QWS near E_F
		MOKE period absent, doubled period present

2.5 Magnetization Dynamics

The time dependence of the magnetization is of great interest. Generally due to reduced dimension dynamics in nanostructures could be faster than in bulk. For example switching of the magnetization in thin films is expected to be faster. Of course, this depends on film thickness, magnetic anisotropy and molecular fields of neighboring magnetic films in a multilayer structure.

To speed up a reversal of the magnetization ($\vec{M} \leftrightarrow -\vec{M}$) within ps– times to fs times, one may use thin magnetic films for example with many excited electrons, hot electrons, resulting from light irradiation. In heterogeneous magnetic film structures transfer of angular momentum may be fast so that a fairly fast switching of the topmost film magnetization may occur.

The magnetic dynamics is described by (see Landau–Lifshitz equation)

$$d\vec{M}_i/dt = - \left(\frac{g\mu_B}{\hbar} \right) \vec{M}_i \times \vec{H}_{eff} + \frac{G}{M_s^2} \vec{M}_i \times (\vec{M}_i \times \vec{H}_{eff}). \quad (42)$$

Here, i refers to a film or a magnetic domain in a nano structured film and \vec{H}_{eff} to a molecular field acting on \vec{M}_i and resulting for example from neighboring films or magnetic domains. The first term describes precessional motion and the second one relaxation. M_s is the saturation magnetization (Note, using $\vec{M}_i \times \vec{H}_{eff} \rightarrow \partial\vec{M}_i/\partial t$ in the 2. term on the r.h.s. of Eq.(42) yields the Gilbert equation with damping parameter G describing spin dissipation).

One gets from Eq.(38) (and also from Boltzmann type theory) that the magnetization in thin films changes during times of the order of (controlled by angular–momentum conservation)

$$\frac{1}{\tau_M} \propto A(T_{el}) |V_{\uparrow\downarrow}|^2 \overline{N\overline{N}} + \dots \quad (43)$$

Here, in case of excited electrons T_{el} may refer to the temperature of the hot electrons and $V_{\uparrow\downarrow}$ to the spin flip scattering potential causing changes in the magnetization (for example: spin–orbit scattering or exchange interactions) and \overline{N} is the average DOS of the electrons. [13]

Note, in case of transition metals with many hot electrons Eq.(35) may yield response times τ_M of the order of 100 fs. Clearly, raising the temperature, $T \rightarrow T_{el}$ due to hot electrons, can speed up the magnetic dynamics.

The Landau–Lifshitz (LL) equation is generally important for spin dynamics. One may use the spin continuity equation ($\partial_t M_i + \partial_\mu j_{i\mu,\sigma} = 0$) to determine the spin currents $\vec{j}_\sigma(t)$ (including spin Josephson one) induced by magnetization dynamics and then describe the latter by using the LL–equation [3].

As will be discussed one gets for magnetic tunnel junctions (presumably best if $\tau_s > \tau_t$) spin current driven by phase difference between magnets of the form

$$\vec{j}_s \propto \partial\vec{M}/\partial t \sim \sin(\Delta\Phi). \quad (44)$$

This follows from the LL–equation and the spin continuity equation (see nonequilibrium magnetism).

2.6 Theory for Magnetic Films during Growth : Nonequilibrium Magnetic Domain Structure

The magnetic structure of thin films can be controlled by film growth conditions, since magnetism depends on the atomic structure of the film. Obviously this is of great interest for

engineering the magnetic properties of films [8, 11].

During growth of the film one has a film structure changing in time. This changes the magnetization. Thus, also the film magnetization changes in time (note, magnetic relaxation processes may occur somewhat time delayed). Then

$$\vec{M}(\vec{r}, t, \{\text{atomic structure (t)}\}) \quad (45)$$

describes the nonequilibrium magnetization of growing films. Clearly, the magnetic structure (domain structure) changes in time t as the atomic structure changes during growth of the film. For simplicity one may use a kinetic MC simulation (MC: Monte Carlo method) for molecular beam epitaxial film growth (MBE) to calculate the film structure and the accompanying magnetic one.. The nonequilibrium behavior reflects sensitively magnetic properties of the film, relaxation processes, range of magnetic forces and magnetic domain structure.

The atomic structure of the growing film is determined from a particular film growth model. For example, in the Eden type growth model the atoms are randomly deposited (to sites i) with probability

$$p_i = \propto e^{-E_i/kT} \quad , \quad (46)$$

where E_i is the atomic binding energy depending on the local coordination number z ($E_i \approx -A\sqrt{z_i}$). For illustration see Fig.9.

Different film growth is obtained by using layer dependent parameters A . One may also take into account diffusion of the deposited atoms. This yields then irregular film structures during growth with varying clusters of deposited atoms (islands of different sizes and shapes).

The resulting magnetic structure consists typically of an ensemble of magnetic domains. The magnetic domains may not be at equilibrium and will respond to the in time changing atomic structure of the growing film. This may occur time delayed. Thus, successively atomic structure and magnetic structure change.

Magnetic relaxation flipping the domain magnetizations is described by using a Markov equation and Arrhenius ansatz for the magnetic transition rates.

In summary, for each obtained atomic structure of the growing film one calculates the corresponding magnetic (domain) structure. Using the Heisenberg type hamiltonian including anisotropy it is obvious how by changing the atomic coordination the exchange interactions change and thus magnetism. For simplicity one uses first Eq.(16). For details of the analysis see Brinzanik, Jensen *et al.* [11].

Spin relaxation assumes coherent rotation of the spins of each atomic cluster (deposited group of atoms). The magnetization (one may use for simplicity an Ising model) of such atomic clusters is directed along the easy axis. Magnetic relaxation is (using Arrhenius type rates for transitions $\vec{M}_i \rightarrow -\vec{M}_i$) given by

$$\Gamma_i = \Gamma_0 e^{-E_i^b/kT} \quad . \quad (47)$$

Here, E_i^b gives the energy barrier against switching of the domain magnetization. Note, if no energy barriers are present then one may use the Metropolis algorithm. The magnetic barrier energy of a cluster controlling the domain relaxation is for example given by

$$E_i = N_i K_i(T) \cos^2 \varphi - g\mu_B H_i S_i \cos \varphi + \dots \quad . \quad (48)$$

The first term is due to magnetic anisotropy and the second due to the field H_i (exchange interaction, external magnetic field, dipolar field) acting on spin S_i .

Generally an energy barrier E_i^b is present for the two magnetic orientations of magnetic cluster i . One applies then as mentioned already a kinetic MC simulation during film growth to obtain the magnetic structure corresponding to a given atomic structure at time t . Correlated relaxation of neighboring magnetic domains must be taken into account. Note, the time for each calculational step is set by the spin precession frequency $\Gamma_0 \approx 10^9 - 10^{12} \text{sec}^{-1}$.

A successful analysis has been derived by Brinzanik and Jensen *et al.* [11]. In their studies first the atomic structure of the film at time t is calculated using a Eden type growth model. Then the corresponding magnetic structure is determined performing a kinetic MC simulation and using Markov equation and for the system of magnetic domains (interacting via exchange and dipolar coupling) the energy

$$E \simeq -(1/4)\sum_{i,j}\gamma_{ij}L_{ij}\vec{S}_i \cdot \vec{S}_j - \sum_i K_i N_i (S_i^z)^2 + \Delta E. \quad (49)$$

Here, γ_{ij} is the domain wall energy, L_{ij} the island surface area, and N_i the number of island atoms. The 2. term describes anisotropy. And

$$\begin{aligned} \Delta E = & \sum_{i>j} (\mu_i \mu_j / r_{ij}^3) [\vec{S}_i \cdot \vec{S}_j - 3(\vec{r}_{ij} \cdot \vec{S}_j)(\vec{r}_{ij} \cdot \vec{S}_i) / r_{ij}^2] \\ & - \sum_i \mu_i \vec{B} \cdot \vec{S}_i \quad . \end{aligned} \quad (50)$$

Here, for simplicity islands with N_i atoms and aligned magnetic moments are treated as particles with magnetic moments $\mu_i(T)$. The film magnetization results from averaging over the domain magnetization.

Typically one gets first for the given nanostructured film magnetism which is not at equilibrium. A non-saturated magnetization is typically obtained. As time progresses magnetic relaxation processes, magnetization reversals of domains, for example, occur. These change the magnetization of the film. Thus, finally equilibrium magnetization is obtained. For growing film thickness one might get an uniformly magnetized film, for details see analysis by Jensen *et al.* [8, 11].

2.7 Tunnel Junctions: Spin Currents

Tunnel junctions ($N_1 | N_2 | N_3$) are interesting nanostructures regarding (ultrafast) switching effects, interplay of magnetism and superconductivity, and in general quantum mechanical interference effects. Note, N_i may refer to material which is ferromagnetic or superconducting, for example. The situation is illustrated in Fig. 20. On general grounds one may get spin currents driven by phase difference between two magnetic systems, ferromagnets or antiferromagnets (which order parameter is also characterized by a phase) [3].

Interesting tunnel junctions are shown in Fig.(20). In Fig. 20(a) is shown a two quantum dot system $n_{i\sigma}$ with energy $\epsilon_{i\sigma}$ controlling the tunnel current $j_{i\sigma}^{i\sigma}$. The position of the energies ϵ_i may depend on occupation (see Hubbard like hamiltonian: $\epsilon_i = \epsilon_i^0 + U n_{i\bar{\sigma}} + \dots$). Note, $n_{i\sigma}$ and thus the current $j_{i\sigma}$ can be manipulated optically.

The tunnel system shown in Fig.(20b) can be used as a sensor for triplet superconductivity. Then the configuration of the angular momentum \vec{d} of the triplet Cooper pairs and of the magnetization \vec{M} of the tunnel medium control characteristically the tunnel current. The Josephson current exhibits interesting behavior, for example upon rotating the magnetization relative to the angular momentum of the Cooper pairs.

In Fig.(20c) is illustrated how tunneling can be used (with the help of a bias voltage) to control magnetoresistance and to determine the magnetization of a ferromagnet (see Takahashi *et al.*) [3]. Note, upon changing ($\uparrow |N_2| \uparrow$) \rightarrow ($\uparrow |N_2| \downarrow$) the magnetoresistance increases, see GMR effect, and accumulation of spin polarized electrons occurs in N_2 . This has been discussed by Takahashi *et al.* [3]. Furthermore, if N_2 becomes superconducting a competition between superconductivity and magnetization occurs for configuration ($\uparrow |N_2| \downarrow$) as a result of accumulating nonequilibrium spin density in N_2 . In Fig.20(b) and Fig.20(c) we assume $\tau_s > \tau_t$, where τ_s and τ_t refer to the spin diffusion and electron tunneling time, respectively. Electrons keep spin while tunneling.

For tunnel configuration ($FM_1|TSC|FM_2$) one expects similar interesting tunneling behavior, for example regarding dependence on relative orientation of \vec{M}_i and angular momentum \vec{d} of the triplet Cooper pairs as for junctions ($TSC/FM/TSC$), see Fig.20(b).

Furthermore, the current j_s^J expected for $\tau_s > \tau_t$ depends on relative magnetization of the two magnets, and on the state of N_2 (normal, superconducting singlet or triplet).

Spin Currents : Using the continuity equation one can find the relationship between spin currents and magnetization dynamics for the magnetic tunnel junction illustrated in Fig.(12). One has

$$\partial_t M_i + \partial_\mu j_{i\mu,\sigma} = 0. \quad (51)$$

This may give under certain assumptions straightforwardly the connection between magnetization and spin polarized electron currents (induced by hot electrons, temperature gradients or external fields). Note, the magnetic dynamics (characterized by $\frac{dM_i}{dt}$) may be described by the LL-equation. This yields generally a spin Josephson current between magnets.

Also according to Kirchhoff the emissivity (e) of the junction is related to its (time dependent) magnetization, magnetic resistance. It is

$$\frac{\Delta e}{e} \simeq a (GMR) \quad , \quad (52)$$

where (GMR) denotes the giant magnetoresistance resulting for the junction if the configuration ($\uparrow |N_2| \uparrow$) changes to ($\uparrow |N_2| \downarrow$). This changes the emissivity to Δe .

Viewing the phase of the magnetic order parameter ϕ_i (magnetization M_i)

$$\vec{M} = |M_i| e^{i\phi_i} \quad (53)$$

similarly as the phase of the S.C. state, one gets for a junction ($FM | N | FM$) a Josephson like current j^J driven by the phase difference of the spin polarizations on both sides of the tunnel junction. Using the continuity equation for the spins, integrating using Gau integral, and the Landau-Lifshitz equation, one gets for the spin current

$$j_\sigma = j_\sigma^1(V) + j^J, j^J \propto dM/dt \propto \vec{M}_L \times \vec{M}_R + \dots \propto |M_L||M_R| \sin(\phi_L - \phi_R + \dots). \quad (54)$$

Here, L and R refer to the left and right side of the tunnel junction, respectively. $j_\sigma^1(V)$ refers to the spin current due to the potential V and may result from the spin dependent DOS. For details of the derivation of the spin Josephson current see Nogueira *et al.* [3].

Note, using the general formula $j = \frac{\partial F}{\partial \phi}$, where F is the free-energy, one gets

$$j = -(e/\hbar) \sum_i \partial E_i / \partial \phi \tanh(E_i/kT). \quad (55)$$

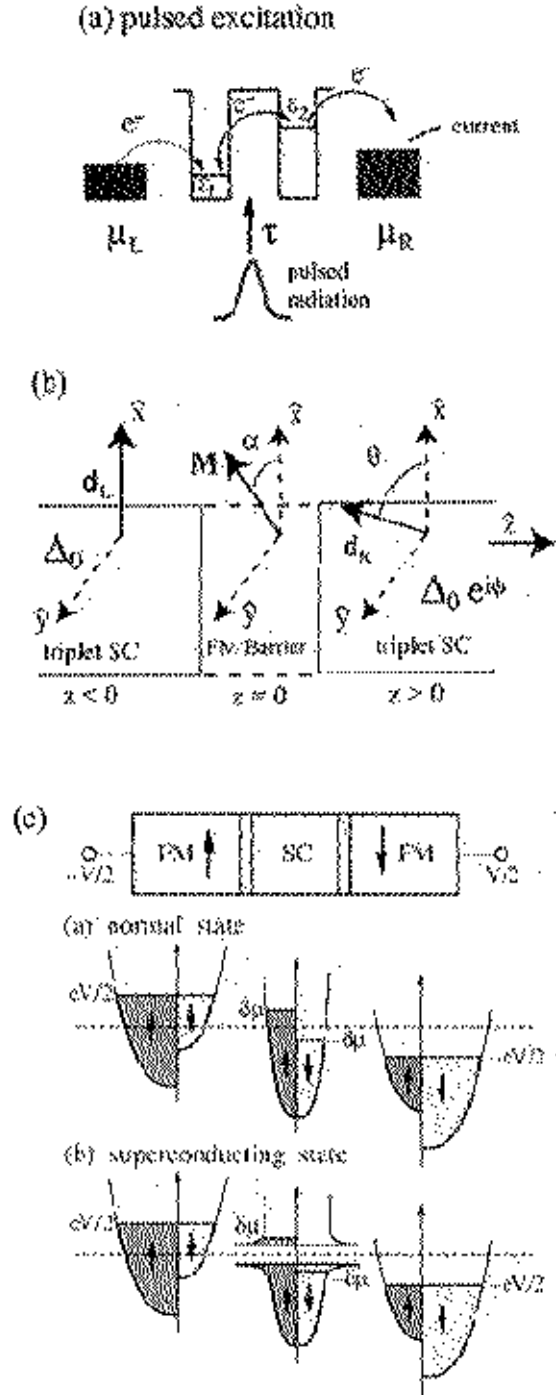


Figure 20: Illustration of various tunnel junctions. (a) A two quantum dot system with spin-dependent levels $\epsilon_{i\sigma}(n_{i\sigma}, t)$ is shown (for example $\epsilon_{i\sigma} = \epsilon_i^0 + U_i n_{i\bar{\sigma}}$). Two levels are separated by an energy barrier which can be overcome using an external electric field. (b) A triplet superconducting Josephson junction ($SC_1 | FM | SC_2$) is sketched. Here, \vec{d} refers to the angular momentum of the Cooper pairs which order parameter has the phase ϕ . (c) A junction ($FM_1 | SC | FM_2$) is illustrated. An external electrical field (potential V) shifts the electronic energy levels (bands). This may control the tunnel current (magnetoresistance), see Takahashi *et al.*. Of particular interest is the interplay of spin current and superconductivity.

Then using $E_i \propto J_{eff} \vec{S}_L \cdot \vec{S}_R + \dots$, one gets also

$$j_\sigma^J \sim J_{eff} \sin(\phi_L - \phi_R) + \dots \quad (56)$$

Here, E_i gives the energy difference between opposite directions of the magnetization (molecular field).

Of course, such a Josephson like spin current is expected on general grounds, since ϕ and S^z are canonical conjugate variables and (approximately)

$$[\phi, S^z] = i. \quad (57)$$

Note, this holds for the Heisenberg hamiltonian as well as for itinerant magnetism described by the Hubbard hamiltonian, for example. The commutator relationship suggests in analogy to the BCS–theory to derive the spin Josephson current from the hamiltonian

$$H = -E_J S^2 \cos(\phi_L - \phi_R) + \frac{\mu_B^2}{2C_s} (S_L^z - S_R^z)^2 + \dots \quad (58)$$

where again L, R refer to the left and right side of the junction and C_s denotes the spin capacitance. In general spin relaxation effects should be taken into account (magnetization dissipation, see LL –equation). Using then the (classical) Hamiltonian equations of motion ($\dot{\phi} = \partial H / \partial S^z$, $\dot{S}^z = -\partial H / \partial \phi$) one gets

$$\Delta \dot{\phi} = 2\mu_B V_s, \quad j_S^J = (2E_J S^2 / \mu_B) \sin \Delta \phi \quad (59)$$

Here, $\Delta \phi = \phi_1 - \phi_2$ and $V_s = (\mu_B / C_s)(S_L^z - S_R^z)$. That $\Delta \dot{\phi} = 0$ if $M_L \parallel M_R$ and $\Delta \dot{\phi} \neq 0$ if M_L is antiferromagnetically aligned relative to M_R can be checked by experiment. It is $j_s^J \sim \sin(\Delta \phi_0 + 4Mt)$. Note, details of the analysis for the a.c. like effect are given by Nogueira *et al.*

Thus, interestingly the spin current in a $FM | FM$ tunnel junction behaves in the same way as the superconductor Josephson current. Of course, as already mentioned magnetic relaxation (see Landau–Lifshitz–Gilbert Eq.) affects j_S^J . For further details see again Nogueira and Bennemann [3].

Clearly, one expects that also junctions involving antiferromagnets (af), (AF/F), (AF/AF) yield such Josephson currents, since using the order parameter for an AF one gets also that S_q^z and ϕ are conjugate variables. (Treat af as consisting of two fm sublattices). Eq.57 should hold for both $J > 0$ and $J < 0$, see Heisenberg hamiltonian.

Note, also $J_{eff} = J_{eff}(\chi)$ is a functional of the spin susceptibility χ , since the effective exchange coupling between the L and R side of a tunnel junction is mediated by the spin susceptibility of system N_2 , see Fig.12.

The analysis may be easily extended if an external magnetic field \vec{B} is present. Then from the continuity equation one gets $j_s \sim \frac{\partial \vec{M}}{\partial t}$ and $\frac{\partial \vec{M}}{\partial t} = a \vec{M}_L \times \vec{M}_R - g \mu_B \vec{B}_L \times \vec{S}_L + \dots$ (and similarly $\frac{\partial \vec{M}_R}{\partial t} = a \vec{M}_R \times \vec{M}_L + \dots$). Alternatively one may use the Hamilton–Jacobi equations with the canonical conjugate variables S^z and ϕ ($\dot{S}^z = \frac{\partial H}{\partial \phi}$, $\dot{\phi} = -\frac{\partial H}{\partial S^z}$) and changing the hamiltonian $H \rightarrow H - g \mu_B (\vec{B} \cdot \vec{S}_L + \vec{B} \cdot \vec{S}_R)$ to derive the currents j_s and j_s^J .

Note, according to Maxwell Eqs. the spin current j_S should induce an electric field E_i given by

$$\partial_x E_y - \partial_y E_x = -4\pi \mu_B \partial_t \langle S^z \rangle = 4\pi j_s \quad (60)$$

Here, for simplicity we assume no voltage and $\partial_t B = 0$ for an external magnetic field B .

Tunnel Junctions with Spin and Charge Current: Generally one gets both a charge current $j_C = -e\dot{N}_L$ and a spin current $j_s = -\mu_B(\dot{S}_L^z - \dot{S}_R^z)$ and these may interfere. This occurs for example for $SCM | SCM$ junctions, where SCM refers to nonuniform superconductors coexisting with magnetic order (see Larkin–Ovchinnikov state), and for a (SC/FM/SC) junction with a ferromagnet between two superconductors. Then one gets after some algebra for the Josephson currents (see Nogueira *et al.*)

$$j_c^J = (j_1 + j_2 \cos \Delta\varphi) \sin\left(\Delta\phi + \frac{2\pi l}{\phi_0} H_y\right) \quad (61)$$

and

$$j_s^J = j_s \sin \Delta\varphi \cos\left(\Delta\phi + \frac{2\pi l H_y}{\phi_0}\right) \quad . \quad (62)$$

Here, ϕ_0 is the elementary flux quantum, H_y an external magnetic field in y -direction, $l = 2\lambda + d$, with λ being the penetration thickness, and d the junction thickness. $\Delta\varphi$ and ϕ refer to the phase difference of magnetism and superconductivity, respectively. The magnetic field H_y is perpendicular to the current direction.

(TSC/FM/TSC) Junction: Regarding switching of tunnel current and analysis of triplet superconductivity the tunnel junction ($TSC | FM | TSC$) is of interest. Here, TSC refers to triplet superconductivity. The Josephson current flows then through low-energy Andreev states. Relative orientation of the magnetization \vec{M} of the ferromagnet (FM) and d -vectors of the triplet superconductors, see Fig.20(b), control the tunnel current. One gets, see Morr *et al.* [3],

$$j_c^J = -\frac{e}{\hbar} \sum_i \frac{\partial E_i}{\partial \phi} \tanh\left(\frac{E_i}{kT}\right) \quad , \quad (63)$$

where ϕ is the phase difference between the two superconductors and E_i are the energies of the Andreev states and which are calculated using Bogoliubov–de Gennes analysis. Thus one derives an unusual temperature dependence of the Josephson current on temperature and even that j_c^J may change sign for certain directions of \vec{M} , although $\Delta\phi$ did not change.

(SC/FM/SC) Junction: As discussed recently by Kastening *et al.* [3] such junctions reflect characteristically magnetism. Again the tunnel current is carried by Andreev states. No net spin current flows from left to right, since the spin polarized current through the Andreev states is compensated by the tunnel current through continuum states as must be due to basic physics. In case of strong ferromagnetism single electrons tunnel, while for weak ferromagnetism Cooper pair tunneling occurs. The Josephson current may change sign for increasing temperature without a change in the relative phase of the two singlet superconductors. Of course, dependent on coherence length, temperature and thickness of the FM and strength of FM one may get $j^J = 0$ for the Josephson current.

(FM/SC/FM) Junction: It is already obvious from Fig.20(c) that in the presence of an applied voltage V junctions ($FM_1 | SC_2 | FM_3$) carry currents which depend sensitively on the relative orientation of the magnetization of the two ferromagnets. If these are directed in opposite direction (AF configuration) one gets a maximal spin accumulation in the superconductor and thus one may suppress (at a critical voltage) superconductivity in singlet superconductors. As a consequence the magnetoresistance changes. Hence, such junctions exhibit currents

$$j_{c\sigma} = j_{c\sigma}(\vec{M}_1, \vec{M}_3, SC_2, T) \quad (64)$$

which reflect sensitively superconductivity and ferromagnetism.

Of course, the current $j_{c\sigma}$ is affected by temperature gradients ΔT between the ferromagnets and resulting for example at nonequilibrium from hot electrons in one *FM*. This may cause interesting behaviour.

Note, also a ring structure hollow at the center (and with magnetic flux Φ) and outer ring superconducting and a neighboring inner ring ferromagnetic and which is also next to the hollow center may exhibit interesting behavior in the presence of an external magnetic field B .

The equation for the current due to $\partial E/\partial\phi$, for the current driven by the phase dependence of the electronic energy, is of general significance. From it one may derive the currents induced in rings, discs etc. due to the Aharonov–Bohm effect if a magnetic field is present.

2.8 Quantum dot Systems

Interesting current pattern and interferences are also expected for the quantum dot grain structure shown in Fig.3. Assuming a mixture of ferromagnetic and superconducting grains (clusters, quantum dots) one has the hamiltonian

$$H = H_T - (ze^2/C) \sum_{i,j} (N_i - N_j)^2 + H' \quad . \quad (65)$$

Here, H_T denotes the tunneling hamiltonian. This includes also spin Josephson currents of the form $E_{ij}^J \cos \varphi_{ij}$ and also Josephson Cooper pair current contributions resulting from the phase difference $\varphi_{ij} = \varphi_i - \varphi_j$ of the phases of the S.C. order parameter of grains i and j . The electrostatic effects due to different charges of grains i, j are given by the second term. H' denotes remaining affects, for example due to ferromagnetic grains. One expects characteristic differences for singlet and triplet superconductivity and interplay of spin currents j_σ between magnetic grains and Josephson–currents.

In grains the interplay of Cooper pair size and distance between Cooper pairs manipulated by confinement is expected to exhibit interesting behavior.

For a lattice like array of quantum dots it is of interest to study phase ordering of the order parameter of the various dots i , its dependence on distance between dots, etc. (see related situation for superconductors when $T_c \propto \rho_s$, here ρ_s is the superfluid density).

As speculated for two–band superconductors and as assumed for *sc q*–bits (strong) phase coupling of two magnetic systems (quantum dots) may cause a covalent splitting like process (mode–mode coupling like process). Thus, for example, one expects for the combined, phase coupled system N_1 and N_3 , see Fig.20, the two covalently like split states $|N_1N_3\rangle_1$ and $|N_1N_3\rangle_2$.

Light irradiation causes interesting responses, since occupation of electronic states (by single electrons, Cooper pairs) can be manipulated.

Also note, for a mixture of superconducting and magnetic quantum dots on a lattice (and presence of an external magnetic field B) one may expect interesting quantum mechanical effects.

These examples may suffice already to demonstrate the interesting behaviour displayed by nanostructures involving tunneling. This holds also for currents across multilayers of magnetic films.

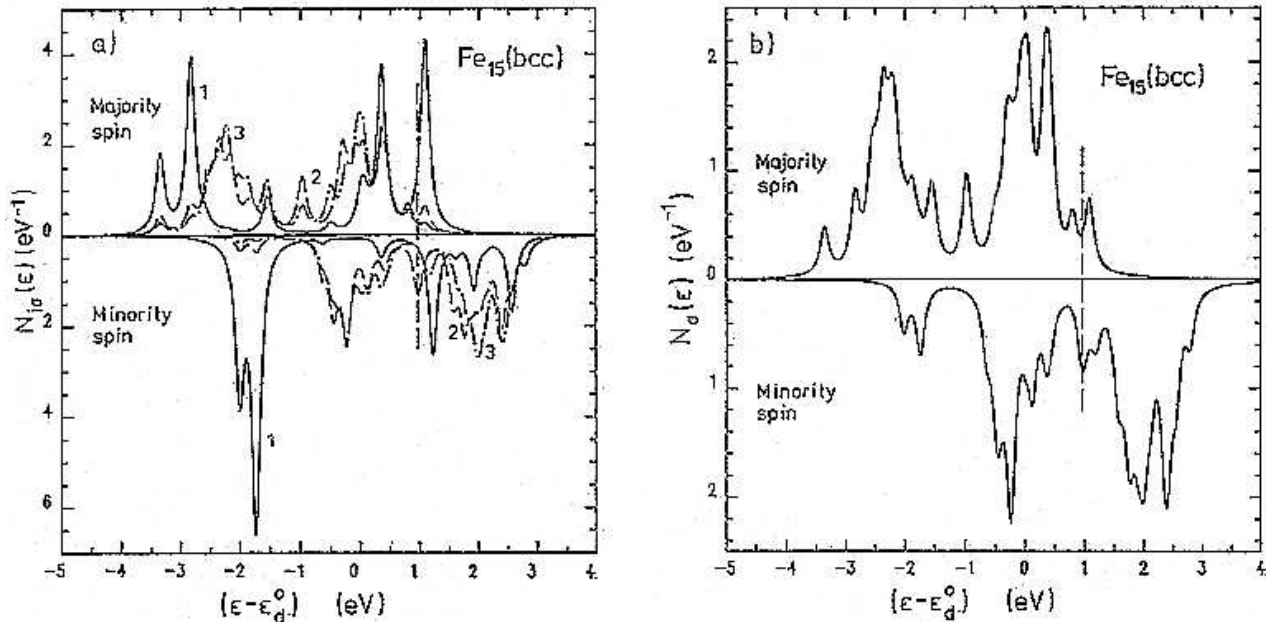


Figure 21: Typical electron density of states (D.O.S.) results for Fe_n clusters, $n=15$. The local D.O.S. refers to the atoms 1, 2, 3, see Fig.1. (a) refers to local DOS, (b) to average cluster DOS.

3 Results

Characteristic results are presented for clusters, films and tunnel junctions.

3.1 Small Magnetic Particles

3.1.1 Single Magnetic Clusters

In small clusters the local D.O.S. exhibits the dependence of the electronic structure on the local atomic environment of a cluster atom. In Fig.21 the local D.O.S. is compared with the average D.O.S. Results were obtained by Pastor et al. using the tight-binding Hubbard hamiltonian.

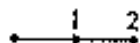
The D.O.S. is the most important property of the electronic structure and determines the thermodynamical and magnetic behavior ($\mu_n, M_n(T)$).

In table 2 results for the bond-length d_n (d_b refers to bulk), cohesive energy $E_{coh}(n)$ and magnetic moments μ_n are given for Ni_n clusters.

In Fig.22 the dependence of the magnetic properties on cluster size is given. The variation of μ_n reflects the atomic structure (shell structure). These results were obtained by S. Mukherjee *et al.*). In accordance with the electronic calculations by Pastor et al. a simple model is used assuming that the moments depend on cluster shell (i) and local atomic coordination, both changing with number of cluster atoms. Such behavior results also for other clusters, for example Ni_n clusters. Note, the discrepancy between theoretical and experimental results for larger clusters. Of course, $\mu_i \rightarrow \mu_B$, bulk behavior as clusters get larger.

In Fig.23 results for μ_n of Fe_n are given. The results were obtained using the Hubbard hamiltonian and a tight-binding type calculation by Pastor *et al.*. For Fe one expects a particular strong interdependence of magnetism and structure (see bcc vs fcc Fe). For each cluster one

Table 2: Results for Ni_n clusters by Pastor *et al.*. E_{coh} denotes the cohesive energy, d_n the bond-length and $\mu(i)$ the local magnetic moments.

	Structure	$E_{\text{coh}}(n)$	d_n/d_b	$\bar{\mu}_n$	$\mu(1)$	$\mu(2)$	$\mu(3)$	$\mu(4)$
Ni_2		0.68 (0.62)	0.92	0.95 (0.36)	0.95 (0.05)			
Ni_3		0.83 (0.68)	0.93	0.38 (0.27)	0.28 (0.27)			
Ni_4		0.87 (0.70)	0.95	0.92 (0.96)	0.87 (0.90)	0.93 (0.99)		
Ni_4		0.93 (0.87)	0.94	0.51 (0.55)	0.51 (0.53)			
Ni_5		0.96 (0.89)	0.96	0.72 (0.95)	0.72 (0.96)			
Ni_5		1.0 (0.90)	0.96	0.96 (0.97)	0.96 (0.97)			
Ni_{10}	fcc	1.05 (1.01)	0.97	0.89 (0.89)	1.20 (1.17)	0.76 (0.79)		
Ni_{12}	iccs	0.99 (0.91)	0.96	0.97 (0.96)	1.07 (1.22)	0.94 (0.94)		
Ni_{15}^a	fcc	0.99 (0.95)	0.97	0.0 (0.0)	0.0 (0.0)	0.0 (0.0)		
Ni_{15}^b	iccs	0.97 (0.97)	0.96	0.0 (0.0)	0.0 (0.0)	0.0 (0.0)		
Ni_{15}^b	fcc	1.15 (1.08)	0.97	0.0 (0.0)	0.0 (0.0)	0.0 (0.0)		
Ni_{15}^b	iccs	1.22 (1.09)	0.96	0.0 (0.0)	0.0 (0.0)	0.0 (0.0)		
Ni_{19}	fcc	1.08 (1.04)	0.99	0.78 (0.78)	1.06 (1.03)	0.78 (0.78)	0.73 (0.73)	
Ni_{43}	fcc	(1.14)		(0.69)	(0.66)	(0.71)	(0.59)	(0.51)
Bulk	fcc	1.18	1.0	0.6	0.6			

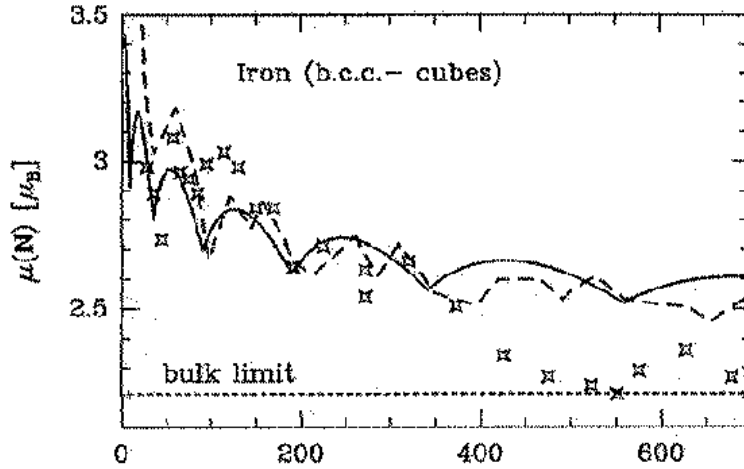


Figure 22: Average magnetic moment $\mu(N)$ of Fe_n clusters as a function of cluster size. The solid and dashed curves refer to calculations by Jensen *et al.* using different cluster shell models for the magnetic moment $\mu(N)$. $\mu(N)$ is calculated by averaging over the shell (coordination) dependent moments μ_i and where these are given by the local atomic coordination (varying with N). Crosses refer to experimental results (de Heer *et al.*). Note, solid and dashed curves refer to calculations using different models for the dependence of the local magnetic moments μ_i on atomic coordination. Of course, for larger clusters $\mu \rightarrow \mu_b$.

assumes a structure which yields the largest cohesion. The variation of $\overline{\mu_n}$ as a function of n is due to the interplay of changes in coordination number and bond-lengths (note, approximately $W_n \propto d^{-5}$, where W is the band-width and d the bond-length). Interestingly, one gets for the small clusters $\overline{\mu_n}$ larger than μ_b , magnetic moments which are larger than the bulk one as expected. The sensitive dependence of the Fe magnetic moments and magnetism on structure is of general importance for nanostructures and of material involving Fe and Fe under pressure.

One may also calculate using molecular field type methods the Curie-temperature T_c as a function of cluster size. Results are shown in Fig.24. Typically one gets that T_c increases for increasing cluster size. Note, the exchange interaction J , q_{eff} and μ_i may change as the cluster grows.

Orbital magnetism: Clusters as other low dimensional systems (surfaces, thin films) exhibit also interesting orbital magnetism. For example, for Ni clusters a remarkable enhancement of the average orbital moment as compared to bulk is observed. Note, one gets for the orbital moment of Ni $\langle L(Ni_7) \rangle \simeq 0.5\mu_B$ while for bulk $\langle L(bulk) \rangle \simeq 0.05\mu_B$. Using the tight-binding Hubbard hamiltonian including the spin-orbit interaction ($H_{so} = -a \sum (\vec{L} \cdot \vec{S})_{i\alpha, i\beta} a^+ a$, here α, β refer to orbitals), Pastor, Dorantes-Davila *et al.* obtain for the average orbital moment $\langle L_\delta \rangle$ the results shown in Fig.25. Here, δ refers to the cluster crystal axis. The important DOS $N_{imo}^\delta(\varepsilon)$ is determined self consistently for each orientation δ of the magnetization with respect to structure. The s-o coupling connects spin up and spin down states (dependent on relative orientation of \vec{M} and atomic structure). $(\vec{L} \cdot \vec{S})_{i\alpha, i\beta}$ are intraatomic matrix elements.

The results show that the orbital magnetic moment is an important contribution to the magnetic moment of clusters and quite generally to the one of nanostructures of transition metals (TM). $\langle \vec{L} \rangle$ depends sensitively on band filling. Also note, for example, $(L_z - L_x)$, etc. reflect magnetic anisotropy. For Ni the orbital moment aligns parallel to the spin moment.

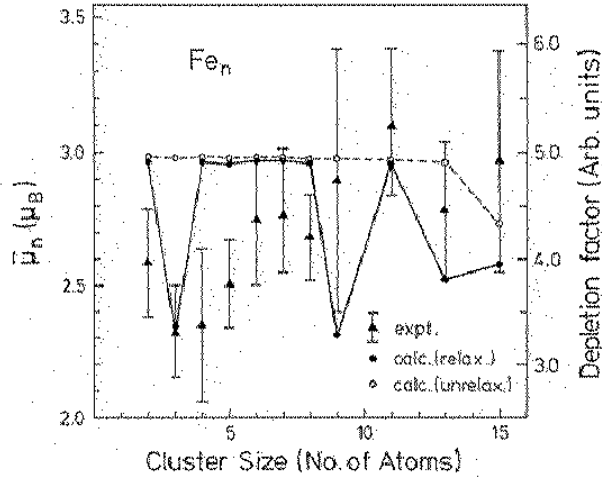


Figure 23: Dependence of average magnetic moment of Fe_n on cluster size. Note, the dependence of the results on the relaxation of the atomic structure, see calculations using an electronic theory by Pastor *et al.*. For each n a structure with largest cohesion is assumed. For Fe-clusters one expects a sensitive dependence on structure and possibly a particular strong interdependence of magnetism and structure. The vertical bars refer to experimental results for the depletion factor and which is assumed to be proportional to the average magnetic moment, at least approximately.

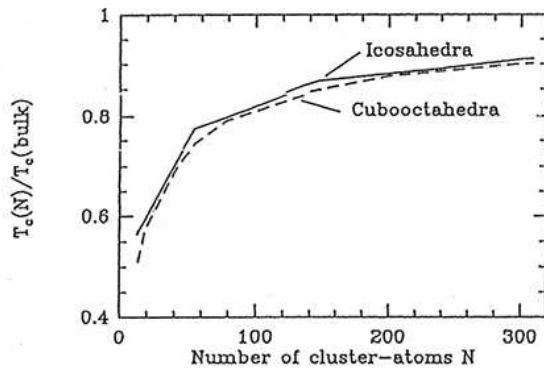


Figure 24: The Curie-temperature T_C ($M(T_C) = 0$) as a function of number of cluster atoms. The calculations by Jensen *et al.* assume two different cluster structures.

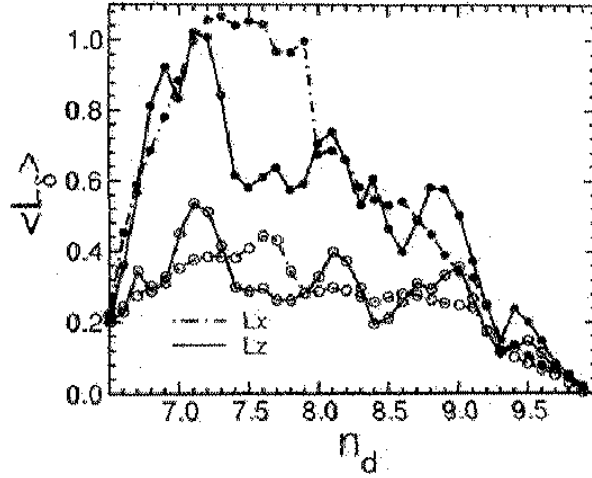


Figure 25: Orbital moment per atom $\langle L_\delta \rangle$ for a pentagonal bipyramid transition metal model cluster of 7 atoms as a function of d-state filling (band-filling) n_d . Bulk n.n. neighbor atomic distances are taken. δ refers to the magnetization direction taken along (principal C_n symmetry) cluster axis ($\delta = z$: full curves, $\delta = x$: dashed curves, for details see Pastor, Dorantes-Davila *et al.*). Note, full and open circles refer to calculations using different electron energies $\epsilon_{i\sigma}$.

Mie scattering: For determining magnetism in small clusters besides Stern-Gerlach deflection experiments (as performed by W. de Heer *et al.*) Mie-scattering could be used. Extending the usual Mie scattering theory to magnetic clusters one calculates from Maxwell equations with spin orbit coupling, coupling the electromagnetic field and the cluster magnetization, and with a dielectric function ϵ of tensor form the Mie backscattering profile. Characteristic differences are obtained for Ni, Co, Fe. For example, magnetic Mie scattering is important for spherical clusters with radius approximately larger than 6 nm for Fe and 10 nm for Co.

Generally \vec{M} has a weak effect on the electromagnetic field. This is strongest when size of cluster is of same order as the wavelength of the electromagnetic field (k^{-1}). In view of the weak coupling one may treat the perturbation due to cluster magnetization \vec{M} in lowest order (with respect to the off-diagonal element $\epsilon_{xy} = a\lambda_{so}M + \dots$ of the dielectric tensor ϵ_{ij} which is frequency dependent). The tensor ϵ_{ij} may be fitted using magneto-optics (Kerr-effect, ellipticity etc.).

Results obtained by Tarento *et al.* are given in Fig.26. Note, the backward scattering and the angle dependent scattering profile reflect magnetism. Magnetic effects are maximal when magnetization is parallel to y, see Mie scattering configuration, Fig.26(a). Note, for angle $\theta = \pi/2$ the backscattering intensity $I(M=0)$ is very small and then the changes due to the cluster magnetization are relatively large. In Fig.26(b) $\epsilon_0 = -1.569 + i5.58$ and $\epsilon_{xy} = -0.059 + i0.122$ is used. Note, in Fig.26(c) we use for the dielectric function $\epsilon_o = -4.592 + i7.778$ and $\epsilon_{xy} = -0.1613 - i0.0733$.

Mie scattering exhibits also characteristic differences regarding the angular dependence of the backscattering intensity for Cr, Fe, Co, and Ni.

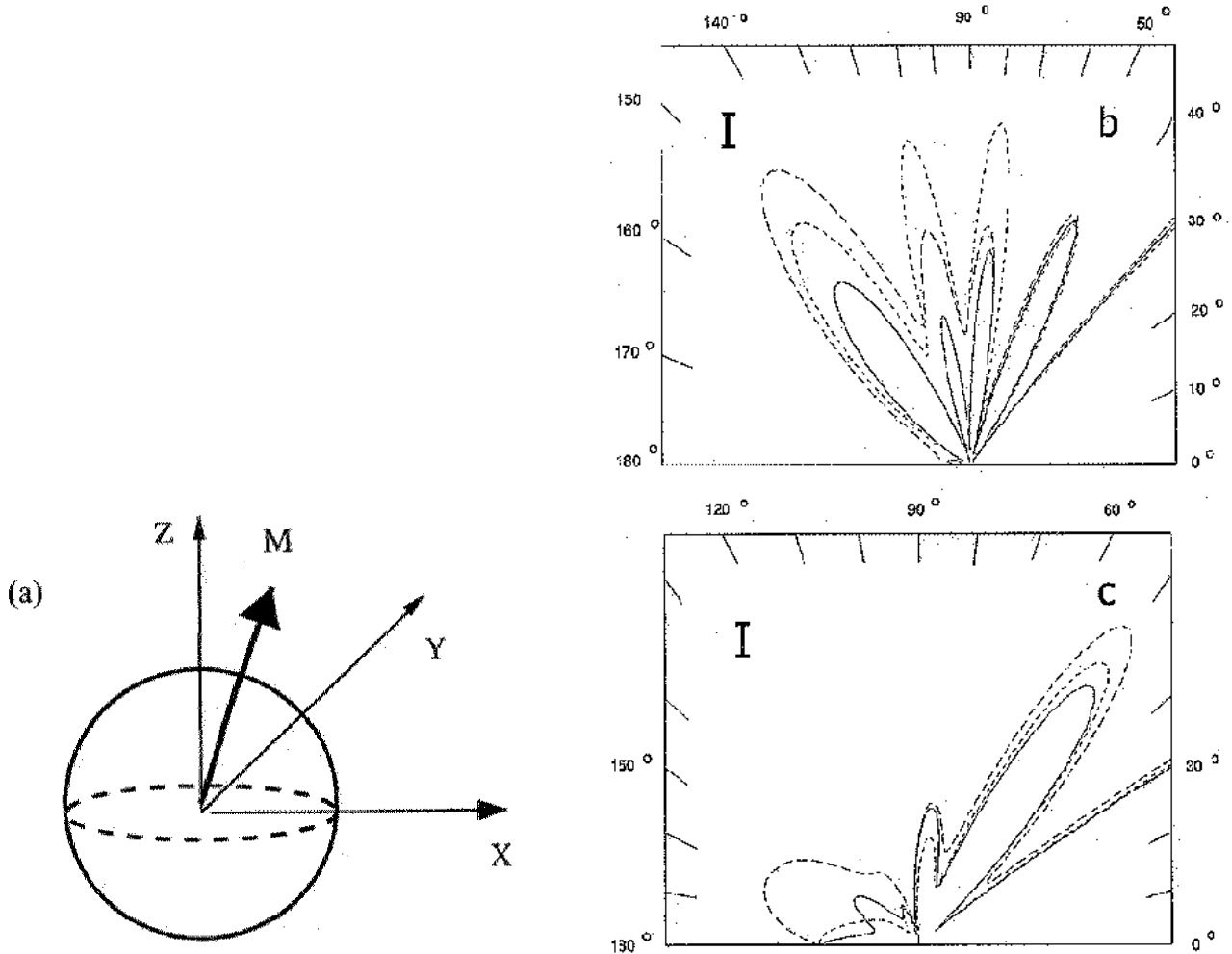


Figure 26: Angular dependence of Mie backscattering: (a) Mie-scattering configuration for magnetic clusters (Co clusters of radius 2600\AA). The incident plane wave propagates along z -direction and electric and magnetic fields are polarized along x - and y -direction. In Figs. (b),(c) different values for the dielectric tensor ϵ_{ij} are used, see text. Results for the angle-dependent backscattering intensity are given, see analysis Tarento *et al.*. The solid curves refer to $M=0$, the dashed ones to magnetic clusters with \vec{M} along y -axis, and the angle to the polar one in the x - z plane. The axis units are arbitrary. In (c) the two dashed curves refer to magnetization taken along the x - and y -axis. (The field frequencies are such that $\hbar\omega=5\text{eV}$ in Fig.(b), and 3.5eV in Fig.(c))

3.1.2 Ensemble of Clusters

The behavior of an ensemble of magnetic clusters is expected to reflect magnetic anisotropy of the cluster and cluster rotation. An external magnetic field H will align the magnetic clusters which magnetization points in the direction of the easy cluster axis. This is set by the anisotropy axis of the cluster. Note, to align the magnetic clusters the pinning of the cluster magnetization to the easy axis has to overcome. This should be reflected then in the dependence of the cluster ensemble magnetization on an external magnetic field.

T_{bl} characterizes the energy which pins the cluster magnetization to its easy axis. Therefore, different behavior is expected for the ensemble magnetization $\langle \mu_Z \rangle$ for temperature $T > T_{bl}$ (Langevin behavior) and $T < T_{bl}$.

In Figs. 27(a) and 27(b) results are given for the magnetization of a system of clusters. Note, in a magnetic field H cluster anisotropy characterized by the blocking temperature T_{bl} and H interfere. For temperatures $T > T_{bl}$ the internal anisotropy needs to be overcome to align the cluster magnetization via the external field.

Results shown in Fig.27 give the magnetization observed in Stern–Gerlach experiments for an ensemble of clusters in a magnetic field H . Obviously magnetic anisotropy within the cluster determines the magnetic behavior. The temperature T_{bl} characterizes the pinning of the magnetization to the easy axis of each cluster. Thermally activated depinning occurs for $T > T_{bl}$ (see calculations by Jensen *et al.*). Clearly, for temperatures larger than the blocking one Langevin type behavior is expected. For lower temperatures one needs a certain strength of the external magnetic field ($\mu H \geq kT$) for unpinning the cluster magnetization from its easy axis.

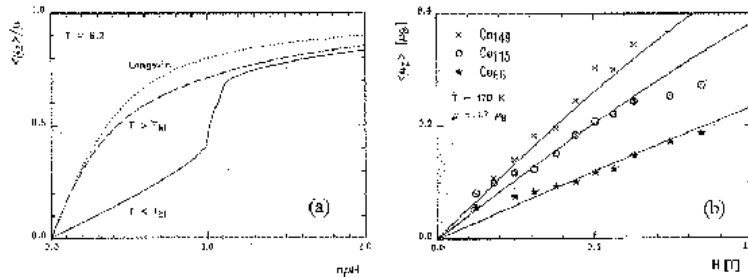


Figure 27: Results for cluster ensemble: The component of the average cluster magnetization in z -direction. (a) Comparison for $T > T_{bl}$ and $T < T_{bl}$, where T_{bl} refers to the blocking temperature. (b) Comparison with experimental results for Co_n clusters, see de Heer *et al.* and Bloomfield and others. Note, here $T_{bl} < T$.

Quantum dot lattices: Typical results for a lattice of quantum dots or anti-dots are shown in the following figures. Of course, one expects that the density of states $N(E)$, generally if magnetism is involved spin dependent, reflects characteristically the nanostructure.

In Fig.28 results for the DOS oscillations are given which demonstrate their dependence on dimension and geometry of the nanostructure. For a sphere mainly paths with $t=1$ and $p=3$ and 4 contribute. Their interference yields a beating pattern. For circular rings path 3 is most important (see Fig.13) and note larger discrepancy between classical and quantum-mechanical calculations. For circular discs note $A_i \sim k^{-1/2}$ (in contrast to spheres with $A_i \sim k^{1/2}$).

Approximately the spin up and spin down DOS are split by the molecular field h_{eff} in case of ferromagnetic nanostructures. It is of interest to study the interplay of superconductivity

and magnetism and magnetic field B .

In Fig.28 the DOS results obtained from the semiclassical Balian–Bloch–Stampfli theory are compared with quantum–mechanical calculations. The oscillating part of the DOS due to the interference of the dominant electronic paths is shown for various nanostructures. The quantum–mechanical calculations were performed using Schrödinger equation and Green’s function theory

$$N(E, ..) = (\gamma/\pi) \int dE' \frac{N(E')}{(E - E')^2 + \gamma^2}. \quad (66)$$

Of course, the parameter γ must be chosen as usual such that it does not affect the structure in the DOS.

Note, in case of magnetism one has a spin dependent DOS $N_\sigma(E)$ and to simplify one may assume that spin up and spin down states are split by the molecular field h_{eff} which may include an external magnetic field B .

Also hollow particles (see coated nanoparticles, for example) can be treated similarly as rings. This is of interest, for example, to study confined and bent 2d electronic systems.

In Fig.29 results are given for the oscillating part of the D.O.S. as a function of energy and external magnetic field for a lattice of anti–dots which repel the electrons. The magnetic field B changes the orbits and thus their interference. As a result DOS oscillations occur. Note, only a few closed electron orbits (1,2,3,...) give the dominant contribution to the electronic structure, the DOS, see theory by Stampfli *et al.* and Eq.(19) and Eq.(21). The magnetic field causes paths deformation and phase shifts. The flux due to the external field B is $\phi = SB$ and for orbits 1, 2, 3 S is approximately independent of B for small field. The cyclotron orbit radius is $R_c = \frac{k}{B}$ and we assume for simplicity $2R_c > (a - d)$ and $R_c \gg R$. Then, $R_c \sim \frac{1}{B}$ and the DOS depends on (d/a) and $\Delta N \sim \cos SB$. This controls also height of oscillations (note $S \propto R_c^2 \propto \frac{1}{B^2}$).

For increasing external magnetic field B the oscillations in the DOS change. Interestingly, the contributions of some orbits may be nearly eliminated. Oscillation period in B decrease for increasing B and decreasing lattice constant a .

Note, an internal molecular field due to magnetism is expected to affect the DOS similarly as the external magnetic field. Note also, the above oscillations in the DOS result from the confinement (closed electronic orbits) and additional structure may result from detailed atomic structure yielding the well known electronic shell structure in clusters etc.

Note, for orbit 4 (see Fig.) and similar ping pong orbits one has $\cos(SB) \approx 1$. Of course, for increasing scattering potential U the amplitude and interference changes ($R_c \sim 1/B$). For decreasing field B dephasing occurs and must be included.

For increasing radius the results for thin rings may be similar to the ones for planar surfaces of thin films. For thin films one may perform the Balian–Bloch type calculations as sketched in the figure below.

3.2 Thin Magnetic Films

Thin films are of central importance for engineering magnetic material on a nanoscale. Thin transition metal (TM) films, for example, exhibit magnetic properties of interest for many technical applications like magnetic recording. In the following typical results are given which show the dependence of film magnetism on the atomic structure, topology of the film and on film thickness. Magnetic anisotropy is very important. Magnetism is characterized by the

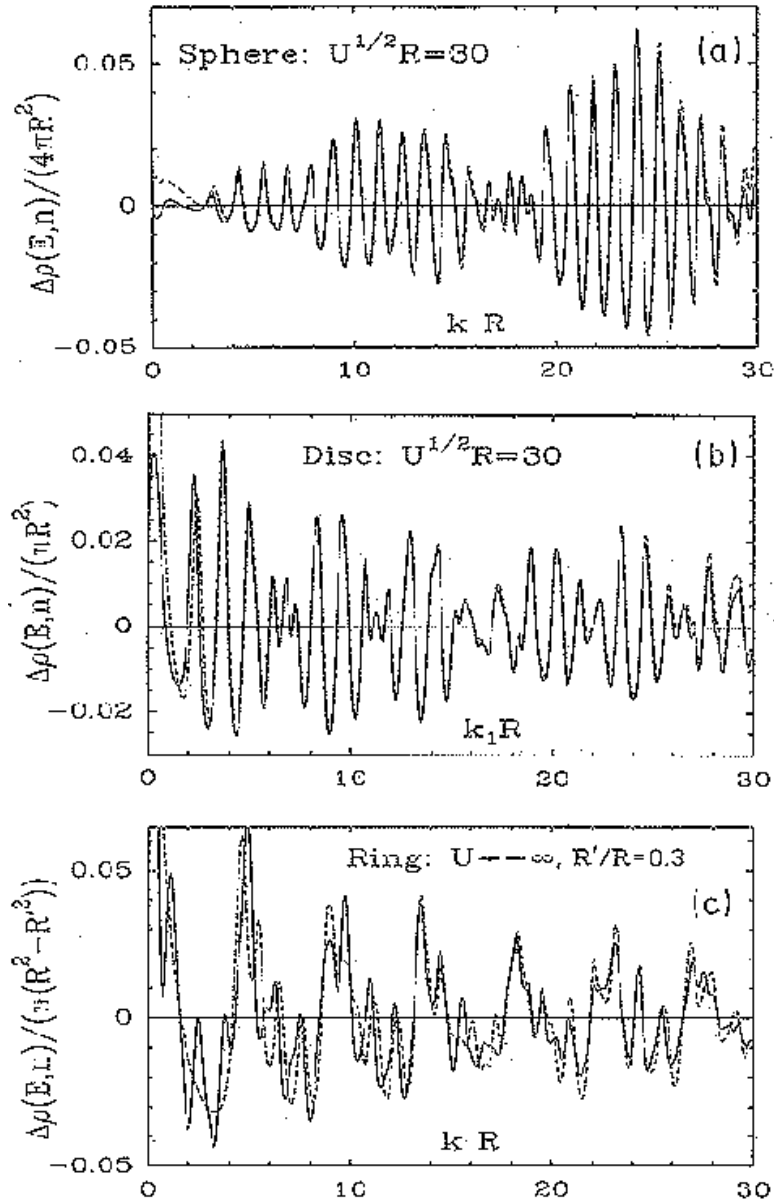


Figure 28: Dependence of the DOS oscillations on dimension and geometry of a mesoscopic system obtained by Stampfli *et al.* using an extension of the Balian–Bloch theory. Results for (a) sphere, (b) disc and (c) ring are given. The electrons are scattered by the potential U . This potential may scatter spin dependently. The dashed curves refer for comparison to quantum–mechanical calculations.

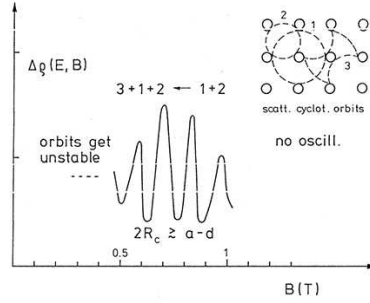


Figure 29: Oscillations of the D.O.S. as a function of magnetic field B for the orbits 1, 2, 3 due to scattering by repelling anti-dots, see calculations by Stampfli *et al.*. The inset shows the lattice of anti-dots. Note, the scattering may be spin-dependent and the density of states is spin split. Note $2R_c \geq (a - d)$ is assumed.

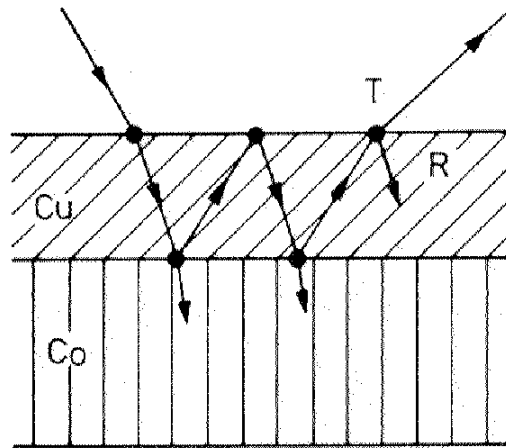


Figure 30: Sketch of the important orbits for thin films. Here, one has to include transmission (T) and reflection (R) coefficients at the corners of the paths. Magnetic films yield spin dependent DOS. Note T and R are spin dependent at interface Cu/Co.

magnetization as a function of film thickness, anisotropy, by the orientation of the magnetization at the film surface and by the Curie-temperature T_c . Nanostructured films exhibit depending on film growth conditions (controlling the film morphology) characteristic magnetic domain structures. Then depending on the distances between the domains various magnetic interactions controlling the global film magnetization come into play.

3.2.1 Magnetic Structure

The magnetic properties of thin ferromagnetic films have been studied intensively. Due to anisotropy long-range ferromagnetic order occurs even for ultrathin, quasi 2d-films. Competing anisotropic forces determine the orientation of the magnetization relative to the atomic lattice. We use the hamiltonian given in Eq.(16) with a local anisotropy

$$H_{anis} = -\sum_i (K_2 \cos^2 \theta_i + K_4 \cos^4 \theta_i + K_s \sin^4 \theta_i) \quad . \quad (67)$$

Note, for $T > 0$ the in-plane anisotropy K_s gets important. After some standard algebra (see Jensen *et al.*) one finds the energy per spin. One gets for

1. uniform magnetic phases:

$$E_u(\theta) = -(9/2)J - K_2 \cos^2 \theta - K_4 \cos^4 \theta - K_s \sin^4 \theta + E_o(\cos^2 \theta - 1/3) \quad , \quad (68)$$

where θ denotes the angle between film normal and magnetization, and for

2. stripe domains with wall width b and domain periodicity $2L$:

$$\begin{aligned} E_{dom}(\theta) = & - J/2(q - \pi^2/bL) - K_2(\cos^2 \theta(1 - b/L) + b/2L) \\ & - K_4(\cos^4 \theta(1 - b/L)) + 3b/8L - K_s(\sin^4 \theta(1 - b/L) + 3b/8L) + \dots \end{aligned} \quad (69)$$

Here, θ denotes the canting angle of the domain magnetization along the z -axis ($\theta = 0$). $q = 4$ for a square monolayer. The domains have the periodicity $2L$ along the y -direction and have an uniform magnetization along the x -direction, inside the domains the magnetization is along $\pm z$ -direction. This domain configuration is assumed for simplicity. One gets rich magnetic behavior for thin films. Magnetic anisotropy is important.

Typical results for the magnetic structure are given in Fig.31. Generally one gets interesting phase diagrams, see Jensen *et al.* [2, 11].

Multilayers of magnetic films reflect how the magnetization of neighboring films interfere, affect each other, act like a molecular field on the magnetization of a particular film.

In Fig.32 results are given for multilayer films Cu-Ni-Cu and Co-Cu-Ni. Note, one finds for the Curie temperature $T_c(Co) > T_c(Ni)$. Clearly, the Co film causes that the magnetization of the Ni film is present at higher temperatures. This results from interlayer exchange coupling.

The results shown in Fig.33 demonstrate the dependence of T_c on film structure. Obviously, interesting characterization of magnetic films is also given by their Curie-temperature.

3.2.2 Reorientation Transition of the Magnetization

The reorientation transition of the magnetization at surfaces (and interfaces) is very important regarding applications, but also regarding understanding of magnetic anisotropy. Such a transition may be driven by temperature, film thickness and film topology (and at nonequilibrium

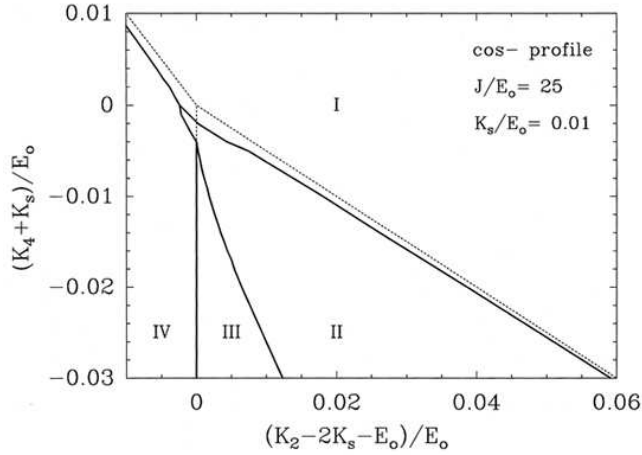


Figure 31: Magnetic structure of thin films obtained at $T = 0$ due to exchange coupling and magnetic anisotropy. Phases *I, II* refer to stripe domain structure with perpendicular and canted magnetization, respectively. Phases *III, IV* refer to uniform magnetization with canted and in-plane magnetization, respectively. (E_o is the demagnetization energy). The anisotropy constants K_2 , K_4 and K_s are given in Eq.(49), their physical significance is clear. The dashed curves indicate what happens if only uniform phases are considered.

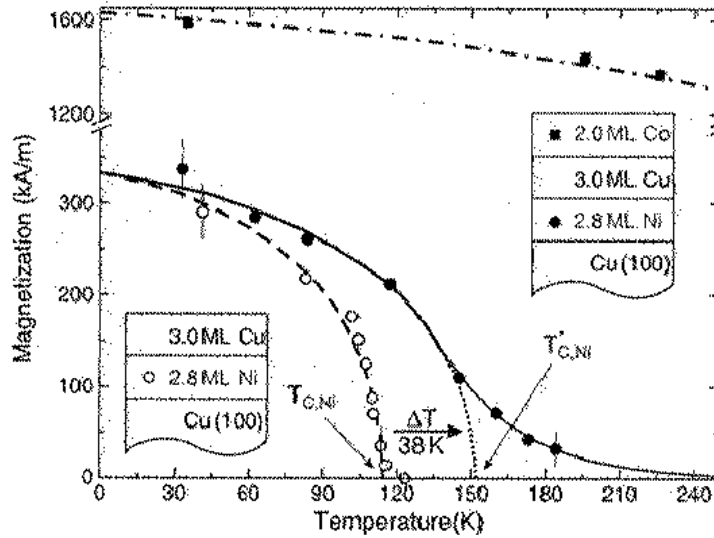


Figure 32: Magnetization of a Co- and Ni-film separated by 3ML Cu-film, see inset Fig.. The experimental results (from XMCD) are indicated by squares and circles. The indicated shift of the Ni Curie-temperature results from interlayer exchange coupling between Ni and Co film.

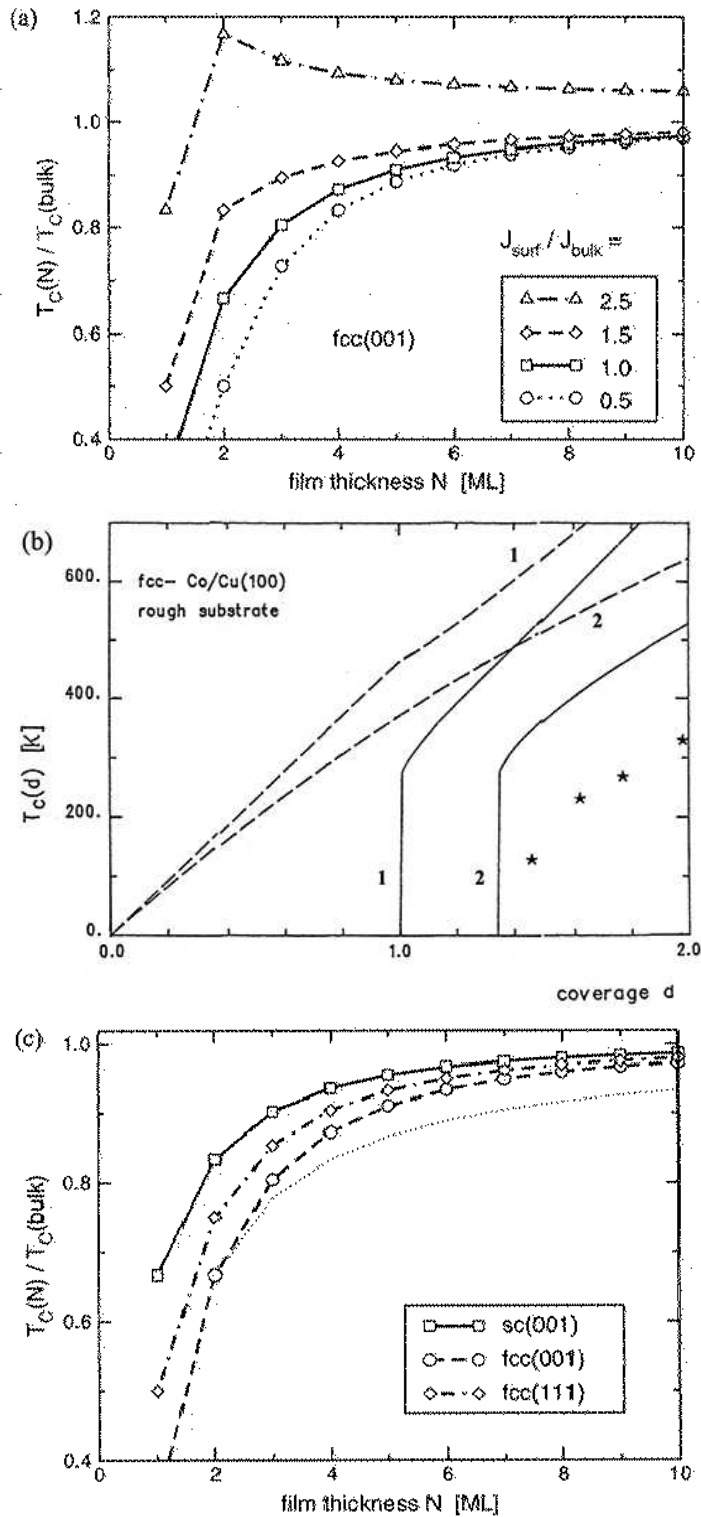


Figure 33: Curie-temperature T_c as a function of film thickness N and morphology. (a) Results obtained using MFA for f.c.c. films. (b) T_c dependence on film topology: (1) Layer by layer film growth. (2) Results refer to rough films and those obtained by random deposition of atoms. The dashed curves refer to Bragg-Williams mean field-theory. The stars refer to experimental results for f.c.c.-Co on Cu(111). (c) Homogeneous ferromagnetic films assuming different film structures, see Jensen *et al.*

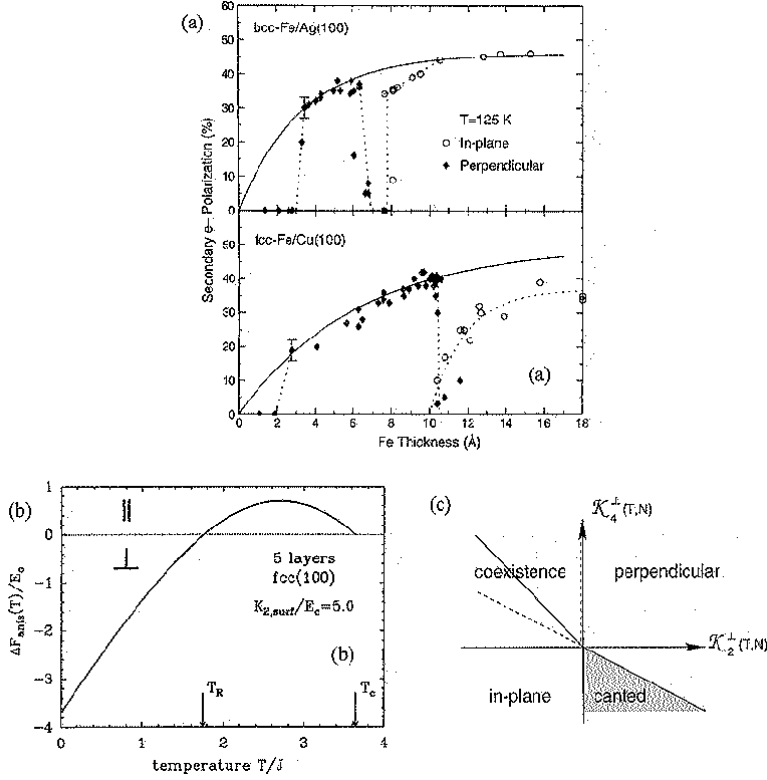


Figure 34: The magnetic reorientation transition. (a) Transition $M_{\perp} \rightarrow M_{\parallel}$. The solid curve gives the magnetization of an uniform (single domain) film, occurring for increasing film thickness and for Fe|Cu films. (b) Free-energy change $\Delta F = F(M_{\perp}) - F(M_{\parallel})$ per spin and for increasing temperature. Magnetic anisotropy is temperature dependent and this causes the reorientation transition at T_R . A fcc(100) film is assumed, see Jensen *et al.*. (c) Phase diagram for the orientation of the magnetization is controlled by the anisotropy parameter $K_2^{\perp}(T, N)$ and $K_4^{\perp}(T, N)$, see Eq.(49). Note, in the coexistence phase the energy minima of the states with perpendicular (\perp) and parallel (\parallel) magnetization are separated by an energy barrier. The P.D. results from minimizing the free-energy (K_4^{\perp} refers to M_{\perp}).

by hot electrons). Magnetooptically the reorientation transition is characterized by the linear response χ_{ij} or the nonvanishing elements of the nonlinear susceptibility χ_{ijl} , for example.

In the following typical results for the reorientation transition of the magnetization are presented. In Fig.34 results are given (a) for thickness induced reorientation transition in b.c.c. Fe films, (b) for temperature induced transition at T_R , and (c) for the dependence of the phase diagram (PD) on anisotropy constants, K_4, K_4^{\perp} and K_4^{\parallel} are included. The free-energy $\Delta F = F(T, \theta = 0) - F(T, \theta = \pi/2)$ is calculated with $F = -\sum_i K_{2i}(m(T)) \cos^2 \theta + \dots$. Here, i refers to the film layer and θ to the angle between film normal and direction of magnetization, see Jensen *et al.* [2, 7]. Note, $\Delta F < 0$ indicates a perpendicular magnetization and $\Delta F > 0$ an in-plane one.

3.2.3 Magnetooptics

Magnetism of thin films and multilayers thereof is well determined by their magneto-optical behavior. In particular SHG sensing sensitively structural symmetry, surfaces and interfaces,

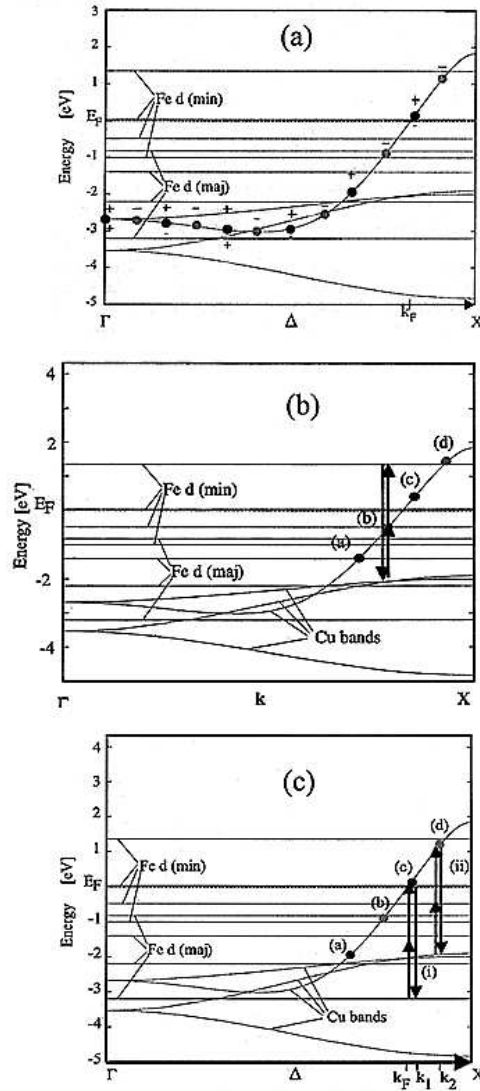


Figure 35: Magnetooptics of thin films (xCu/Fe(001)) involving quantum well states (QWS) due to confinement. As a consequence of QWS presence the SHG is strongly film thickness dependent. SHG involving QWS exhibits characteristic SHG oscillations. (a) QWS in thin films, the parity of the wave functions is indicated by (+) and (-). Energies of QWS along $\Gamma \rightarrow X$ direction of BZ are given. Black dots refer to a 6ML film and black and grey dots to a 12ML film. The parity of the states is indicated. (b) SHG involving as intermediate state an occupied QWS below the Fermi-energy, the final state is a Fe d-state. Transitions contributing dominantly to SHG are shown. One gets corresponding SHG oscillations as a function of film thickness. (c) Interference of SHG from surface and interface is negligible (for example (xCu/Fe(001))). The important SHG optical transitions involving QWS as final states are indicated. Transitions (i) are possible for Fe films with 6ML and 12ML, (ii) only for films with 12 ML Fe. Thus, one gets SHG oscillations having a 6ML period. For details see discussion by Luce and Bennemann (*Nonlinear Optics, Oxford*).

is very useful for studying magnetic properties of nanostructures. Magnetic thin films cause characteristic SHG reflecting magnetism, since the nonlinear susceptibility χ_{ijl} determining the light intensity $I(2\omega)$ of SHG depends on magnetization \vec{M} .

As usually one splits the susceptibility in parts even and odd in M and then the magnetic contrast

$$\Delta I(2\omega) \propto I(2\omega, M) - I(2\omega, -M) \quad (70)$$

yields sensitively the magnetic behavior. Resonantly enhanced SHG transitions of the ferromagnet which states are spin split are a sensitive measure of magnetism. Note, the interference of SHG from the film surface and interface (film/substrate) is of interest, in particular if magnetism is different at surface and interface, see Fig.11.

In table 1 characteristic features of SHG response from thin films are given. We refer to weak interference of SHG when $\chi^i \gg \chi^s$ and to strong interference when $\chi^i \approx \chi^s$. Note, the wave vector \vec{k} selectivity is controlled by band-structure. For the film system Cu/Fe/Cu the dipole matrix elements with d -states cause $\chi^i \gg \chi^s$. For Au/Co/Au films no Co d -states are involved and therefore $\chi^i \approx \chi^s$. The periodic appearance of QWS for increasing film thickness may cause oscillations in SHG.

In thin films (which may be described with respect to their electronic structure by potential wells) one gets QWS (quantum well states) and corresponding contributions to MSHG (magnetic second harmonic light). As supported by experiments QWS in thin films may contribute strongly to SHG (quasi resonantly enhance SHG). Since the occurrence of QWS is dependent on film thickness, one gets QWS involving characteristic oscillations in SHG as a function of film thickness. These oscillations depend of course on light frequency, magnetism, parity of the QWS, inversion symmetry of the film and interference of SHG from surface and interface.

If interference of nonlinear light from surface and interface is important, then SHG response depends on QWS parity. As a consequence only a period twice as large as for the linear Kerr effect optics appears. If this interference is not so important, then SHG exhibits typically two oscillation periods. For details of such behavior see Luce, Bennemann ([12]) and also discussion given previously, see Fig.18 etc..

SHG involving QWS is shown in Fig.35. In Fig.35(a) thin film QWS and their parity are sketched. The Figs. refer to xCu/Fe(001) system. For other systems the analysis is similar. Fig.35(a) shows the energies of the QWS. The parity is indicated by (+) and (-). Note, at the Fermi energy a parity change occurs. The spin polarized d -states of Fe are also shown. In Fig.35(b) dominant SHG contribution resulting from an occupied QWS below the Fermi-energy is illustrated (final state of SHG transition is a d -state of Fe). In Fig.35(c) SHG involving unoccupied QWS is shown. Note, states along $\Gamma \rightarrow X$ direction in the Brillouin zone (BZ) are most important. Interference of surface and interface SHG is negligible. Dominant SHG transitions are indicated: (i) are possible for 6ML and for 12ML of Cu. This gives oscillations with a period of 6ML. (ii) possible only for 12ML. Thus, one gets two different oscillations (which are frequency dependent, at k_1, k_2 in the BZ).

Note, for $\chi^i \chi^s \rightarrow -1$ one gets a cancellation of the thickness dependent contribution to SHG due to QWS. If χ^i and χ^s become comparable parity of QWS gets important. For example, for a dominant QWS close to the Fermi-energy one gets oscillations only for one with odd parity, see discussion by Luce *et al.* [12].

This shows the interesting magneto-optical behavior of thin films.

3.2.4 Nanostructured Thin Films with Magnetic Domains

General remarks: In the following the magnetic properties of generally irregular nanostructures at equilibrium and nonequilibrium are discussed. Generally one observes that the magnetic properties of nanostructured films depend on the film growth conditions. During growth irregular film structures with varying island sizes, shapes appear. Competing interactions between islands (exchange, dipole,...) occur. Magnetic anisotropy controls the formation of domains, their size and shape and magnetic relaxation of the domains. The relaxations determine the transition from nonequilibrium to equilibrium. In view of the complex behavior one may use Monte Carlo simulations. To describe the transition from isolated islands to connected ones correlations of magnetic relaxation (of neighboring islands) must be taken into account. For example cluster (island) spin flips will lead to a much faster magnetic relaxation than single spin flips.

Main questions are (1) what is the domain structure, (2) what is the time dependent approach of the film magnetization towards equilibrium, (3) what are the controlling forces. If only short range interactions (exchange ones) are active then one expects that percolating atomic structures (coverage $\theta \geq \theta_p$) are necessary for long range global magnetic ordering. Ordering for coverages below θ_p might indicate dipolar interactions.

The time-dependent structural and magnetic behavior of films during growth reveals many interesting properties and in particular the important interplay of atomic structure and formation of magnetic domains and global film magnetization. As the film growth the size of the domains, its surface roughness and the orientation of the domain magnetization changes. Magnetic relaxation occurring typically on a ps to ns time scale causes in thin films a time dependent magnetization which approaches only at relatively long times (via thermal activation etc.) the equilibrium magnetization. Depending on the domain size and distances between the domains exchange or magnetic dipole coupling may dominate and cause corresponding, different relaxation. Thus, the approach of inhomogeneous ultrathin films towards equilibrium magnetization and its dependence on film topology requires careful studies.

Important parameters controlling film behavior are the blocking temperature T_{bl} ($T_{bl} \sim KN/k_B \ln(t_{exp}\Gamma_o) \sim 5K$), for $N \simeq 1000$ atoms resulting from magnetic anisotropy and the percolation coverage θ_p . While magnetic ordering due to exchange coupling occurs for $T < T_c \sim J$, long-range magnetic dipolar coupling causes ordering for $T \leq T_{dip} \sim (N\mu)^2/R^3$ (which for $N=1000$ atoms gives about 5K). R refers to the distance between domains. As mentioned due to its complexity analysis requires generally Monte Carlo simulations, see Jensen *et al.* [8, 11]. In Fig.36 magnetic domain relaxation is sketched and the typical energy barriers against reversal of the direction of an island (domain) magnetization are shown.

The magnetic relaxation is calculated using a Monte Carlo method and a Markov master equation

$$dP(x, t)/dt = -\Sigma\Gamma(x \rightarrow x')P(x, t) + \Sigma\Gamma(x' \rightarrow x)P(x', t) \quad ,$$

where P gives the probability of a spin state $x = S_1, S_2, \dots$ at time t . $\Gamma(x \rightarrow x')$ denotes the transition rate. $\langle M(t) \rangle \propto \Sigma_i M_i(t)$, i = time steps taking into account possibly coherent spin flips of connected domains, see Brinzanik, Jensen *et al.* [11]. The Markov equation in combination with the M.C. statistical methods yields the time dependent non-equilibrium magnetization and its relaxation towards the equilibrium one. Depending on the density of the domains, their distance, correlated relaxation of neighboring domains occurs. This is demonstrated in Fig.36(c) where results obtained assuming cluster spin relaxation vs. single spin relaxation are

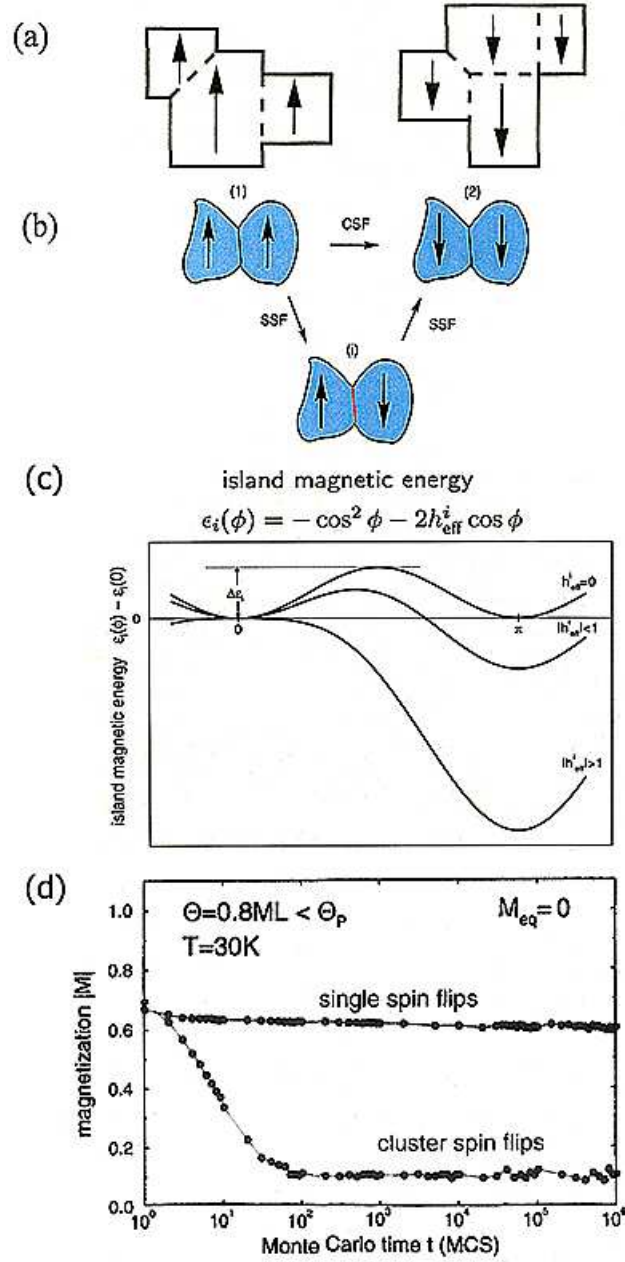


Figure 36: Sketch of (a) coherently relaxing connecting magnetic domains. (b) relaxing domains illustrating model assuming coherent relaxation and successively single domain relaxation used by Jensen *et al.* (CSF: Coherent spin flip of neighboring domains, SSF: Single domain spin flip). (c) energy barrier of a domain on which a molecular field h_{eff}^i acts for magnetization reversal. The barrier energy ($\epsilon_i = E_i^b / KN$) controls the reversals of the domain magnetization and results from magnetic anisotropy ($\sim K$) and (interdomain, interlayer) molecular field h_{eff}^i . (d) Test results for the relaxation of the magnetization using CSF approximation.

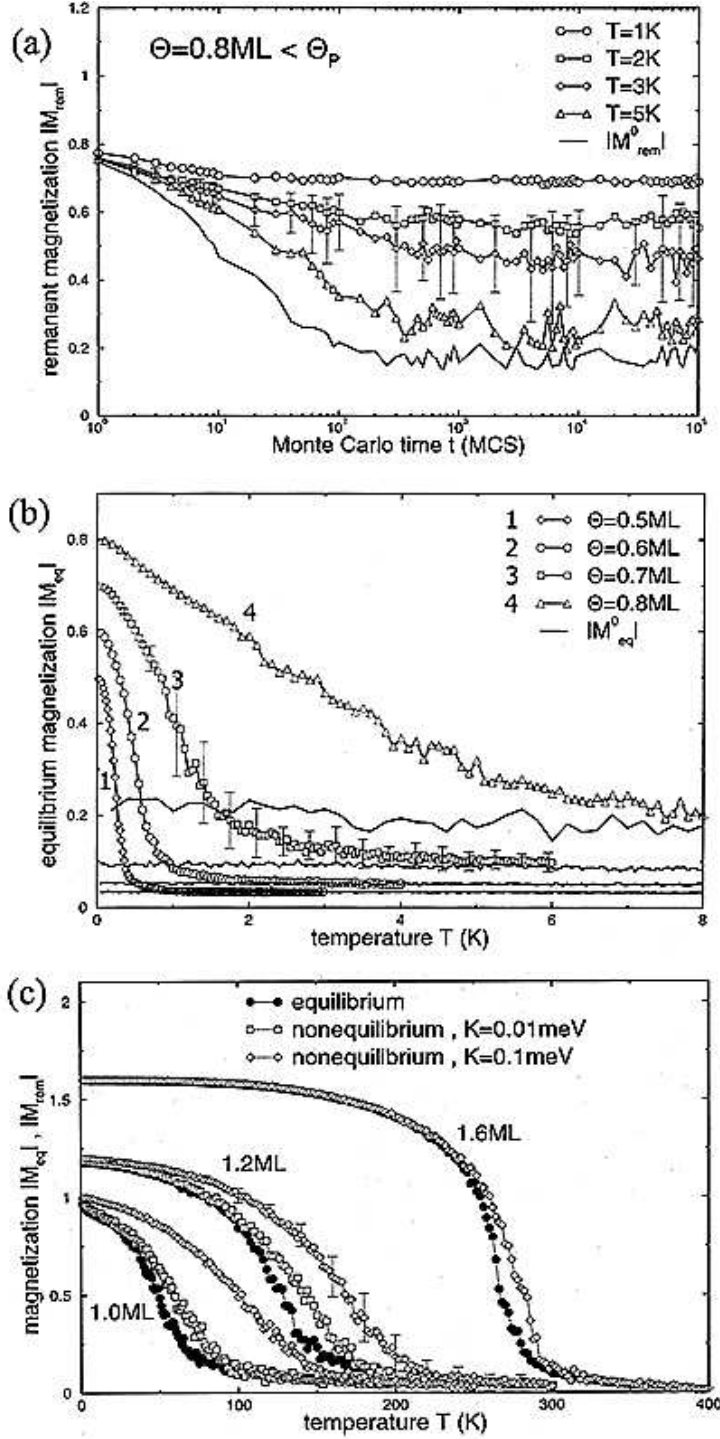


Figure 37: Magnetic relaxation in thin films for different film thickness and temperature. (a) Time dependent long range ordering in case of exchange and dipole coupling and for varying temperature. Note, $\theta < \theta_p$. The relaxation starts from fully aligned domain magnetization. At low temperatures ($T \sim 1K$) a stable magnetization due to dipole interactions is obtained. (b) Equilibrium magnetization as a function of temperature for $\theta < \theta_p$. Here, θ_p denotes the percolation coverage ($\theta_p = 0.9ML$). (c) Equilibrium magnetization as a function of temperature for different anisotropy (K) and film thickness. Note, the difference between nonequilibrium and equilibrium magnetization.

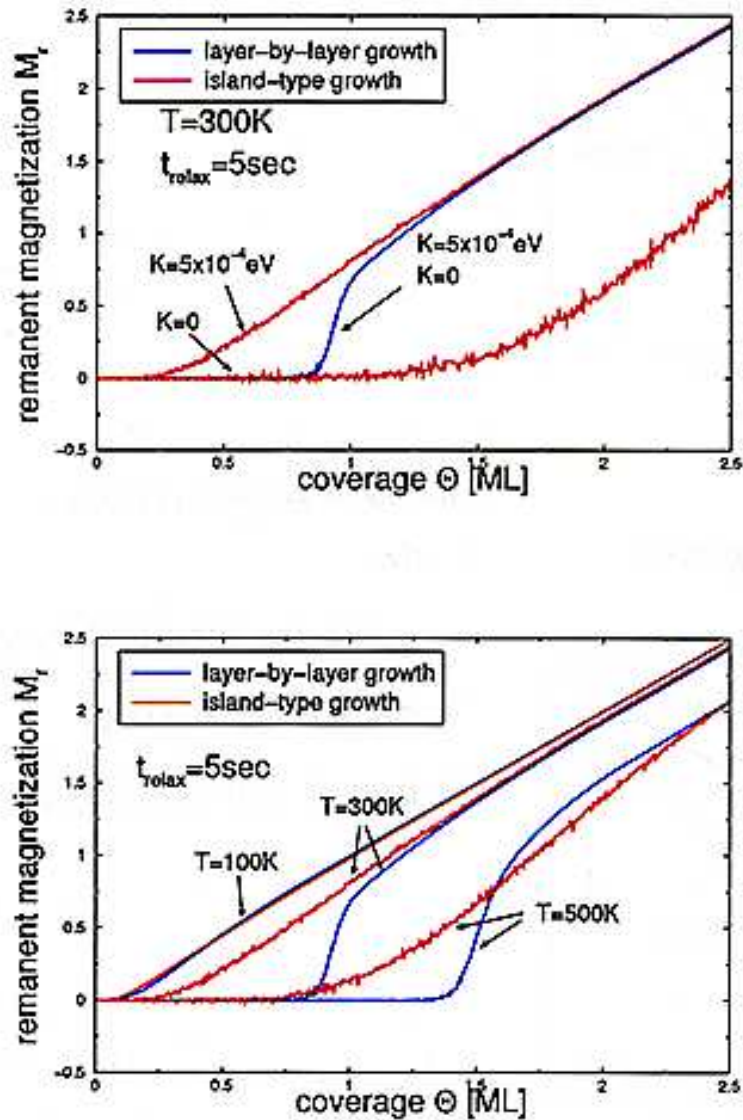


Figure 38: Magnetic relaxation dependence on film structures, on growth mode, layer by layer vs. island growth. Note, dependence on anisotropy K and temperature. (upper Fig.) For island growth the magnetization depends strongly on magnetic anisotropy (K). (lower Fig.) Magnetization in case of layer by layer growth depends strongly on exchange interactions between islands.

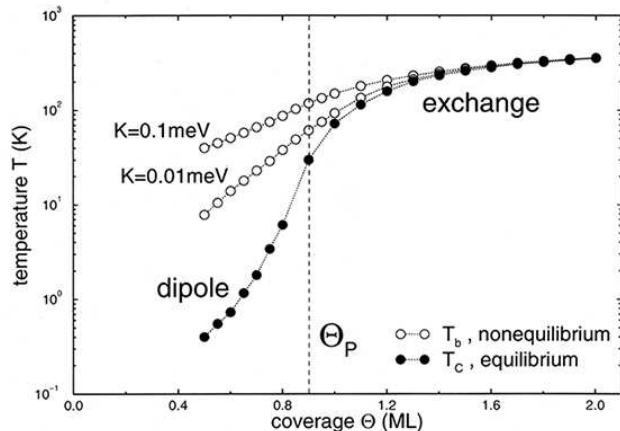


Figure 39: Dependence of Curie-temperature T_c and blocking temperature T_b on film thickness (coverage θ). θ_p denotes the percolation coverage. Note, a semilogarithmic plot is used. The curve for the ordering temperature due to dipole coupling neglects for simplicity domain wall energy. As $\theta \rightarrow \theta_p$, the exchange interactions begin to dominate, for $\theta < \theta_p$ dipole coupling plays a role and yields a small T_c . The nonequilibrium behavior is mainly due to magnetic anisotropy.

shown.

For a domain structured film the film magnetization is given by

$$\vec{M} \propto \sum_i m_i N_i \langle \vec{S}_i \rangle, \quad (71)$$

where \vec{M} points along the easy axis and i refers to the i -th island with m_i aligned magnetic moments. Here, one averages over the magnetization directions of the domains. (The kinetic Monte Carlo method gives after equilibration for the average magnetization $\langle M \rangle \approx (1/R) \sum_{r=1}^R M_r(t)$).

In Fig.37 magnetic relaxation of thin films is shown (for details see Jensen *et al.*) [11]. Results obtained below and above percolation coverage θ_p are compared. Note, (for $\theta > \theta_p$) the strong influence of single island anisotropy K on relaxation. For increasing connectivity of the islands faster relaxation results from exchange interactions between islands. Note, the temperature and film thickness dependence of the relaxation.

The MC results demonstrate that faster relaxation occurs for correlated spin flips (CSF), as expected of course. As also expected different T_c behavior occurs below and above percolation coverage (θ_p).

In Fig.38 it is shown how the relaxation of the magnetization depends on the atomic film structure. The dependence of the remanent magnetization of a film on its growth mode, layer by layer or island type one is given. Note, the dependence of the results by Jensen *et al.* on anisotropy and temperature.

In Fig.39 ordering in thin films is characterized. Depending on the density of domains exchange and dipolar coupling act differently. Clearly the percolation coverage is an important control-parameter for the magnetic behavior and range of magnetic interactions. At low coverage dipole coupling may dominate and then ordering occurs at low temperatures.

In Fig.40 the dependence of magnetic behavior, of domain structure on film morphology is shown. Results were obtained by Jensen *et al.* using a kinetic M.C. simulation and Markov equation for the relaxation of the magnetic domains are given. Film structures resulting from an

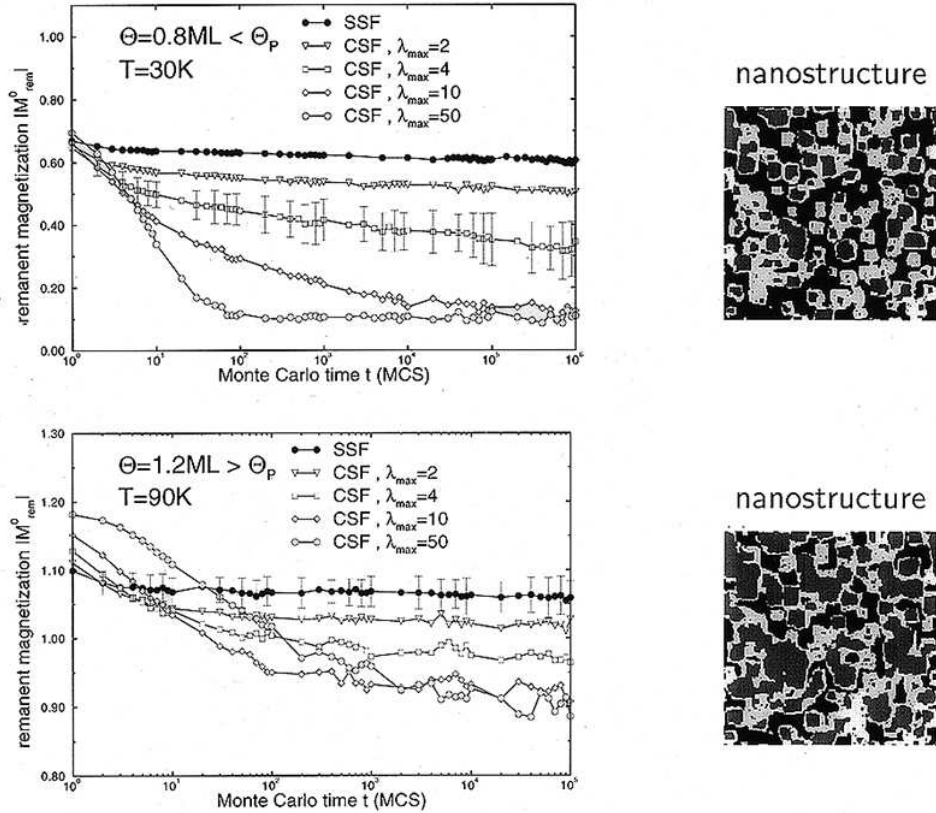


Figure 40: Magnetic relaxation in domain structured thin films using Monte Carlo type calculations performed by Jensen *et al.* [11]. λ refers to different spin clusters and θ_p to the percolation coverage. CSF refers to correlated cluster (island) spin flips. For comparison also results are given assuming single spin flips (SSF). The atomic nanostructures corresponding to the magnetic domain structures are also shown and were obtained using an Eden growth model, for details see Jensen *et al.*. Regarding nanostructures white and grey areas refer to magnetic domains and black areas to uncovered surface of the thin film.

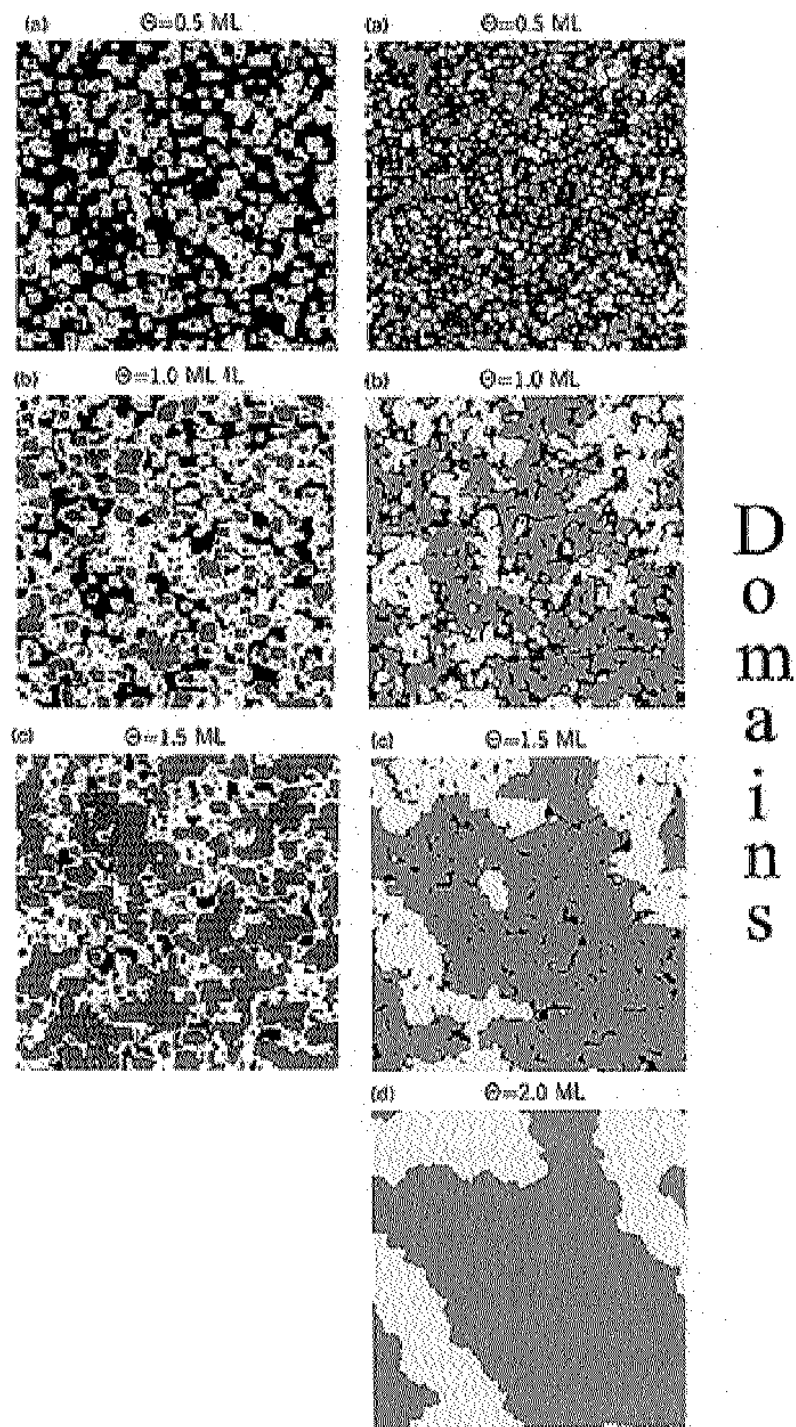


Figure 41: (left) Film nanostructures using Eden type growth model, (black: uncovered surface, grey (light) to first layer atoms, dark to first layer atoms); (right) corresponding resulting magnetic domains and their dependence on film thickness. (black: uncovered surf., grey: two opposite magnetic directions). Only domains at the surface are marked, see results by Brinzanik *et al.*.

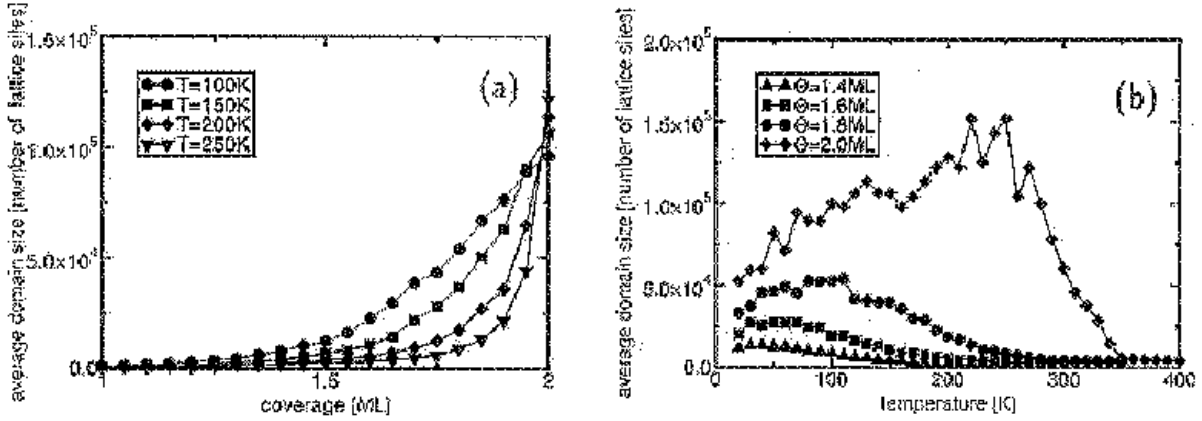


Figure 42: Average magnetic domain size as a function (a) of coverage (film thickness) and (b) temperature. The film growth model is described in the text (see Jensen *et al.*). The percolation threshold is $\theta_p \sim 0.9ML$.

Eden growth model and resulting magnetic domains are shown [8, 11]. Regarding calculations an area of 500×500 lattice constants is taken which contains about 1250 islands. λ refers to different spin cluster sizes.[2, 8, 11]

Of course, magnetic ordering in thin films depends sensitively on topology and film thickness and the dominant magnetic coupling between domains. Results presented demonstrate this.

The results presented in Fig.41 for the domain size (and results on their roughness and surface) are very important regarding understanding of magnetic behavior of irregular thin films and applications.

In Fig.41 results are given for the magnetic domain structure in thin films having different thickness. Of course, the magnetic domain structure changes and the size of the domains increases as the film thickness increases.

In Fig.42 results for magnetic domains and their size dependence on film thickness and temperature are given. These were obtained using the previously discussed analysis by Jensen *et al.*. Note, as a function of temperature one may get a maximum in the domain size. The reason is that for low temperatures domain growth is hindered by energy barriers and at higher temperatures thermal activation disintegrates domains.

Note, generally for increasing film thickness the domains which are first isolated begin to merge and form larger connected areas, still markedly affected by the atomic nanostructure of the film. The roughness of the domains is affected by the nanostructure and decreases for thicker films and for increasing temperature. Of course, this is expected on general physical grounds.

3.3 Tunnel Junctions: Magnetic Effects

Nanoscaled tunnel junctions offer interesting physics in particular regarding quantum mechanical effects and spin dependent currents, separation of charge and spin currents and their interdependence. Also one may use such nanostructures ($FM | M | FM$), M = normal state, superconducting state, etc.) as interesting fast switches and magnetoresistance devices. Note,

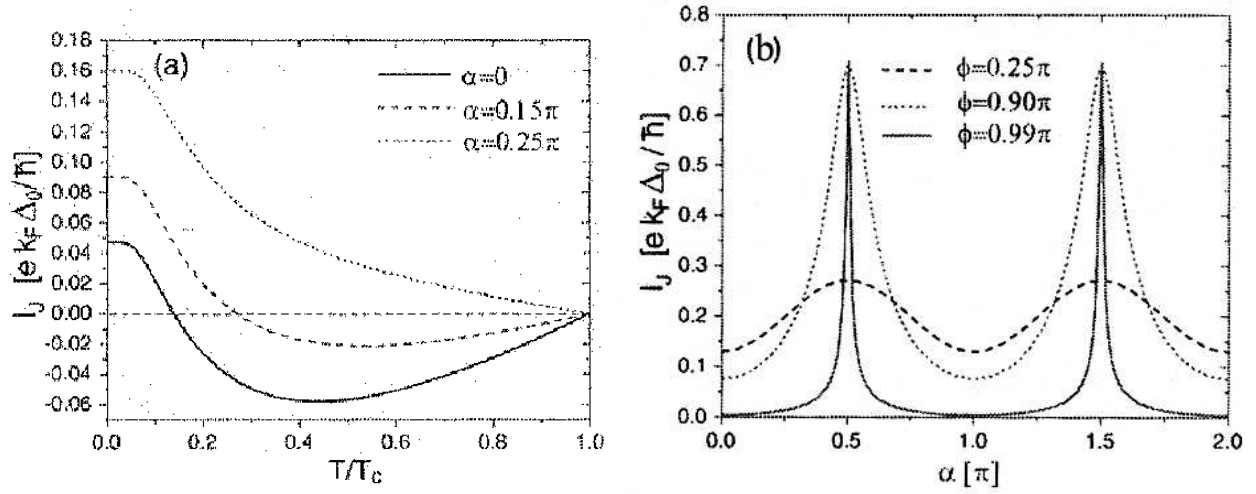


Figure 43: Tunnel junction ($TSC | FM | TSC$), where FM and TSC refer to a ferromagnet and triplet superconductor, respectively, ϕ to the phase of the superconductor: (a) Josephson current I_J as a function of temperature (changing sign), (b) I_J as a function of α , the angle between magnetization \vec{M} and direction normal to the current. Note, I_J may be switched between zero and a finite value.

the Josephson tunnel current is carried by Andreev–states, see Kastening, Morr *et al.*. In the following some examples are discussed. Note, different behavior may result dependent on times τ_{CP} , τ_s , and τ_t referring to Cooper pairs, spin diffusion and tunneling transport time, respectively.

For a tunnel junction

$$(TSC | FM | TS) \quad (72)$$

where TSC denotes a triplet superconductor and FM a ferromagnet, one gets interesting behavior of the Josephson current j_J as a function of temperature, α and θ . The angles α and θ determine the direction of the magnetization of the ferromagnet and the direction of the TSC–order parameter, see Fig.20(b) for illustration. The Andreev states are determined from $H\psi_j = E\psi_j$ using Bogoliubov–de Gennes method.

As shown by Fig.43 the Josephson current may change sign as a function of temperature and may be switched between zero and finite value upon varying the angles α , θ . The unconventional change of sign of I_J (without change of phase) for increasing temperature results from the changing occupation of the Andreev states and from the factor $\frac{\partial E_i}{\partial \phi}$ in the expression for the tunnel current. Note, this sign change is different than the one observed for singlet superconductors with a ferromagnetic barrier in between. The behavior of I_J for rotating magnetization, as a function of α , suggests to use such junctions as switching devices. Note, for increasing ϕ the current changes more drastically.

Of particular interest is the behavior of I_J as a function of phase ϕ (for $T=0$) shown in Fig.43(b). Then only the states $E_i < 0$ are occupied. For (1) $M \parallel d_{L,R}$, $\alpha \neq \pi/2$, the ferromagnet (FM) couples Andreev states, and (2) for $\vec{M} \perp \vec{d}_{L,R}$ the Andreev states are not coupled by the FM and spins are well defined.

Clearly the above junction would be a sensitive probe to detect triplet superconductivity, see results by Morr *et al.* [3].

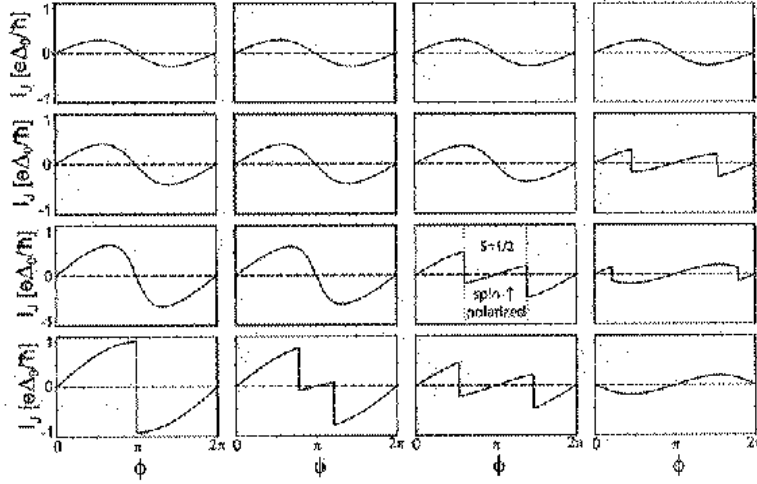


Figure 44: Josephson current I_J at $T = 0$ for a junction (SC/FM/SC) as a function of phase ϕ of the superconductor for several values of the scattering strength g and z of the magnetic and nonmagnetic potential, respectively ($g = 0, 1/3, 2/3, 1$ from left to right, $z = 0, 1/3, 2/3, 1$ from bottom to top), see results by Kastening, Morr *et al.*. Note, the ferromagnet is approximately represented by a potential barrier.

Another tunnel system is one involving singlet superconductors,

$$SC | FM | SC \quad . \quad (73)$$

The FM is approximately represented by a barrier potential scattering spin dependently the electrons (g refers to the magnetic scattering strength, z to the non-magnetic one). Again, depending on nonmagnetic and magnetic scattering of the tunnelling electrons the Josephson current may change sign as a function of temperature T and furthermore as a function of the relative phase of the two superconductors, see Fig.43 and Fig.44. (Note, $I_J = I_\uparrow + I_\downarrow$, $I_s = I_\uparrow - I_\downarrow$, the Josephson current I_J is solely carried by the Andreev states, the total spin current $I_s = 0$, since spin current through Andreev states is canceled by the one through the continuum states).

For $z \gg g$ one gets $I_J = (e\Delta_0/\hbar) \frac{\sin \phi}{2z^2}$ and non magnetic current is dominated by Cooper pairs. For $g \gg z$ one has $I_J = -(e\Delta_0/\hbar) \frac{\sin \phi}{2g^2}$ and current is carried by single electrons. Note, then the phase shift by π . Results assume for the thickness of the tunnel junction d to be smaller than the coherence length, otherwise the situation is more complicated.

Note, the sign change of the Josephson current as a function of temperature shown in Fig.45 results not from a transition of the junction from a π -state at low temperature to a 0-phase at high temperature, but from a change in the population of the Andreev states (while the relative phase between the superconductors remains unchanged).

Also interestingly, the total spin polarization of the two superconductors ground state changes from $\langle S_z \rangle = 0$ to $\langle S_z \rangle = 1/2$.

Of course, as mentioned already interesting results are also expected for $(FM_1/SC/FM_2)$ junctions. The tunnel current depends on the superconducting state, singlet vs. triplet. Also a spin current is expected for $\tau_s > \tau_t$, times refer as before to times without spin flip and tunneling time. Singlet superconductivity may block tunneling. For a triplet superconductor the angle between Cooper pair angular momentum \vec{d} and \vec{M} may control the tunneling.

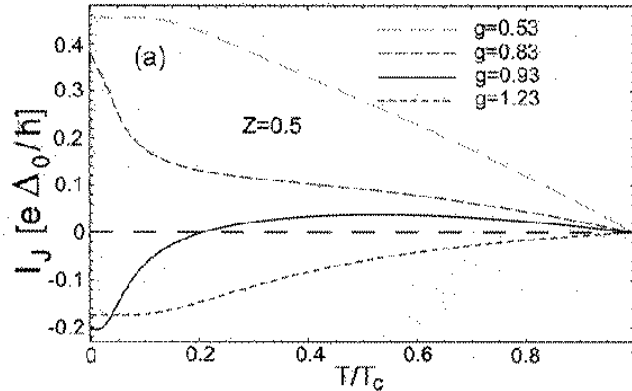


Figure 45: Josephson current I_J of a tunnel junction (SC/FM/SC) as a function of $\frac{T}{T_c}$ for $\phi = \pi/2$ and nonmagnetic scattering strength $z = 0.5$ and several values of g , the magnetic scattering strength.

Transport between quantum dots: An interesting case of electron transport (electron pump model) between two quantum dots involving possibly Coulomb- and spin-blockade (see Hubbard hamiltonian with spin dependent on-site interaction) is illustrated in Fig.20(a). Driving the current with a pulsed (polarized) external field to overcome an energy barrier one gets spin-dependent charge transport with v. Stückelberg oscillations due to bouncing forth and back of the electrons between the two quantum dots.

In Fig.46 results are given for the photon assisted tunneling between two quantum dots. The applied electromagnetic field is given by $V(t) = V_0 \cos(\omega t)$. Note the dependence of the charge transfer on the duration of the applied light pulse and the Rabi oscillations due to the bouncing back and forth of the electrons. The Rabi oscillation frequency is $\Omega = 2\omega J_N(E = V_0/\hbar\omega)$. Here J_N is a Bessel function of order N , where N refers to number of photons absorbed to fulfill resonant condition $N\hbar\omega = \sqrt{\Delta\varepsilon^2 + 4\omega^2}$. Different frequencies are used which cause resonant absorption of one, two and three and possibly more photons. Of course this affects the charge transfer. The time resolved analysis of the occupation of the electronic states shows that system if connected to reservoirs acts as electron pump. Before action of the external electromagnetic field the initial state is $n_1 = 1$ and $n_2 = 0$. After the pulse is over oscillations disappear and one gets again the initial state via transferring one electron to the right quantum dot and the left reservoir donating one electron to the left quantum dot, see Garcia *et al.* [3]. Spin dependent quantum dot electron states cause spin currents.

Of interest is also the coherent control of photon assisted tunneling between quantum dots and its dependence on the shape of the light pulse, see Grigorenko, Garcia *et al.* [3]. The shape of the external electric (or magnetic pulse) may be optimized to get a maximal charge or spin current between the quantum dots connected to two metallic contacts.

Note, these results are also of interest for Fermion or Boson systems on optical lattices, its dynamics and interaction with external fields. Optical manipulation of molecular binding, in particular Boson formation induced by an electromagnetic field is an option. In intense fields nonlinear behavior may be particular interesting. Furthermore, on optical lattices one may study in particular the interplay of magnetism and lattice structure, the transition from local, Heisenberg like to itinerant behavior of magnetism. Important parameter for the occurrence of ferromagnetism (antiferromagnetism) are Coulomb interactions and particle hopping (kinetic energy) between lattice sites, and possibly also spin-orbit coupling. Note, as indicated

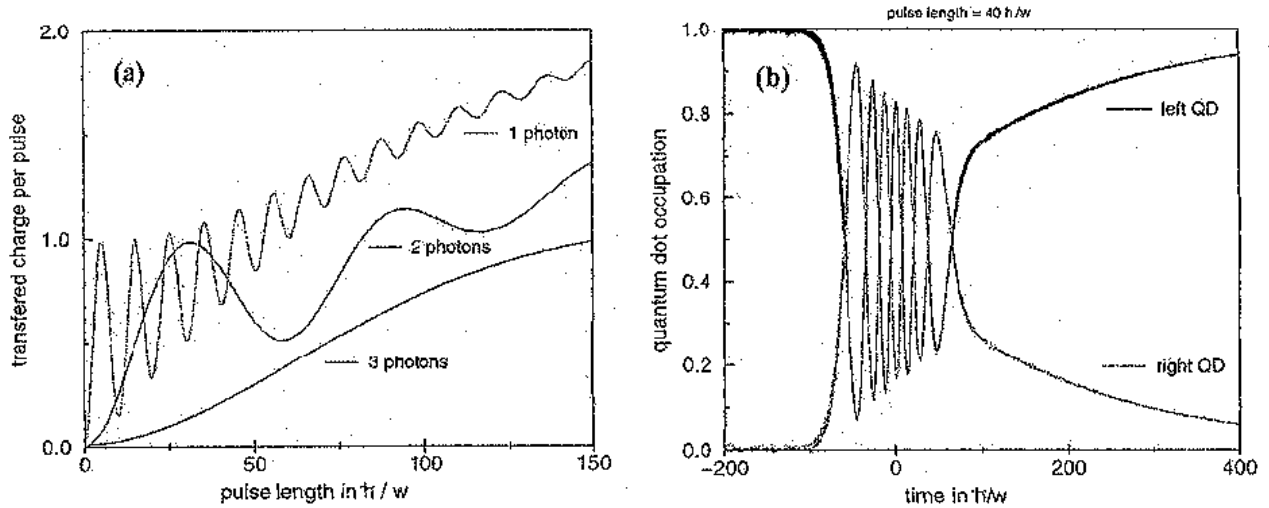


Figure 46: Charge transfer between two quantum dots exhibiting Rabi (v.Stückelberg) oscillations due to bouncing electrons between the quantum dots. (a) Dependence of transferred charge on pulse duration of external field and for different frequencies $\omega_1, \omega_2, \omega_3$ which cause resonant tunneling by absorption of one, two and three photons, respectively; (b) Time dependent occupation of quantum dot states, see results by Garcia *et al.*. Note, for spin dependent quantum dot states (magnetic quantum dot), see Fig.20(a), the results depend on the light polarization and may involve spin dependent currents.

by Hund's rules ferromagnetism could occur already for a Fermi-liquid with strong enough repulsive Coulomb interactions, quasi irrespective of the lattice structure, since spin polarization (together with the Pauli principle) may minimize the repulsive Coulomb interactions. In case where a.f. dimerization of neighboring lattice sites yields Boson formation and resulting BEC condensation optical influence, also of the magnetic excitations, is an important option.

In Fig.47 the possibility of manufacturing optically an ultrafast switching device is sketched. Note, in general changing in nanostructures the magnetization generates in accordance with Maxwell-equations light.

Via hot electrons fast changing temperature gradients may yield interesting and novel behavior of tunnel junctions. Possibly in such way Onsager theory can be tested for nanostructures.

For further discussion of the interesting physics realized by tunnel systems, the interplay of spin and charge currents (see continuity equation for the spin density) and of accompanying light (see Maxwell equations), one should study the literature, see Nogueira, Bennemann *et al.* [3] and Bennemann [13].

Currents in Mesoscopic Structures: As mentioned already for mesoscopic structures like discs, quantum dots and rings, for example, one might get interesting topological effects and persistent currents driven by phases resulting from the Aharonov-Bohm effect [14]. One may derive such currents induced by a magnetic field B from $j = \frac{\partial \Delta F}{\partial \phi}$, where F refers to the free-energy. From symmetry considerations one gets $\Delta F \propto \cos BS$, where BS is the flux enclosed by a ring for example, and for the current

$$j \propto \sin BS. \quad (74)$$

Here, the phase shift $\Delta\phi = \pm BS$ results from encircling the center (of the ring, disc, etc.)

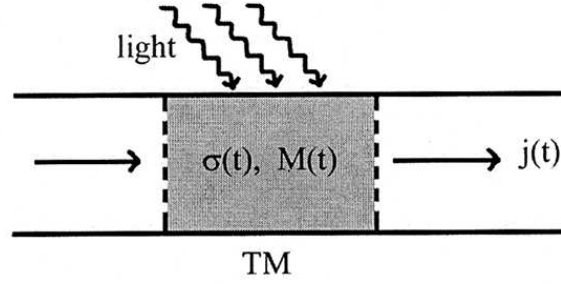


Figure 47: Illustration of a tunnel junction which may act as an ultrafast switching device due to optical excitation of (hot) electrons. Magnetization changes as the electronic temperature changes.

clockwise or counterclockwise. Note, as in the case of superconductors flux quantization may occur. Dynamics due to $B(t)$ or $M(t)$ is of course reflected in the induced current. Also electron scattering causes dephasing etc. and affects the current.

The induced currents due to the Aharonov–Bohm effect with details of their oscillations can be calculated from

$$j = \partial\Delta F/\partial\phi = -e/\hbar \sum \partial E_i/\partial\phi \tanh(E_i/kT) \quad (75)$$

and using the Balian–Bloch type theory developed by Stampfli *et al.* for calculating $E_i(\phi)$ and taking into account clockwise and anticlockwise encircling the center. For narrow rings one expects that mainly orbits 1, 2, 3 are important. A magnetic field B causes the phase shift $\Delta\phi = \Delta\phi_1 + \Delta\phi_2$ due to path deformation and flux, respectively ($\Delta\phi_2 = BS_{\pm}$, where S refers to the area enclosed by the orbit and \pm to clockwise or counterclockwise encircling of B), see Aharonov–Bohm effect. Thus, one gets for the current induced for example by the field B into a narrow ring the expression

$$j \propto \sum_t \sum_p a_{tp} \sin \phi_n \sin \phi_{tp}(\dots) + \dots \quad (76)$$

Here, $\phi_n = BS_0$ denotes the quantized flux in units of hc/e of the orbit characterized by t and p (describes Aharonov–Bohm effect) and ϕ_{tp} results from the path deformation due to the field B . Note, the factor (...) causes rapid oscillations described by exponentials, see Stampfli *et al.* Interference of contributions from different paths may yield a beating pattern for the current oscillations. Generally the oscillations resemble those discussed for the DOS, see Figs. Since the coupling of the induced currents is given by terms $j_{\mu}A_{\mu}$, where A_{μ} refers to the vector potential of B , one gets generally that the induced current decreases quadratically with the ring radius R ($j \propto R^{-2}$). [14] The fine structure of the current oscillations reflects the quantization of the enclosed flux. In accordance with le Chatelier principle the magnetic field associated with the induced current should counteract the external field B .

Of course, dephasing expected for strong scattering of the electrons and large rings (and discs) weakens and possibly destroys the current. Also for ferromagnets (Ni, Fe, ...) one expects spin currents (due to DOS-effects etc.). For spin currents also spin orbit coupling may play a role, see Aharonov–Casher effect. [14]

As noted a ring shows similar behavior as a (repulsive) antidot covered by a thin film. Of interest would be also to study a ring of graphene, due to the remarkable properties of

graphene, or conducting nanotubes. To study interplay of electric and magnetic fields (Maxwell equations at action in nanostructures) double-rings are of interest. Generally the discussion and results for superconducting cylinders, rings, squids, tunnel junctions, can be frequently applied somewhat to the topologically closed mesoscopic structures in case of relatively long free path of the electrons (see dominant paths in Balian–Bloch–Stampfli theory). This demonstrates the interesting properties of nanostructures.

4 Summary

Magnetic effects in nanostructures have been discussed. Typical properties of clusters, cluster ensembles, single films and film multilayers and microscopic tunnel systems are presented. Due to the reduced dimension and system size external fields may change sensitively the behavior. Spin dependent transport on a nanoscale, involving optical manipulation, temperature gradients etc., see corresponding Onsager theory, offers interesting possibilities. Also (strong) nonequilibrium behavior of nanostructure needs be studied.[13]

Acknowledgements

Essential general help in particular regarding organisation of the review, technical assistance and critical reading was given by Christof Bennemann. Furthermore, discussions and many results by P. Jensen, M. Garcia, P. Stampfli, G. Pastor, W. Hübner, K. Baberschke, M. Kulic, and many others are gratefully acknowledged. I am particular grateful to F.Nogueira for ideas, discussions and help. This review was supported by D.F.G through S.F.B.

References

- [1] Pastor G.M., Bennemann K.H. (1999), *Magnetism in Clusters in Metal Clusters*, Editor Ekardt W. (Wiley, New York, 1999); Pastor G.M. in *Atomic Clusters and Nanoparticles*, p. 335 (EDP Sciences, Les Ulis/Springer, Berlin, 2001); Pastor G.M., Ph.D. thesis, F.U.Berlin (1989); Sugano S., *Microcluster Physics*, Springer Series in Mat. Science **20** (1991); Tomanek D., Mukherjee S., Bennemann K.H., *Phys. Rev. B* **28**, 665 (1983); Jellinek J., *Theory of Atomic and Molecular Clusters*, Springer Series in Cluster Physics (1999), also *Proceedings of ISSPIC-conferences*
- [2] Jensen P.J., Bennemann K.H., *Magnetic Structure of Films*, *Surface Science reports* **61**, 129 (2006); Brinzanik R., Jensen P.J., Bennemann K.H., *Study of nonequilibrium magnetic domain structure during growth of nanostructured ultrathin films*, *J. of Magnetism and Magnetic Materials* **238**, 258 (2002); Brinzanik R., Ph.D. thesis F.U. Berlin (2003), *Monte Carlo study of Magnetic nanostructures during Growth*; Jensen P.J., Bennemann K.H., *Magnetism of 2d-nanostructures*, in book *Magnetic Material* (Editor A.V.Narlikar, Springer, 2004)
- [3] Kastening B., Morr D.K., Alff L. and Bennemann K.H., *Charge Transport and Quantum Phase Transition in Tunnel Junctions*, *Phys. Rev.B* **79**, 144508 (2009); Kastening B., Morr D.K., Manske D. and Bennemann K.H., *Novel Josephson Effect in Tunnel Junctions*, *Phys. Rev. Lett.* **96**, 47009-1 (2006); Nogueira F. and Bennemann K.H., *Spin Josephson effect in ferromagnetic/ferromagnetic tunnel junctions*, *Europhysics Lett.* **67**,

- 620 (2004); Takahashi S., Imamura H., Maekawa S., *Spin Imbalance and Magnetoresistance of Tunnel Junctions*, *Phys. Rev. Lett.* **82**, 3911 (1999); Garcia M., *Habilitation thesis, FU Berlin (1999)*; Speer O., Garcia M., Bennemann K.H. *Phys. Rev.***62**, 2630 (1996)
- [4] Tarento R.J., Bennemann K.H., Joyes P., van de Walle J., *Mie Scattering of Magnetic Spheres*, *Phys. Rev. E* **69**, 166 (2004)
- [5] Stampfli P., Bennemann K.H., *Electronic Shell Structure in Mesoscopic Systems: Balian–Bloch type theory*, *Z. Physik D* **25**, 87 (1992); *Phys. Rev. Lett.* **69**, 3471 (1992); Tatievski B., *Diploma thesis, Balian–Bloch type theory for Spheres, Discs, Rings and Anti-Dot Lattices (F.U. Berlin, 1993)*; Tatievski B., Stampfli P. and Bennemann K.H., *Analytical results for the electron shell structure in Mesoscopic Systems*, *Ann. der Physik* **4**, 202 (1995)
- [6] Jensen P.J., Bennemann K.H., *Magnetic Properties of Ferromagnetic Clusters in Stern–Gerlach Deflection Experiments*, *Comput. Mat. Science* **2**, 488 (1994); Jensen P.J., Mukherjee S., Bennemann K.H., *Theory for Spin Relaxation in Small Magnetic Clusters*, *Z. Phys. D* **21**, 349 (1991); Dorantes–Davila J., Guirado R.A., Pastor G.M., *Orbital Magnetism*, in *Physics of Low Dimensional Systems (Editor J.L.Moran–Lopez, Kluwer Academic Publ., New York, 2001)*; Pastor G.M., Dorantes–Davila J., Bennemann K.H., *Transition Metal Clusters*, *Physica B* **149**,22 (1988); *Phys. Rev.B* **40**, 7642 (1989); Dorantes–Davila J., Dreysse H., Pastor G.M., *Physical Rev. Lett.* **91**, 197206 (2003); Pastor G.M., Dorantes–Davila J., Bennemann K.H., *Spin Fluctuations in T.M. Clusters*, *Phys. Rev. B* **70**, 1 (2004)
- [7] Jensen P.J., Morr D.K. and Bennemann K.H., *Reorientation Transition in Thin ferromagnetic films*, *Surface Science* **307**, 1109 (1994); Jensen P.J. and Bennemann K.H., *Temperature Induced Reorientation of Magnetism at Surfaces*, *Solid State Communic.* **100**, 585 (1996)
- [8] Jensen P.J. and Bennemann K.H., *Theory for Domain Wall Width*, *Ann. Physik* **2**, 475 (1993)
- [9] Jensen P.J., Dreysse H., and Bennemann K.H., *Magnetism and Curie–temperature in thin transition metal films*, *Europhys. Lett.* **18**, 463 (1992), *Surf. Sci.* **269–270**, 627 (1992)
- [10] Moran–Lopez J.L., Bennemann K.H., Avignon M., *Magnetism in transition metals*, *Phys. Rev. B* **23**, 5978 (1981); Liu S.H., *Itinerant Magnetism*, *Phys. Rev. B*, **17**, 3629 (1978)
- [11] Jensen P.J., Bennemann K.H., *Thin Film Magnetic Phase Diagram*, *Phys. Rev. B* **52**, 16012 (1995) and Jensen P.J. in Ref.2; Brinzanik R., Jensen P.J., Bennemann K.H., *Nonequilibrium Magnetic Domain Structure during Film Growth*, *J. Magn. Magn. Mat.***238**, 258 (2002)
- [12] Bennemann K.H., *Nonlinear Optics in Metals (Oxford University Press, 1998)*
- [13] Bennemann K.H., *Ultrafast Dynamics in Solids*, *Ann. Physik* **18**, 480 (2009)

- [14] *Butiker M., Imry I., Landauer R., Phys.Lett. 96A, 365 (1983); Riedel E.K., v.Oppen F., Phys. Rev. B 47, 15449 (1993); Balatsky A.V., Altshuler B.L., Phys. Rev. Lett. 70, 1678 (1993)*